CHALMERS
UNIVERSITY OF TECHNOLOGY

Excavation in Soft Clay

Class A prediction of excavation in central Gothenburg

Master's thesis in Master Program Infrastructure and Environmental Engineering

MATILDA HARLÉN

GABRIELLA POPLASEN

Department of Architecture and Civil Engineering
CHALMERS UNIVERSITY OF TECHNOLOGY
Master's thesis ACEX30-19-44
Gothenburg, Sweden 2019

Master's thesis ACEX30-19-44

Excavation in Soft Clay

Class A prediction of excavation in central Gothenburg

MATILDA HARLÉN
GABRIELLA POPLASEN

CHALMERS
UNIVERSITY OF TECHNOLOGY

Department of Architecture and Civil Engineering
Division of Geology and Geotechnics
Geotechnics Research Group
Chalmers University of Technology
Gothenburg, Sweden 2019

Excavation in Soft Clay
Class A prediction of excavation in central Gothenburg

MATILDA HARLÉN
GABRIELLA POPLASEN

Supervisor: Industrial Doctoral Student Johannes Tornborg, Department of Architecture and Civil Engineering
Examiner: Senior Lecturer Mats Karlsson, Department of Architecture and Civil Engineering

Department of Architecture and Civil Engineering
Division of Geology and Geotechnics
Geotechnics Research Group
Chalmers University of Technology
SE-412 96 Gothenburg
Telephone +46 31 772 1000

Cover: Picture of studied excavation (Tornborg, 2018)

Typeset in LaTeX
Department of Architecture and Civil Engineering
Gothenburg, Sweden 2019

Excavation in Soft Clay
Class A prediction of excavation in central Gothenburg
MATILDA HARLÉN
GABRIELLA POPLASEN
Department of Architecture and Civil Engineering
Division of Geology and Geotechnics
Chalmers University of Technology

Abstract

The densification of urban areas implies a higher demand on sustainable infrastructure, where deep excavations play an important role. Therefore, satisfactory modelling of the unloading response of clay, both in short and long term perspective, is of importance. To capture the complex behaviour of soft clay and include the effect of surrounding structures, numerical modelling is essential to ensure an adequate level of design.

The purpose of this thesis is to perform a Class A prediction of an excavation for the Hisings bridge project in Gothenburg. The area of the studied excavation is a busy area, adding to the complexity of the project. An advanced numerical model, Creep-SCLAY1S, was chosen for several reasons. It is an effective stress based visco-plastic model, which accounts for creep, anisotropy, bonding and destructuration. Thus, many properties inherent to Scandinavian clays are taken into account. The excavation design in Plaxis 2D was already finalized by Skanska Teknik, but with NGI-ADP, a total stress based elasto-plastic model, that also accounts for anisotropy. In addition to the Class A prediction with Creep-SCLAY1S, a comparison with the results from the NGI-ADP model is also made.

The result shows that both numerical models, Creep-SCLAY1S and NGI-ADP, predict similar unloading response. The difference between the model results lies in the magnitude of the predicted values, where Creep-SCLAY1S gives larger values for displacements and lower values for structural forces/bending moments. When comparing to some preliminary results from field measurements, both models seem to overestimate deformations. Even though NGI-ADP tends to give a reasonable prediction for the short term (undrained) case, it could be for the wrong reason. In comparison to NGI-ADP, it is clear that Creep-SCLAY1S predicts the development of deformations/stresses with time in a more realistic way. Further, there may be many reasons for the difference in model results, such as not incorporating installation effects, lack of 3D effects or using incorrect stress state in the soil.

In conclusion, numerical modelling is a very useful tool when modelling soil behaviour, but it should be used as an indication on the expected behaviour more than for prediction of definite answers. Another thing that is important to consider when using different numerical models is what purpose the study has. Both studied numerical models have their advantages and drawbacks. Creep-SCLAY1S seemingly incorporates many aspects of Scandinavian clay behaviour, in comparison

to NGI-ADP. By allowing for consolidation analysis which could be crucial for design of excavations, the Creep-SCLAY1S model has an obvious advantage. However, the complexity of Creep-SCLAY1S is a drawback which could lead to uncertainties. Finally, if modelling long-term performance of excavations (or other underground structures) and their surroundings, rate-dependent models such as Creep-SCLAY1S that account for effects of on-going background creep settlements should be used.

Keywords: Creep-SCLAY1S, soft clay, creep, numerical modelling, bottom heave, deep excavation, sample disturbance, small strain stiffness, total stress based model, effective stress based model

Acknowledgements

We would like to thank our supervisor Johannes Tornborg and our examiner Mats Karlsson for introducing us to the subject and for guidance and contribution with expertise throughout the whole process. We would also like to thank everyone at Skanska Teknik (Geoteknik) in Gothenburg, that have shown interest in our thesis. A special thanks to Anders Kullingsjö, David Ekstrand, Robert Oskarsson and Torbjörn Edstam at Skanska for valuable thoughts and discussions during the project.

Matilda Harlén & Gabriella Poplasen
Gothenburg, June 2019

Contents

Nomenclature

Roman letters

a_s	Swelling index	[-]
b	Load factor for which swelling exceeds creep	[-]
c'	Cohesion intercept	[kPa]
c'_{ref}	Reference cohesion intercept	[kPa]
c_u	Undrained shear strength	[kPa]
c_{uk}	Corrected undrained shear strength	[kPa]
C_α	Secondary compression index	[%]
e	Void ratio	[-]
e_0	Initial void ratio	[-]
E'	Drained Young's modulus	[kPa]
E'_{50}	Drained Young's modulus at 50% of peak strength	[kPa]
E	Young's modulus	[kPa]
E_{oed}	Oedometer modulus	[kPa]
E_u	Undrained Young's modulus	[kPa]
EA	Axial stiffness	[kN/m]
EI	Bending stiffness	[kNm^2/m]
G	Shear modulus	[kPa]
G_0	Small strain shear modulus	[kPa]
G_{ur}	Unloading/reloading shear modulus	[kPa]
G_{ur}/s_u^A	Ratio unloading/reloading shear modulus over (plane strain) active shear strength	[-]
k	Permeability	[m/s]
K'	Drained bulk modulus	[kPa]
K	Bulk modulus	[kPa]
K_0	Coefficient of lateral earth pressure at rest	[-]
K_0^{NC}	Coefficient of lateral earth pressure at rest for normally consolidated state	[-]
K_u	Undrained bulk modulus	[kPa]
$L_{spacing}$	Out-of-plane spacing	[m]
m	Ratio between M_e & M_c	[-]
M'	Stiffness increase at large strains from oedometer curve	[-]
M	Stress ratio at critical state	[-]
M_0	Elastic stiffness ($\delta\sigma/\delta\varepsilon$) from oedometer curve	[kPa]
M_c	Stress ratio at critical state in triaxial compression	[-]
M_e	Stress ratio at critical state in triaxial extension	[-]
M_{ed}	Bending moment	[kNm/m]
M_L	Stiffness ($\delta\sigma/\delta\varepsilon$) for compression after σ'_c from oedometer curve	[kPa]

M_p	Maximum bending moment	[kNm/m]
M_{re}	Reloading modulus	[kPa]
M_{ul}	Unloading modulus	[kPa]
$N_{p,1}$	Maximum force in 1D	[kN/m]
$N_{p,2}$	Maximum force in 2D (anisotropy)	[kN/m]
p'	Mean effective stress	[kPa]
p'_{eq}	Mean effective stress at Current state surface	[kPa]
p'_m	Mean effective stress at Normal compression surface	[kPa]
p'_{mi}	Mean effective stress at Intrinsic compression surface	[kPa]
q	Deviator stress	[kPa]
r_s	Time resistance number (or creep number)	[-]
r_{si}	Intrinsic time resistance number (or intrinsic creep number)	[-]
R	Time resistance	[s]
R_{inter}	Strength reduction factor	[-]
s'	Principal effective stress in the plane of shearing (centre of Mohr circle)	[kPa]
s_u^{DSS}/s_u^A	Ratio of direct simple shear strength over (plane strain) active shear strength	[-]
s_u^P/S_u^A	Ratio of (plane strain) passive shear strength over (plane strain) active shear strength	[-]
$s_{u,inc}^A$	Increase of shear strength with depth	[kN/m^2/m]
$s_{u,ref}^A$	Reference (plane strain) active shear strength	[kN/m^2]
S_t	Sensitivity	[-]
t_0	Initial time	[s]
t	Maximum shear stress in the plane of shearing (radius of Mohr circle)	[kPa]
t	Time	[s]
t_r	Reference time	[s]
u	Pore pressure	[kPa]
V_{ed}	Shear force	[kN]
V_p	Pressure wave velocity	[m/s]
V_s	Shear wave velocity	[m/s]
w	Specific weight of plate	[kN/m/m]
w	Water content	[%]
w_L	Liquid limit	[%]
w_N	Natural water content	[%]
w_P	Plastic limit	[%]
y_{ref}	Reference depth	[m]

Greek letters

α_0	Initial anisotropy	[-]
α_s	Creep parameter or secondary compression index	[-]
χ_0	Initial bonding	[-]
δW	Increment in work	[kPa]
δW_d	Increment in distortional work	[kPa]
δW_v	Increment in volumetric work	[kPa]
$\Delta\chi$	Destructuration or degradation of bonding	[-]
$\Delta\varepsilon$	Relative strain	[-]
$\Delta\varepsilon_{cr}$	Relative creep strain	[-]
$\Delta\varepsilon_p^c$	Relative volumetric viscoplastic strain	[-]
$\Delta\varepsilon_q^c$	Relative deviatoric viscoplastic strain	[-]
Δe/e_0	Relative void ratio	[-]
Δt	Relative time	[-]
$\dot{\varepsilon}$	Total strain rate	[1/s]
$\dot{\varepsilon}_p^c$	Volumetric creep strain rate	[1/s]
$\dot{\varepsilon}_p^e$	Volumetric elastic strain rate	[1/s]
$\dot{\varepsilon}_q^c$	Deviatoric creep strain rate	[1/s]
$\dot{\varepsilon}_q^e$	Deviatoric elastic strain rate	[1/s]
$\dot{\varepsilon}^c$	Creep strain rate	[1/s]
$\dot{\varepsilon}^e$	Elastic strain rate	[1/s]
ε_{cr}	Creep strain	[%]
ε_p	Volumetric strain	[%]
ε_q	Deviatoric strain	[%]
η	Stress ratio	[-]
η_{K0}	Initial stress ratio	[-]
γ	Unit weight	[kN/m^3]
γ_f^C	Shear strain at failure in triaxial compression	[%]
γ_f^{DSS}	Shear strain at failure in direct simple shear	[%]
γ_f^E	Shear strain at failure in triaxial extension	[%]
γ_{sat}	Saturated unit weight	[kN/m^3]
γ_{unsat}	Unsaturated unit weight	[kN/m^3]
κ^*	Modified swelling index	[-]
λ^*	Modified compression index	[-]
λ_i^*	Modified intrinsic compression index	[-]
μ^*	Modified creep index	[-]
μ_i^*	Modified intrinsic creep index	[-]
ν'	Poisson's ratio	[-]
ν_u	Undrained Poisson's ratio	[-]
ω	Absolute effectiveness of rotational hardening	[-]
ω_d	Relative effectiveness of rotational hardening	[-]
ϕ'	Friction angle	[°]
ϕ'_c	Friction angle at critical state in compression	[°]
ϕ'_{cv}	Critical state friction angle	[°]
ϕ'_e	Friction angle at critical state in extension	[°]
ψ'	Dilatancy angle	[°]

ρ	Density	[kg/m^3]
σ'_1=σ'_2=σ'_3	Principal effective stresses	[kPa]
σ'_c	Apparent preconsolidation pressure	[kPa]
σ'_h	Effective horisontal stress	[kPa]
σ'_{h0}	Effective horisontal in-situ stress	[kPa]
σ'_v	Effective vertical stress	[kPa]
σ'_{v0}	Effective vertical in-situ stress	[kPa]
τ	Reference time	[days]
τ_0/s_u^A	Initial mobilization	[-]
θ	Lode angle	[rad]
$\dot{\lambda}$	Visco-plastic multiplier	[-]
ξ	Absolute rate of destructuration	[-]
ξ_d	Relative rate of destructuration	[-]

Abbreviations

CADC	Consolidated Anisotropic Drained Compression
CRS	Constant Rate of Strain
CSL	Critical State Line
CSS	Current State Surface
ESP	Effective Stress Path
FEM	Finite Element Method
ICS	Intrinsic Compression Surface
IL	Incremental Load
MCC	Modified Cam Clay
NC	Normally Consolidated
NCS	Normal Compression Surface
OC	Over Consolidated
OCR	Over Consolidation Ratio
POP	Pre-Overburden Pressure
SPW	Sheet Pile Wall
SQD	Specimen Quality Designation
TSP	Total Stress Path
YS	Yield Surface

List of Figures

List of Tables

1
Introduction

As cities densify and the demand for sustainable infrastructure is increasing, there will also be a higher demand for underground constructions. Consequently, satisfactory modelling of the unloading behaviour of clay will come to play a more important role. Especially since deep and complex excavation works may stay open a longer time period than previously. Thus, the modelling of time-dependent response of clay will be important since the stability of excavations often gets more critical with time. To be able to capture the complex behaviour of clay and include the effect of surrounding structures, numerical modelling is essential to ensure adequate design. It is of extra importance to get reliable predictions in urban areas since there often are high demands on safety and restrictions of deformations. Therefore, it is of interest to further investigate how numerical models perform considering unloading behaviour.

1.1 Case Study

This study investigates a deep excavation located in the central parts of Gothenburg, see Figure 1.1. To build excavations in Gothenburg, and larger buildings/infrastructure in general, is rather complicated due to the difficult ground conditions. A characteristic ground profile in Gothenburg consists of thick layers of soft and sensitive clay which leads to challenges with ongoing creep settlements.

Figure 1.1: Location of the studied area (Google Maps, 2019).

The construction site is located between Nordstan and Nils Ericson terminalen, see Figure 1.2. The area is highly exploited and busy, which in addition to the ground conditions adds to the complexity of the project. The excavation is carried out in order to construct a ramp, where the upper part is connected to the new Hisings bridge and the lower part is a loading ramp going into Nordstan, see Figure 1.2. The studied excavation will be up to 7 m in the deeper parts.

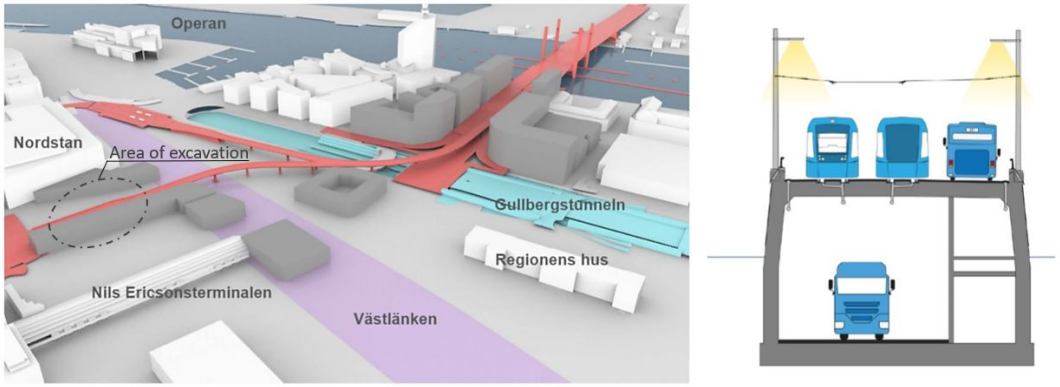

Figure 1.2: Visualization of location and section of the ramp (Ekholm, 2017) (red=new bridge, grey=future buildings, white=existing).

The ramp is a part of the new Hisings bridge project, which itself is a part of the "Västsvenska paketet". The project is ordered from the city of Gothenburg, and their vision is to facilitate and increase the capacity of public travelling which will allow for a growth of western Sweden (Trafikverket, 2016b). The companies responsible for the Hisings bridge project (including the excavation for the ramp) are Skanska and MT Højgaard. This thesis will be conducted in collaboration with Skanska Teknik. The design of the retaining structure for the excavation has already been finalized by Skanska Teknik using analytical Rankine earth pressures and numerical (FEM) analysis with the NGI-ADP model in Plaxis 2D. However, since the NGI-ADP model is total stress based, it does not include time-dependent response. Another interesting aspect of clay is the bonding and destructuration effects. It would therefore be of interest to study the response of a more advanced numerical model that is effective stress based and that includes these aspects. Therefore, it is chosen to analyze the designed system with the Creep-SCLAY1S model.

1.2 Aim and Objectives

The aim of this Master's thesis is to make a Class A prediction for the excavation located between Nordstan and Nils Ericsson terminalen, which is preparing for the new Hisings bridge ramp. The prediction will be performed by numerical analysis, using Plaxis 2D with the Creep-SCLAY1S model. Both short and long term performance will be assessed. Further, the study aims at mapping important behaviour of soft clay and understand how the model affects the results. It also aims at identifying uncertainties when modelling deep excavations and approaches to reduce those.

The following objectives are set:

- Create a soil profile and retrieve parameters for the Creep-SCLAY1S model which are representative for the soil behaviour
- Validate the Creep-SCLAY1S model
- Study how deformations and structural forces develop with time
  - Which magnitude of bottom heave could be expected?
  - Which magnitude of settlement could be expected?
- Compare and evaluate the main differences between the results of the Creep-SCLAY1S and NGI-ADP model
  - What are the main limitations of the studied models, and what effect does it have?
- Asses which parameters that have large influence in the Creep-SCLAY1S model
- Analyze what could be improved in order to get more reliable results

1.3 Limitations

As always, it is not possible to replicate reality and get exact predictions. The following are the main limitations that are identified for this thesis:

- The geometry of the excavation and the properties of the retaining structure in Plaxis 2D is designed by Skanska Teknik
- Only one section of the excavation is considered
- By using 2D plane strain, it does not account for corner effects and other 3D-effects like step-wise excavation
- The soil profile and properties are retrieved from a limited number of boreholes, which may not be representative for the soil surrounding the excavation
- Limitations with modelling soil with Creep-SCLAY1S:
  - the isotropic elastic behaviour is modelled as linear
  - does not account for small strain stiffness
  - does not describe non-linear variation of OCR (or strength) with depth
- Installation effects from piles and sheet pile walls are not be considered

1.4 Method

The main steps of the Method used in this thesis are presented in this section. Figure 1.3 shows an overview of the steps that are described.

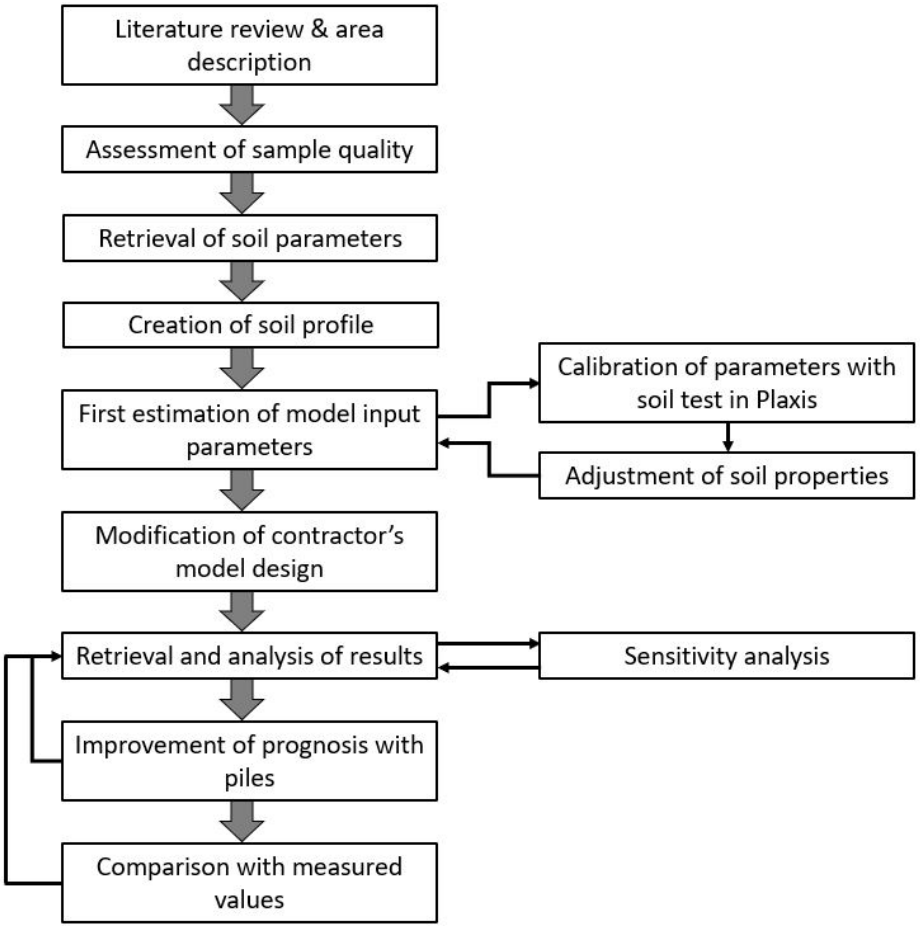

Figure 1.3: Methodology for this thesis.

First, a literature review was executed to get a better understanding on the subject of this thesis. Both printed books and online scientific databases were used. In addition to this, information about the studied area was retrieved to get an understanding of the soil in the area, expected behaviour and problems that could occur. The description of the area and the literature review, can be found in Chapter 2 and 3, respectively.

Before the laboratory test data was analyzed, a sample quality assessment was performed in order to only include representative data. After that, the screened laboratory tests together with the borehole data were analyzed to retrieve a soil profile. In addition to this, the remaining input parameters to the Creep-SCLAY1S model were calculated. All model specific parameters were then calibrated with soil test in PLAXIS 2D. Further information about the input parameters for the Creep-SCLAY1S model can be found in Section 3.3. A more detailed description of the parameter retrieval and soil profile, can be found in Section 4.1.

After this, the NGI-ADP model design by Skanska Teknik, was modified to be able to use the Creep-SCLAY1S model parameters. The changes done were alterations in the soil profile and changing plastic calculation to consolidation calculation. Further, the original boundaries of the models were changed in order to avoid boundary effects. More detailed information about the PLAXIS 2D modelling can be found in Section 4.2.

The main results consist of a comparison of the results from the Creep-SCLAY1S and NGI-ADP model. In the soil, vertical and horizontal displacements were analyzed in points of interest, while bending moment and normal forces were analyzed for the structural entities. Further, a sensitivity analysis was performed in order to validate the accuracy of the results from the Creep-SCLAY1S model. The results and sensitivity analysis can be found in Chapter 5.

To further improve the prognosis for the studied excavation (and also make it more similar to reality), piles beneath the excavation bottom were added to the Creep-SCLAY1S simulation in PLAXIS 2D. The results for this can be found in Section 5.5. In addition to this, measured data on the bottom heave from the studied excavation was compared to all numerical predictions. The comparison can be found in Section 5.6.

2

Area Description

The purpose of this chapter is to give a background on the history of the excavation area as well as a description of the local ground conditions. Thus, giving a picture of the expected soil characteristics and behaviour.

2.1 History of the Area

The northern part of central Gothenburg or more specifically the areas of Vallgraven and Nordstaden (where the excavation is located), are the oldest parts of the city and have been populated since 1620 (Stadsmuseet, 1999). From then and until the beginning of the 1800's, Gothenburg was a fortificated city. Figure 2.1 shows the evolution of the city from year 1809 until today. From 1806 Gothenburg was not a fortificated city anymore, and large areas were converted into land mass and piled to make space for new buildings. Thus, the Göta älv river started to resemble today's appearance more and more. The studied area was before 1840 a reed area, where the Göta älv river was much wider than it is today. From 1855 and further on, a major expansion of the railway system was executed. In Figure 2.1 under year 1872, it can be seen that there was a building, more precise a train storage and workshop, located at the studied excavation site. During early excavation of the studied area, the foundation wall and 8 m long wooden piles from this building were found and have now been removed. Between the 1950's and 1960's, Gothenburg was a fast growing city, where some of the most extensive changes in the area of the studied excavation were made.

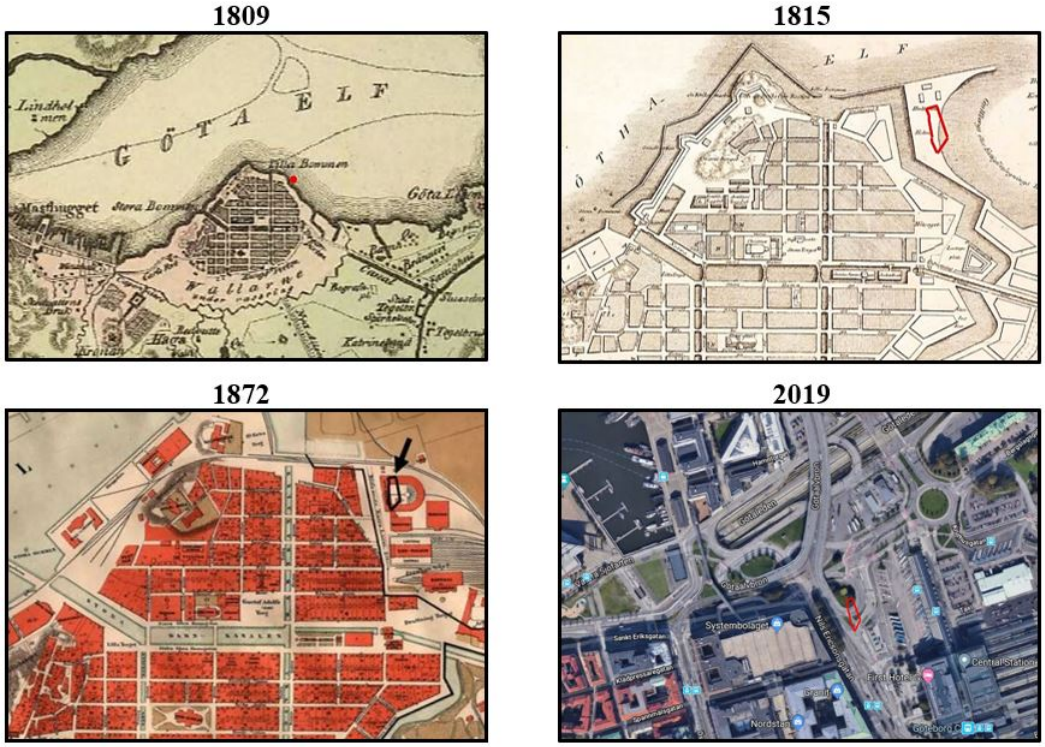

Figure 2.1: Maps of studied area from different time periods, where the studied excavation is marked with red or black (Google Maps, 2019; Lantmäteriet, 2019; Stadsbyggnadskontoret, 2019).

2.2 Geology and Hydrogeology

The geological history of the Gothenburg region is rather complex, consisting of different kinds of deposits, both glacial and post-glacial (SGU, 2019; Trafikverket, 2016a). Gothenburg's topography consists of lowland valleys including rivers with surrounding mountain-landscape. The soil in the valleys generally consists of a top layer of filling, followed by a thick layer of clay deposit. The clay could be assumed to be illite, which has rather strong bonding. Although, since the clay has been deposited in saltwater, the microstructure is more open resulting in a highly compressible deposit (Rankka, 2003). The bedrock consists mainly of felsic magmatic rock, such as gneiss and quartz-rich granite. Furthermore, glacial clay composes the largest share of the soil, where some is covered by post-glacial clay or post-glacial sand (SGU, 2019). The limit between glacial and post glacial clay is around 19 m $\pm$ 1m below sea level (T. Wood, 2015). In Figure 2.2 the location of the excavation is marked on regional maps showing soil type (Quaternary map) and depth to bedrock. It can be seen from the Quaternary map that the excavation is located on the converted reed area close to the old shoreline. Further, the Quaternary map shows that the top layers (the fill) consist of artificial fill and an underlying bed of young fluvial sediment. The thickness of the filling material in the area of the excavation varies between 3.6-4.7 m (Skanska Teknik, 2018a). The bottom 0.5-1.5 m of the filling are found to consist of mainly clay, with elements of sand, silt and bricks. Further, clay makes up the remaining soil, down to approximately 90 m

below ground surface, where a thin layer of friction material is found on top of solid bedrock. From the second map in Figure 2.2, it can also be seen that the excavation is located in a lowland area (valley), where some of the thickest clay deposits in the region are located.

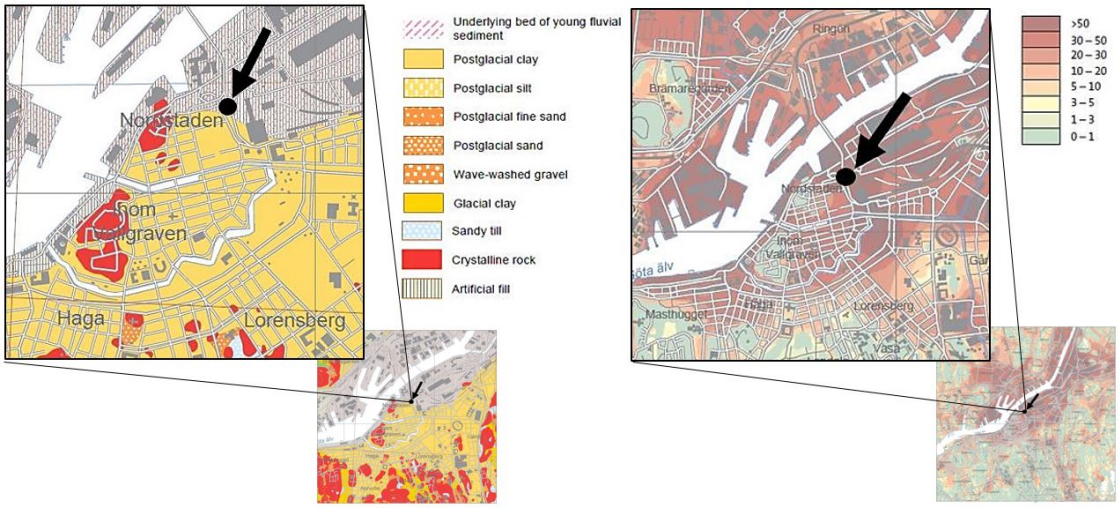

Figure 2.2: Regional maps of soil type and depth to bedrock (SGU, 2019).

Investigations from the area indicate on a homogeneous clay which is slightly over-consolidated (OCR around 1.1-1.4). No intermediate permeable layers of sand or silt have been identified (Skanska Teknik, 2018b). The topography in connection to the excavation is rather flat, except for an embankment for the existing Göta älv bridge next to it, resulting in a variation in ground surface level. In general the ground surface is located at +3 m above sea level, and the groundwater table is located at +1 m above sea level (Skanska Teknik, 2018b). The clay has a water content of 60-90% and a sensitivity around 10-30 (Skanska Teknik, 2018b), which is classified as medium sensitivity according to Rankka et al. (2004) (Swedish definition). One challenge with excavating in these conditions, except the stability, is to prevent deformations of nearby structures, which will be extra challenging due to the urban location. A potential problem will be the risk of lowering the groundwater table which could damage foundations due to consolidation or an acceleration of degradation processes (due to extra contact with oxygen). The potential risk of damage will depend on proximity to the excavation and the foundation type (Trafikverket, 2016c). A building which will be in the risk zone is Nordstan which is a large building close to the excavation where wooden piles have been used for the foundation. To see foundation types for buildings in the area, see Figure A.1 in Appendix A.1. Another structure in the risk zone would be the road embankment next to the excavation, where the tracks for the trams are sensitive to deformations.

3
Theoretical Background

In this chapter the main findings from the literature review are presented. The chapter starts with explaining important characteristics and behaviour of clay, with focus on soft clay and unloading response. Then, different ways of simplifying (model) the soil behaviour are introduced, where numerical modelling is explained. Further, the difference between effective and total stresses based models are made clear since the studied models differ in this aspect. Also, small strain stiffness is included since it has not been incorporated in the studied models but is expected to influence the results. At last the used models, Creep-SCLAY1S and NGI-ADP are described in more detail, where Creep-SCLAY1S is the main focus.

3.1 Behaviour of Soft Clay

Soil particles naturally have different shapes, where clay particles are mostly flat and platy which implies a low ability to resist deformations (D. M. Wood, 1990). In contrast to more coarse grained soils, clay particles are not held together by direct contact. Instead they are held together by molecular forces, allowing for a soil structure with a large void ratio (Sällfors, 2013). The voids are filled with pore fluids, most commonly air and water. Due to the large share of voids and the poor contact between the particles, clay tends to exhibit large irrecoverable deformations (D. M. Wood, 1990). The low stiffness and large deformation is extra prominent in soft clay, where the void ratio (and water content) is larger. The deformation of soils consists of both change in volume and shape, and the magnitude varies in different directions due to the anisotropic properties of clay. Further, the magnitude of deformation is dependent on properties like density, water content, mineral composition and organic content (Larsson, 2008). It is also dependent on the current stress state as well as the stress history. Volume change in soils occurs most commonly when it is sheared, where this mechanism is called dilatancy (D. M. Wood, 1990). When the volume changes, the pore fluid will move as well. Here, the permeability, k, indicates how easy it is for the water to move through the soil. As clays are composed mostly of very small particles, the permeability will be very low as opposed to coarse grained soils, such as sand. The flow of water in the soil is governed by excess pore pressures that are created if equilibrium of the pore water is disturbed. The response of the soil is thus dependent on the effective stresses that the soil is experiencing.

One important mechanism of soft clays is the consolidation process (Knappet & Craig, 2012). Consolidation is a volume reduction by dissipation of excess pore pressure from saturated soils, i.e. change in effective stress. The opposite mechanism is called heave, where an increase in volume is incorporating dissipation of negative excess pore pressure. The classical theory of consolidation (1D) was first introduced by Terzaghi (1923) and assumes that time is independent of the relationship between effective stress and strain. Although, it has later been shown, by for instance Larsson (1986), that this theory is not valid for e.g. Swedish clays by analyzing measured settlements and pore pressures. Another important, also time-dependent, process to consider when modelling soft clay behaviour is creep (Persson, 2004), which is described in more detail in the next section.

3.1.1 Creep

Deformations can be both elastic and plastic and are also either instantaneous or time-dependent (Larsson, 2008). Instantaneous deformations in undrained saturated soils consist only of shape change, while time-dependent deformations include consolidation and creep. The consolidation process is, as mentioned, driven by the gradient due to the excess pore pressures, while the creep is defined as a time-dependent volume change under constant effective stress. Further, creep can be described as the rearrangement of soil particles to a more stable state, and can include both change in volume and shape (Knappet & Craig, 2012).

Šuklje (1957) was first to introduce a model where creep is incorporated in the whole consolidation process as opposed to that it only could occur when excess pore pressures have dissipated. This implies that primary and secondary compression (consolidation and creep) are not separate processes, but rather occur simultaneously. According to Hansbo (1960), creep occurs most likely due to viscous deformations in microstructural fracture zones which originate from the primary compression. Due to the stress increment that arises, a rearrangement of particles with time occurs. If the rearrangement is followed by a volume increase, the soil dilates (Larsson, 2008). If the rearrangement is followed by a volume decrease, the soil contracts. The rearrangement of soil particles leads to an increased deformation resistance or bulk modulus, resulting in that the creep rate decreases with time (Hansbo, 1960).

To quantify the creep rate, there are several parameters to describe creep. Examples are the parameters C_α, α_s and r_s which all describe a linear relationship between time and creep deformations if the time axis is logarithmic. Taylor (1942) introduced a secondary compression index, C_α, which is most commonly used internationally. In Sweden it is more common to use α_s (Olsson, 2010). The difference between them is that α_s is described with strain and C_α with the void ratio (Claesson, 2003). Janbu (1969) presented the time resistance number, r_s, which just like α_s is described with strain, but with the natural logarithm instead. In Equations (3.1)-(3.3) the definitions of the creep parameters can be seen.

$$C_\alpha = \frac{\Delta e}{\Delta log(t)} \tag{3.1}$$

$$\alpha_s = \frac{\Delta \varepsilon_{cr}}{\Delta log(t)} \tag{3.2}$$

$$\frac{1}{r_s} = \frac{\Delta \varepsilon_{cr}}{\Delta ln(t)} \tag{3.3}$$

The relationship between α_s and r_s can be described with Equation (3.4).

$$\alpha_s = \frac{ln10}{r_s} \approx \frac{2.3}{r_s} \tag{3.4}$$

C_α and α_s can be derived from the slope of the consolidation/compression in an Incremental load, IL, Oedometer test when all excess pore pressures have dissipated, see Figure 3.1 (Claesson, 2003; Olsson, 2010).

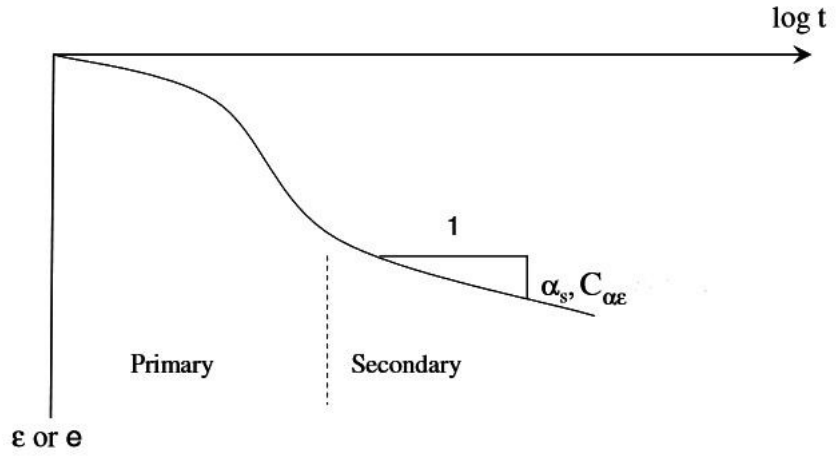

Figure 3.1: Evaluation of secondary compression (creep) indices (Olsson, 2010).

Creep deformations are strongly dependent on the effective stress during increasing strain (Meijer & Åberg, 2007). An illustration of this can be seen in Figure 3.2, where α_s starts to increase significantly when approaching σ'_c. Thus, the highest probability of creep occurrence is in normally consolidated, NC, and slightly over consolidated, OC, clays.

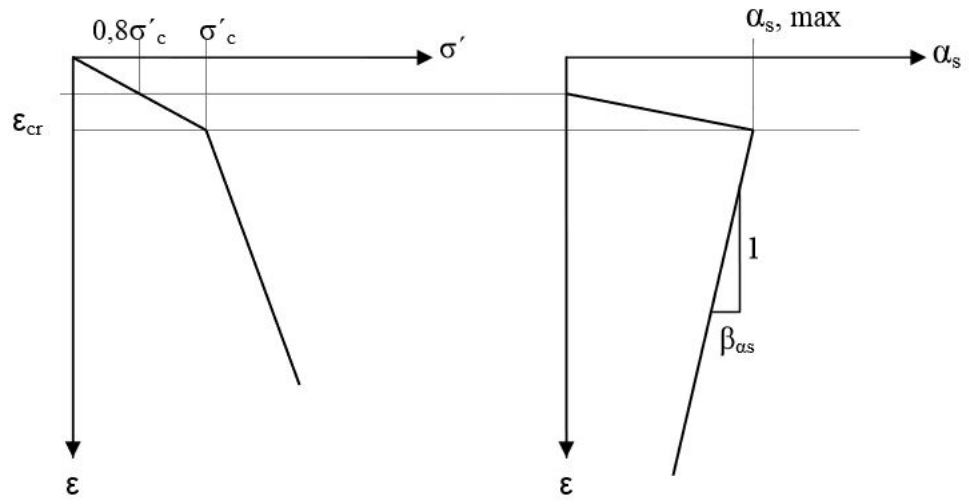

Figure 3.2: Variation of α_s with strain (Meijer & Åberg, 2007).

The time resistance, R, explains the stress- and time-dependent soil behaviour during compression, swelling and recompression (Olsson, 2010). R is evaluated from a single load step in an Oedometer test. If time is seen as an act and deformation as its response, R can be described with Equation (3.5).

$$R = \frac{\Delta t}{\Delta \varepsilon} \tag{3.5}$$

Figure 3.3 shows that R increases linearly with time at t_0 (Olsson, 2010), which corresponds to when excess pore pressures have dissipated.

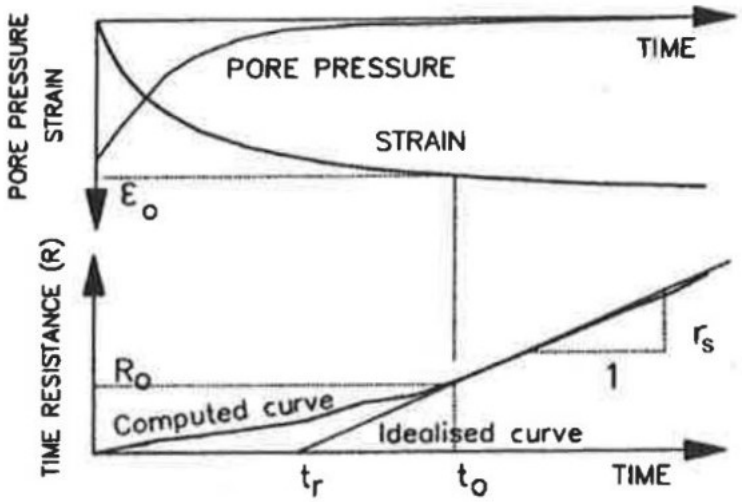

Figure 3.3: Time resistance with time during one Oedometer load step (Svanø, 1991).

Here, the relationship between R and t is linear and only "pure" creep is occurring. The gradient of the linear relationship can be defined with the time resistance number, r_s, which can be described with Equation (3.6).

$$R = r_s(t - t_r) \tag{3.6}$$

The creep strain due to linear time resistance can be expressed by integrating over a time-span, t_0 to t, see Equation (3.7).

$$\Delta\varepsilon_{cr} = \frac{1}{r_s}\int_{t_0}^{t}\frac{dt}{(t - t_r)} = \frac{1}{r_s}ln\frac{t - t_r}{t_0 - t_r} \tag{3.7}$$

3.1.2 Deep Excavations in Soft Clay

The main factor adding to the difficulty of excavation design is an increment in complexity with depth (Wang, Liu, & Liu, 2009). Especially soft clay is more challenging when designing and constructing deep excavations, due to its low stiffness (Kempfert & Gebreselassie, 2006). Its low stiffness can cause large deformations, both inside and outside the excavation, which is particularly problematic in urban areas. Also, urban areas are a more complex environment for excavations as current structures exist and must be dealt with (Kullingsjö, 2007). Thus, the design needs to be executed properly, as large settlements or collapse could occur, leading to damage of infrastructure or injuries of individuals (Ahmad, 2017). An example of a severe collapse, is the excavation of Nicoll Highway in Singapore, which except adding to large economic losses, caused 4 deaths and was cutting of traffic and electricity in large areas (COI, 2005).

With increased depth of excavation, an increased yielding of soil is occurring if no support is present (Knappet & Craig, 2012). Therefore, a support system is installed, which most commonly consists of a retaining wall, and struts or anchors to keep the wall in place. For a deep excavation, struts at several levels is commonly used. If the retaining structure is not designed adequately, a slip surface could form as plastic equilibrium is reached in the lower part of the excavation, for an example see Figure 3.4. Normally, failure of a braced excavation is due to failure in one strut (Knappet & Craig, 2012).

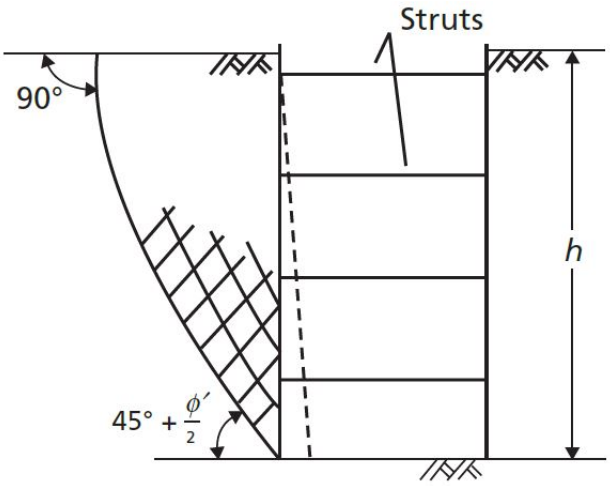

Figure 3.4: Simplified example of wall deformation and slip surface (Knappet & Craig, 2012).

There are several factors that affect the performance of the retaining system, such as soil behaviour, stiffness of the support system, geometry of the excavation and distance to adjacent structures (Kullingsjö, 2007). However, the soil response is the most complex. When studying the unloading of soil, it is crucial to know the stress history of the soil in order to understand the response (Ladd & Foott, 1974). Further important soil characteristics when studying unloading, are non-linear stress strain response, anisotropy, rate-effects and hysteresis behaviour. However, all these aspects are rarely taken into account when designing retaining systems (Kullingsjö, 2007).

The stress changes that occur when excavating will be both due to the loss of lateral support and due to the vertical unloading (Kullingsjö, 2007). This in turn leads to different drainage conditions around the excavation, which will cause different effective stresses. The effective stresses may change "more or less" with time after excavation depending on the consolidation process. The drainage conditions could be either ideally drained (no excess pore pressures), ideally undrained (constrained volume change in soil and excess pore pressure) or more likely partly drained (excess pore pressure dissipates over time). All excavations are theoretically most similar to the third drainage type, but due to the low permeability, clay is often treated as undrained. Although, this could lead to underestimation of stability since the effective stresses decrease with time as the excess pore pressure equalizes.

3.1.2.1 Bottom Heave

When excavating, the soil will experience a stress relief which in turn results in heave of the excavation bottom. The heave in clay is induced by the negative excess pore pressures which are created when the soil is unloaded. The bottom heave is a crucial design factor for deep excavations, especially in urban areas as large deformations could cause damage to nearby structures and softening in sensitive clays (Karlsrud & Andresen, 2008). It is extra important to consider bottom heave

in soft clays due to its low shear strength (Ergun, 2008). The heave mechanism can be described as an upward vertical displacement, due to soil expansion caused by unloading (Knappet & Craig, 2012). Heave is a reverse consolidation process and is governed by the unloading modulus, M_{ul} (Persson, 2004). The mechanism is induced by the weight of the excavated soil and surcharge next to the excavation, which results in upward movement of the bottom, see Figure 3.5. If the shear strength of the soil is not sufficient to withstand deformations, the soil can fail due to the bottom heave mechanism. Thus, these potential problems should be constantly monitored.

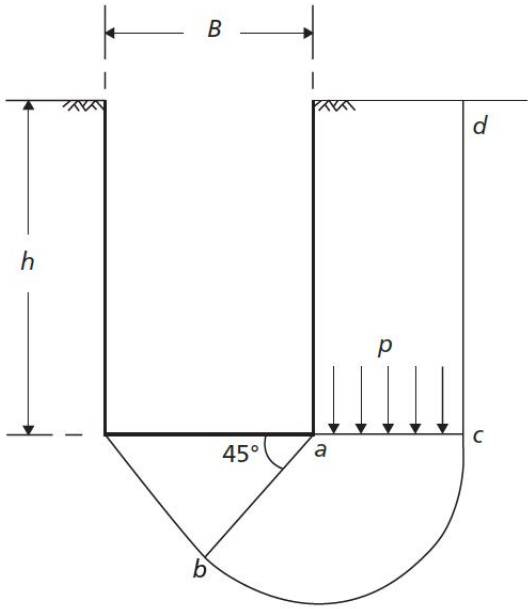

Figure 3.5: Illustration of bottom heave mechanism (Knappet & Craig, 2012).

Like the process of consolidation settlement, the heave in low permeable soils is hydrodynamically delayed in time (Tornborg, 2017). As stated before, the unloaded soil will initially experience negative excess pore pressures. Those pore pressures will even out with time and thereby also gradually decrease the effective stress. Swelling, which often is confused with heave, is a similar mechanism which instead of unloading gives an upward vertical displacement due to changes of chemicals or water content in the clay. Swelling is however not of interest in this study.

Larsson (1986) did several IL Oedometer tests on Swedish clay and found that loading stresses near the preconsolidation pressure gave very large M_{ul} due to creep effects. Also, unloading of OC clays gives lower M_{ul} than for NC clays (Persson, 2004). Figure 3.6 shows that according to the Larsson (1986) model, M_{ul} decreases linearly if vertical stress decreases in relation to 80% of the preconsolidation pressure. Figure 3.7 shows that for $\sigma'_v > 0.8\sigma'_c$, the unloading instead becomes infinitely large. The unloading modulus is stress dependent and can simplified be described with Equations (3.8)-(3.9) (Persson, 2004).

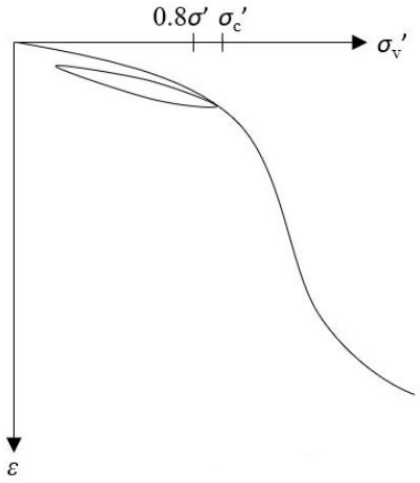

Figure 3.6: Unloading modulus related to stress behaviour in laboratory test (Larsson, 1986).

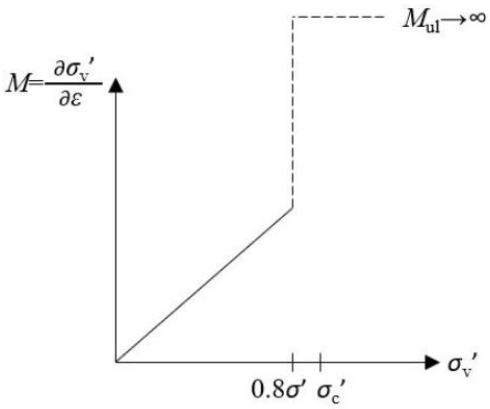

Figure 3.7: Simplified model for unloading modulus (Larsson, 1986).

$$M_{ul} = \frac{\sigma'_v}{a_s} \quad \text{for} \quad \sigma'_v \leq b\sigma'_c \tag{3.8}$$

$$M_{ul} \to \infty \quad \text{for} \quad \sigma'_v \geq b\sigma'_c \tag{3.9}$$

where
a_s=swelling index [-]
b=load factor for which swelling exceeds secondary compression [-]

Further, Karlsrud (2003) showed that a non-linear relationship for the unloading modulus, where stiffness relates to the stress level of the soil and preconsolidation pressure should be more accurate. Also, a reloading modulus, M_{re}, was defined using reload steps in the IL tests.

Persson (2004) also performed IL Oedometer tests, but also triaxial tests and field measurements as well, where the unloading behaviour of soft Gothenburg clay was studied. Similar behaviour as for the results from Larsson (1986) and Karlsrud (2003) was observed. The relationship for M_{ul} proposed by Persson (2004) is presented in Equation (3.10).

$$M_{ul} = 35\sigma'_c \, e^{\frac{3.5}{OCR}} \tag{3.10}$$

3.2 Soil Modelling and Numerical Modelling

When dealing with geotechnical structures it is of importance to be able to predict deformations and to ensure stability, especially in urban areas (Karstunen & Amavasai, 2017). Due to the complexity of the interaction between the soil, the structure and the surroundings, the system has to be idealized. To simplify the behaviour of the soil there exist several different constitutive models (Karstunen & Amavasai, 2017). In Figure 3.8 four different constitutive models are shown.

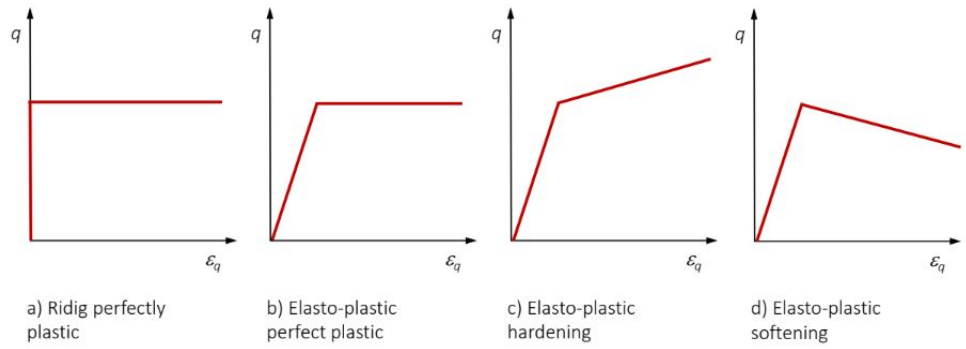

Figure 3.8: Different constitutive models (Karstunen & Amavasai, 2017).

The rigid-perfectly plastic model implies that soil is not deforming until failure occurs (Karstunen & Amavasai, 2017). The elasto-plastic perfectly-plastic model, i.e. Mohr-Coulomb model, has linear elastic behaviour until failure occurs. Neither the rigid-perfectly plastic nor the elasto-plastic perfectly plastic model are suitable for simulating the behaviour of soft clay, which is NC or slightly OC, since this type of clay tends to have a significant change in volume during shearing. For soft clays, the elasto-plastic hardening or elasto-plastic softening models are more suitable. The elasto-plastic hardening model accounts for increase of undrained shear strength during consolidation of NC clay. The elasto-plastic softening model accounts for degradation of mobilised shear strength, which is common in sensitive soft clay. Most common in geotechnical modelling is to use isotropic elasto-plastic soil models, for instance those in Figure 3.8 (Wheeler, Näätänen, Karstunen, & Lojander, 2003). However, soft clays are mostly anisotropic due to the clay particles' platy shape, the deposition process and the consolidation history of the deposit (Karstunen & Koskinen, 2008).

The simplified behaviour of soils is usually described with principal stresses in either s'-t plane or in p'-q plane (D. M. Wood, 1990). The principal stresses are explained in Figure 3.9 while the definitions of s' & t and p' & q are presented in Equation (3.11) and Equation (3.12), respectively.

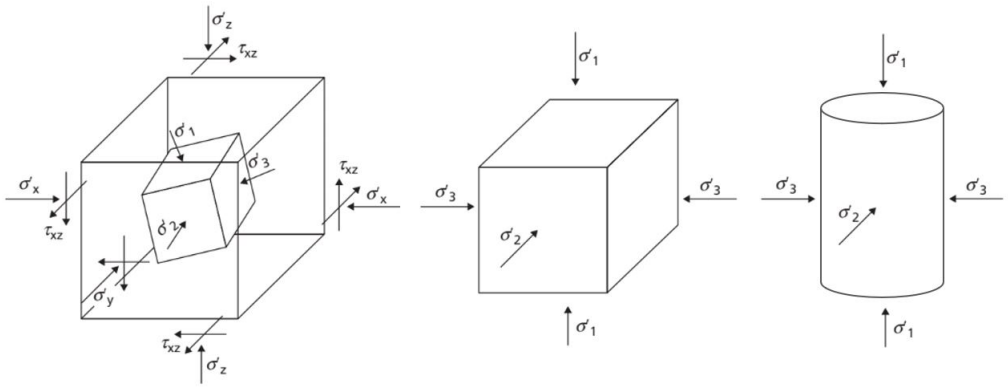

Figure 3.9: Visualization of principal stresses (Knappet & Craig, 2012).

$$s' = \frac{\sigma'_1 + \sigma'_3}{2} \qquad t = \frac{\sigma'_1 - \sigma'_3}{2} \tag{3.11}$$

where
σ'_1, σ'_2 and σ'_3 = principal effective stresses
s' = principal effective stress in the plane of shearing (center of Mohr circle)
t = maximum shear stress in the plane of shearing (radius of Mohr circle)

$$p' = \frac{\sigma'_1 + \sigma'_2 + \sigma'_3}{3} \qquad q = \sigma'_1 - \sigma'_3 \tag{3.12}$$

where
σ'_1, σ'_2 and σ'_3 = principal effective stresses
p' = mean effective stress
q = deviator stress

Changes in the soil during different processes can according to D. M. Wood (1990) be described with increment in work, see Equation (3.13). p' is here linked to volumetric work, while q is linked to distortional work (shape change).

$$\delta W = \delta W_v + \delta W_d = p' \delta \varepsilon_p + q \delta \varepsilon_q \tag{3.13}$$

Altogether, there are three possible methods to solve idealized problems: empirical, analytical and numerical (Petalas, 2018). If possible, it is best to solve the problem analytically, however due to complexity of the system it is not always possible to

solve the problem analytically. Further, empirical methods would require extensive knowledge of similar previous projects or much resources such as time and money. Due to the limitations of analytical and empirical methods, numerical methods are more suitable for predictions of complex structures in urban areas. The numerical approach often involves using Finite element methods, FEM, which is based on discretizing the continuous soil (Karstunen & Amavasai, 2017). The discretized elements are then assigned the same properties for the whole element. Further, the elements are connected by nodes where the parameters and values of interest could be evaluated (Plaxis, 2018c). The number of nodes can be adjusted according to the desired level of accuracy. In short, the infinite amount of soil particles and their bonding is reduced to a finite amount of nodes with 2 or 3 degrees of freedom (depending on if modelling in 2D or 3D). A common commercial software for modelling geotechnical structures is Plaxis. Although software such as Plaxis are handy and useful tools, the results could be misleading if proper care is not taken (Karstunen & Amavasai, 2017). It is important to remember that the prediction can never be better than the input data and that the choice of constitutive model in combination with the experience of the engineer are major factors affecting the results.

3.2.1 Total Stress vs Effective Stress Based Model

In numerical modelling, there exist different kinds of material models. Depending on the material model chosen and in turn the drainage type used, there exist different types of analyses (Plaxis, 2018b). The most common analysis types are total stress analysis and effective stress analysis, respectively (Jamal, 2017).

The total stress analysis is used when the soil is considered to behave undrained, i.e. for short term conditions in low permeable soils. In total stress analysis the soil is assumed to be a one-phase material, and thus pore pressures, u, are not distinguished from the stresses. Therefore both total strength (c_u, ϕ=0, ψ=0) and total stiffness parameters (E_u, ν_u) are used (Jamal, 2017; Plaxis, 2018b). Even though c_u is an input value, the analysis does not give an increase or decrease in shear strength with time, as consolidation is not analyzed (Plaxis, 2018b). A further drawback with the total stress analysis is that the rate-dependent response of soil is not accounted for.

The effective stress analysis is used when the soil is considered to behave drained, i.e. for long-term conditions (Jamal, 2017). In effective stress analysis, u is accounted for, and changes in excess pore pressures are analyzed. Here, effective strength (c', ϕ', ψ'=0) and effective stiffness (E_{50}', ν') parameters are used (Jamal, 2017; Plaxis, 2018b). The development of excess pore pressures is used to obtain the effective stress path, ESP (Plaxis, 2018b). However, a drawback with the effective stress analysis is that the wrong undrained shear strength may be predicted, as it is based on the effective strength parameters. An advantage with the effective stress analysis is that an increase (hardening) or decrease (softening) of shear strength is accounted for. In Figure 3.10 the total stress path, TSP and ESP are illustrated.

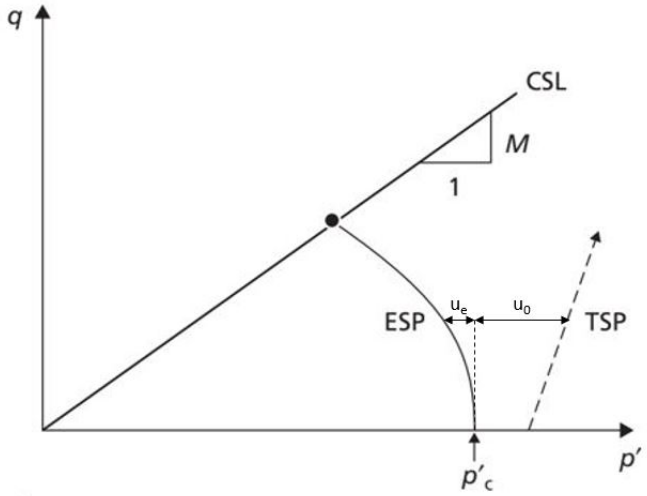

Figure 3.10: Illustration of TSP and ESP for NC clays (Knappet & Craig, 2012).

3.2.2 Small Strain Stiffness

Today, there is no existing constitutive model that accounts for all characteristics of Swedish soft clay, such as structure/destructuration, anisotropy (in elastic and plastic regions), small strain stiffness (and its degradation) and creep (T. Wood, 2016). However, T. Wood (2016) claims it to be necessary for the construction projects that are ahead in Sweden. The stiffness is the resistance to withstand deformations under applied force. Small strain stiffness is important since it has been shown that field stiffness is much larger than the one derived from laboratory tests, when looking at back-analysis of constructions, meaning that conventional laboratory tests underestimate soil stiffness (Clayton, 2011; Persson, 2004).

For urban excavations which are designed to be far from failure state, strains in the ground are small (Clayton, 2011). Clayton (2011) claims that especially for these cases, it is important to account for small strain stiffness to obtain more realistic ground movement predictions, as this can affect adjacent buildings or underlying structures. Small strains are considered to lie below $10^{-5}\%$, and to have an elastic behaviour with no plastic deformations (Persson, 2004; T. Wood, 2016). Skeletal stiffness of unconsolidated soil depends on the effective stress (Clayton, 2011). Therefore, for saturated soils, two different parameter sets may be needed; parameters for the "undrained" or "short-term" case and the "drained" or "long-term" case. For isotropic soil, the most common stiffness parameters can be seen in Table 3.1.

Table 3.1: Drained and undrained stiffness parameters (Clayton, 2011).

Case	Parameter set 1		Parameter set 2	
Undrained	Undrained Young's modulus, E_u	Undrained Poisson's ratio, ν_u	Shear modulus, G	Undrained bulk modulus, K_u
Drained	Effective Young's modulus, E'	Effective Poisson's ratio, ν'	Shear modulus, G	Drained bulk modulus, K'

Parameter set 1 can be obtained from a triaxial tests (assuming isotropy) (Clayton, 2011). Parameter set 2 is convenient as the shear modulus, G, is the same for the drained and the undrained case. The relationships between drained and undrained shear modulus, Young's modulus, Poisson's ratio and bulk modulus for assuming isotropic conditions can be seen in Equations (3.14)-(3.16).

$$G = \frac{E'}{2(1+\nu')} = \frac{E_u}{2(1+\nu_u)} \tag{3.14}$$

$$K' = \frac{E'}{3(1-2\nu')} \tag{3.15}$$

$$K_u = \frac{E_u}{3(1-2\nu_u)} \tag{3.16}$$

It is practical to consider stiffness parameters as constant at very small strains, but usually the stiffness reduces as strains increase above those levels (Clayton, 2011), see Figure 3.11.

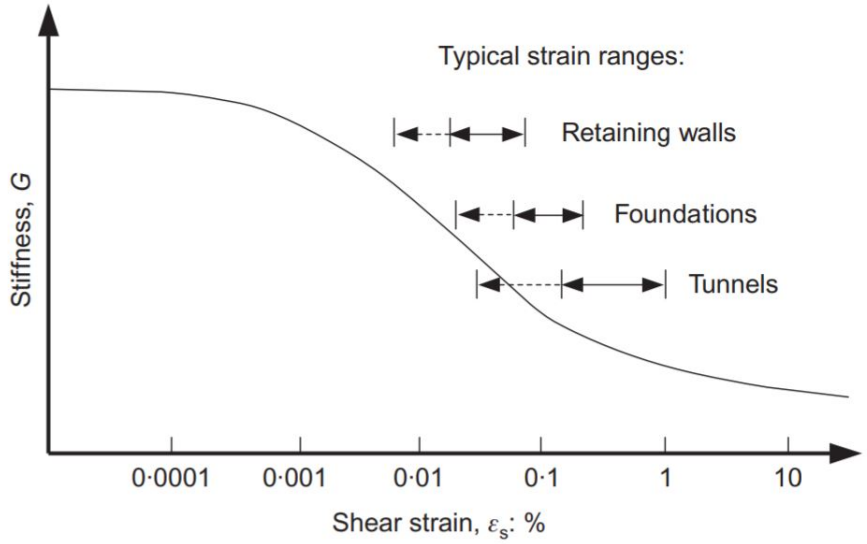

Figure 3.11: Strain ranges and stiffness variation for geotechnical structures (Clayton, 2011).

Strain levels around geotechnical structures like tunnels, foundations and retaining walls are generally small, which can be seen in Figure 3.11 (Clayton, 2011). To analyse this, both parameters at very small strain levels, preferably reference strains like G_0, and stiffness parameters are needed (Clayton, 2011; T. Wood, 2016). These can be obtained from field methods like seismic geophysical methods and laboratory tests such as triaxial apparatus with bender elements and resonant column tests. However, none of these methods are ideal, as they give different results since layering of the soil, the testing procedure and sample disturbance have an impact. Nevertheless, compared to field tests, laboratory tests can give a greater range of stiffness data. Laboratory tests could also be used to derive stiffness degradation with strain.

3.3 Creep-SCLAY1S Model

Creep-SCLAY1S is an advanced constitutive model which can be used in PLAXIS 2D or 3D. It originates from the elasto-plastic Modified Cam Clay model, MCC, but in addition includes anisotropy, destructuration, bonding and creep (rate-dependency), which all are important aspects to include when modelling natural soft clay (Grimstad et al., 2010; Karstunen & Amavasai, 2017). The model is an elastic-viscoplastic constitutive model, where the total strain rate can be described with Equation (3.17)-(3.20) (Karstunen & Amavasai, 2017; Leoni, Karstunen, & Vermeer, 2008). The total strain rate contains an elastic part based on Hooke's law, and an inelastic part that represents irreversible and time-dependent strains i.e. creep (Leoni et al., 2008).

$$\dot{\varepsilon} = \dot{\varepsilon}^e + \dot{\varepsilon}^c \tag{3.17}$$

where

$$\dot{\varepsilon}^e = \dot{\varepsilon}^e_p + \dot{\varepsilon}^e_q = \frac{\dot{p'}}{K} + \frac{\dot{q}}{3G} \tag{3.18}$$

and

$$\dot{\varepsilon}^c = \dot{\varepsilon}^c_p + \dot{\varepsilon}^c_q = \dot{\lambda}\frac{\delta p'_{eq}}{\delta p'} + \dot{\lambda}\frac{\delta p'_{eq}}{\delta q} \tag{3.19}$$

where $\dot{\lambda}$ is the visco-plastic multiplier

$$\dot{\lambda} = \frac{\mu^*_i}{\tau}\left(\frac{p'_{eq}}{p'_m}\right)^{\beta}\left(\frac{M_c^2 - \alpha_0^2}{M_c^2 - \eta^2_{K0}}\right) \quad \text{where} \quad \beta = \frac{\lambda^*_i - \kappa^*}{\mu^*_i} \tag{3.20}$$

The Creep-SCLAY1S model is able to model reliable stress strain behaviour for natural clays which are NC or slightly OC and is therefore suitable for modelling Gothenburg clay, see for example Dijkstra, Karstunen, Gras, and Karlsson (2015); Karstunen and Amavasai (2017). Since Creep-SCLAY1S considers creep effects it

is also suitable for modelling deformations in urban environments, especially the long-term performance can be analyzed (Karstunen & Amavasai, 2017). In contrast to elasto-plastic models, Creep-SCLAY1S does not have a conventional yield surface since it does not have a purely elastic region. Instead of a yield surface the model has a Normal compression surface, NCS, which is the transition between small and large irrecoverable creep strains, and is defined by the preconsolidation pressure (Amavasai et al., 2018). The NCS for Creep-SCLAY1S is visualized in general stress space in Figure 3.12. Equation (3.21) shows the equation for NCS in triaxial space (Karstunen & Amavasai, 2017).

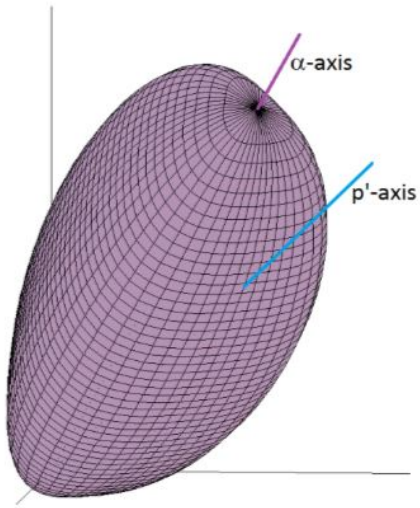

Figure 3.12: Illustration of 3D reference surface for the Creep-SCLAY1S model (Sivasithamparam, 2012).

$$f_{NCS} = (q - p')^2 - (M(\theta)^2 - \alpha^2)[p'_m - p']p' = 0 \tag{3.21}$$

Since the model does not include any consistency condition it is possible to go outside the NCS. Although, the "price" for going outside the NCS is large permanent strains. Except the NCS there are two more reference surfaces (which are defined in the triaxial space): the Current state surface, CSS, and the Intrinsic compression surface, ICS. All reference surfaces for Creep-SCLAY1S are illustrated in the triaxial space in Figure 3.13 d). Figure 3.13 also includes the yield surfaces for the "predecessors" (MCC, SCLAY1 and SCLAY1S) (a-c) of Creep-SCLAY1S, in order to visualize what happens with the yield surface when adding anisotropy, bonding/destructuration and rate-dependency. 3.13 a) represents the yield surface of the MCC model, which is the simplest of the models, assuming isotropic behaviour, and as can be seen the surface is symmetric around the p'-axis. In contrast to the MCC model, S-CLAY1 model includes anisotropy which can be seen by the inclined surface. In the S-CLAY1S model, the bonding and destructuration is also included, which relates to the appearance of the ICS.

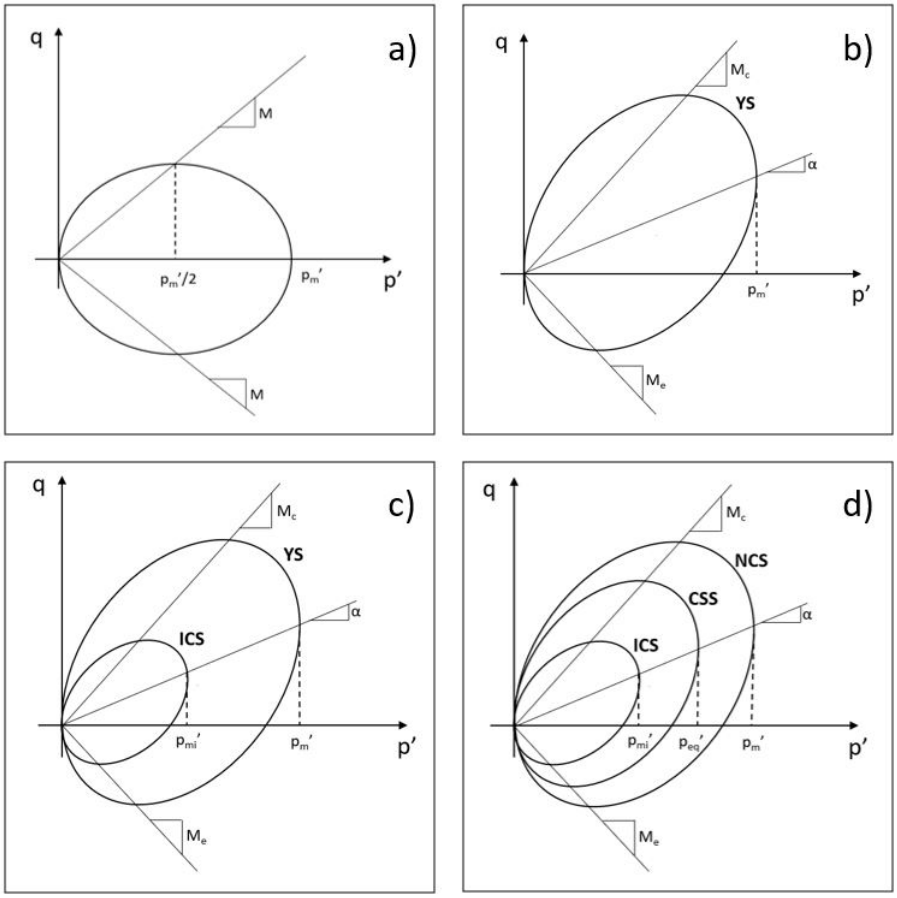

Figure 3.13: Illustration of yield and reference surfaces.
a) MCC, **b)** S-CLAY1, **c)** S-CLAY1S, **d)** Creep-SCLAY1S

Since Creep-SCLAY1S accounts for many aspects of soft clay behaviour, it involves many parameters, which are not always straight forward to derive or calibrate. Therefore, the following sections will present the input parameters and their meaning. In Table 3.2 all input parameters to the model are summarized.

Table 3.2: Input parameters to the Creep-SCLAY1S model (Amavasai et al., 2018).

Type	Parameters	Symbol	Required tests
Initial stress parameters	Apparent preconsolidation pressure	σ'_c	Oedometer IL (alt. CRS test)
	Lateral earth pressure at rest for NC state	K_0^{NC}	See eq. (3.22)
	Lateral earth pressure at rest	K_0	See eq. (3.23)
	Overconsolidation ratio	OCR	Oedometer IL test
	Pre-overburden pressure	POP	Oedometer IL test
	(Inital void ratio	e_0	Oedometer IL test)
Conventional parameters	Poisson's ratio	ν'	Triaxial test
	Modified intrinsic compression index	λ_i^*	Oedometer IL (alt. CRS test)
	Modified swelling index	κ^*	Oedometer IL (alt. CRS test)
	Stress ratio at critical state in triaxial compression	M_c	Triaxial compression test
	Stress ratio at critical state in triaxial extension	M_e	Triaxial extension test
Anisotropic parameters	Initial anisotropy	α_0	See eq. (2.6)
	Absolute effectiveness of rotational hardening	ω	Triaxial extension test
	Relative effectiveness of rotational hardening	ω_d	See eq. (2.7)
Bonding and Destructuration parameters	Initial bonding	χ_0	Estimated from sensitivity
	Absolute rate of destructuration	ξ	Back calculated from CRS and Triaxial tests
	Relative rate of destructuration	ξ_d	Back calculated from CRS and Triaxial tests
Creep parameters	Modified intrinsic creep index	μ_i^*	Oedometer IL (creep) test
	Reference time (days)	τ	Average time step used in Oedometer tests

3.3.1 Parameters

In this section the input parameters for the Creep-SCLAY1S model are presented.

3.3.1.1 Initial Stress Parameters

The apparent preconsolidation pressure, σ_c', is an important parameter in geotechnical design as it distinguishes the elastic and reversible deformations from the inelastic and partially irreversible deformations (Yang, Jia, Liu, & Shan, 2009). It also indicates the point where high compressibility of the soil starts. As OCR and POP depend on this parameter and are input parameters into the Creep-SCLAY1S model, it is crucial to estimate the preconsolidation pressure correctly (Karstunen & Amavasai, 2017). In addition to this, the model response is very sensitive to those parameters, adding to its importance. When retrieving the preconsolidation pressure from laboratory tests, the value obtained also depends on the strain rate used, as higher strain rates result in a higher preconsolidation pressure. Therefore, it is not advised to use constant rate of strain, CRS, tests for this model. Thus, incremental load, IL, Oedometer tests are needed. The OCR and POP are calculated using the in-situ vertical effective stress, σ_v', together with the apparent preconsolidation pressure.

The coefficient of lateral earth pressure at rest for the NC state, K_0^{NC}, and for the OC state, K_0, are retrieved with equation (3.22) and (3.23), respectively (Karstunen, Krenn, Wheeler, Koskinen, & Zentar, 2005).

$$K_0^{NC} = 1 - \sin\phi'_{cv} \quad \text{(Jaky's formula)} \tag{3.22}$$

$$K_0 = (1 - \sin\phi'_{cv})\, OCR^{\,\sin\phi'_{cv}} \tag{3.23}$$

where ϕ'_{cv} is the friction angle at critical state. K_0 is valid during expansion and not recompression (Karstunen & Amavasai, 2017).

Another method of estimating K_0 proposed by Larsson et al. (2007) is presented in Equation (3.24)-(3.25).

$$K_0 = K_0^{NC} OCR^{0.55} \tag{3.24}$$

where

$$K_0^{NC} = 0.31 + 0.71(w_L - 0.2) \tag{3.25}$$

This relationship is empirical, and is like most such relationships for clays, based on the liquid limit, w_L (Larsson et al., 2007). The liquid limit is often used as a general measure of the influence of for example clay minerals, depositional environment, chemistry of pore water at deposition and changes in it. Therefore, it is of importance to use this empirical relationship only on soils with as similar as possible properties as the soil used in the retrieval of the empirical relationship. In this case, the relationship in Equation (3.24)-(3.25) is only valid for homogeneous clay layers with properties representative for Swedish clays.

The initial void ratio, e_0, is not an required input parameter to the model, but is needed in consolidation analysis if taking account for change in permeability, k, as a function of change in void ratio (Karstunen & Amavasai, 2017).

3.3.1.2 Conventional Parameters

The Creep-SCLAY1S model uses similar parameters to the ones used in the MCC model (Sivasithamparam et al., 2015). Among them are Poisson's ratio, ν', stress ratio at critical state, M, modified compression index, λ^*, and modified swelling index, κ^*. One difference is that this model uses the modified intrinsic compression index, λ_i^* instead (Karstunen & Amavasai, 2017). It is derived in the same way as λ^*, but with reconstituted clay preferably. If reconstituted clay is not available, IL Oedometer tests on natural clay at a high strain level enough to destroy all effects of apparent bonding can be used. For clarification of Swedish conventional designation and the modified swelling and compression indices, see Figure 3.14.

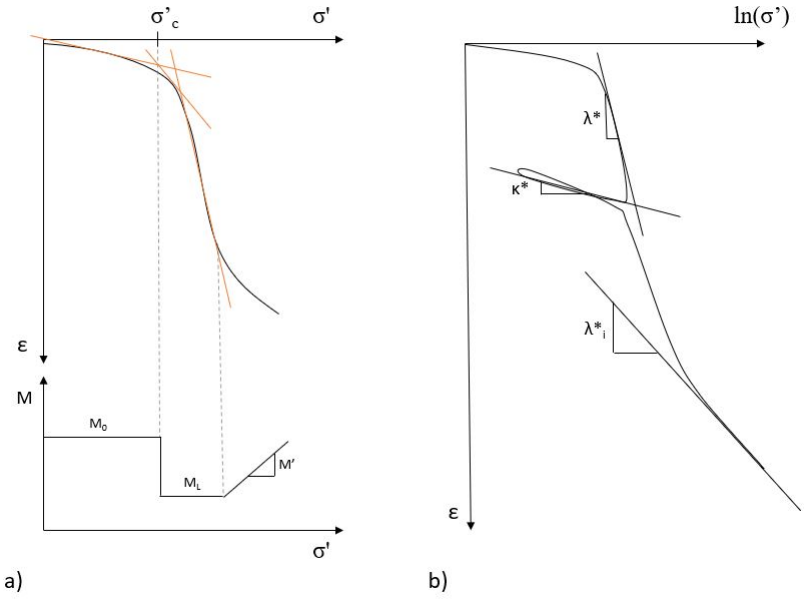

Figure 3.14: Relation between different swelling and compression parameters. **a)** Swedish designation **b)** Creep-SCLAY1S

The stress ratio at critical state, M, is defined for triaxial compression, M_c, and for triaxial extension, M_e (Karstunen & Amavasai, 2017). Incorporating Lode angle dependency, gives a smooth yield surface as opposed to the Mohr-Coulomb failure surface (Sivasithamparam, 2012). By using a Lode angle dependent yield surface, corners are avoided and numerical computations are made easier. In Figure 3.15, the Lode angle dependency is shown for different m-values. The m-value is the ratio between M_e and M_c, where m=1 corresponds to the Drucker-Prager failure criterion (used in the MCC model without α_0-inclination/anisotropy).

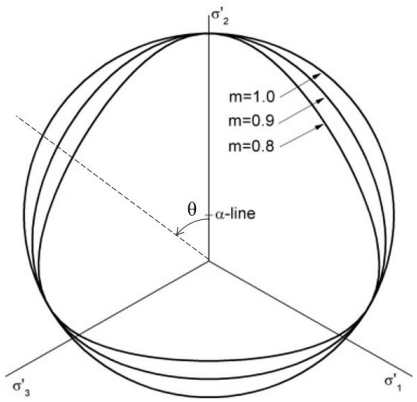

Figure 3.15: Illustration of Lode angle dependency in π-plane (Sivasithamparam et al., 2015).

Including M_e allows for more accurate predictions when modelling unloading situations. Equation (3.26) and (3.27) show how to determine M_c and M_e from ϕ'_{cv} (D. M. Wood, 1990).

$$M_c = \frac{6 \sin \phi'_{cv}}{3 - \sin \phi'_{cv}} \tag{3.26}$$

$$M_e = \frac{6 \sin \phi'_{cv}}{3 + \sin \phi'_{cv}} \tag{3.27}$$

where ϕ'_{cv} is derived from compression respectively extension tests.

If no triaxial extension tests are conducted, M_e can be redeemed from Equation (3.28), using the friction angle at critical state in compression, ϕ'_c, i.e. for Mohr Coulomb failure (Karstunen & Amavasai, 2017). However, this would likely underestimate M_e.

$$\sin \phi'_c = \frac{3M_e}{6 - M_e} \tag{3.28}$$

3.3.1.3 Anisotropic Parameters

In natural clays the anisotropy is an important aspect to consider when modelling the response of loading (Grimstad et al., 2010). The anisotropy in clay is a result of the shape of clay particles, the process of deposition and the history of consolidation (Karstunen & Koskinen, 2008). In Creep-SCLAY1S the initial anisotropy of the soil is described by the parameter α_0, which corresponds to the inclination of the reference surface, see Figure 3.13 (Karstunen & Amavasai, 2017). If assuming that the soil mainly has been exposed to one dimensional consolidation, resulting in close to NC clay and horizontal layering, the initial anisotropy could be estimated with Jaky's formula resulting in an α_0 according to Equation (3.29) (Leoni et al., 2008).

$$\alpha_0 = \frac{\eta_{K0}^2 + 3\eta_{K0} - M_c^2}{3} \quad \text{where} \quad \eta_{K0} = \tfrac{3M_c}{6-M_c} \tag{3.29}$$

If the soil is subjected to plastic straining, the initial anisotropy will be changed which is represented by change of the inclination/position of the reference surface. The change in position of the reference surface is determined by so called rotational hardening laws (Sivasithamparam et al., 2015). In Creep-SCLAY1S, the evolution of anisotropy is represented by the parameters ω (rate of rotation) and ω_d (rate of rotation due to deviatoric stress) (Karstunen & Amavasai, 2017). ω_d and ω can be estimated with Equation (3.30) and (3.31), respectively. Even though it is possible to estimate ω, it will require calibration against laboratory test data.

$$\omega_d = \frac{3}{8}\frac{(4M_c^2 - 4\eta_{K0}^2 - 3\eta_{K0})}{(\eta_{K0}^2 - M_c^2 + 2\eta_{K0})} \tag{3.30}$$

$$\omega \approx \frac{1}{(\lambda_i^* - \kappa^*)}\, ln\left(\frac{10M_c^2 + 2\alpha_0\,\omega_d}{M_c^2 + 2\alpha_0\,\omega_d}\right) \tag{3.31}$$

3.3.1.4 Bonding and Destructuration Parameters

The bonding between the clay particles and the degradation of bonding are also important effects to consider when studying the response of clay (Grimstad et al., 2010). The interparticle bonding for a natural soil (initial bonding) is dependent on the composition of minerals and porewater when the soil was deposited (Karstunen et al., 2005). The bonding gives additional strength/resistance to the soil and allows for a higher void ratio during deposition. However, when the soil is exposed to plastic straining, the particles will slip and rearrange which will cause degradation of bonding, i.e. the process called destructuration (Karstunen et al., 2005). If the soil is sensitive enough, and if the rate of destructuration is larger than the rate of plastic straining, the soil could exhibit a loss in shear strength during compression (Karstunen et al., 2005). An example where the effects of destructuration can be seen is presented in Figure 3.16.

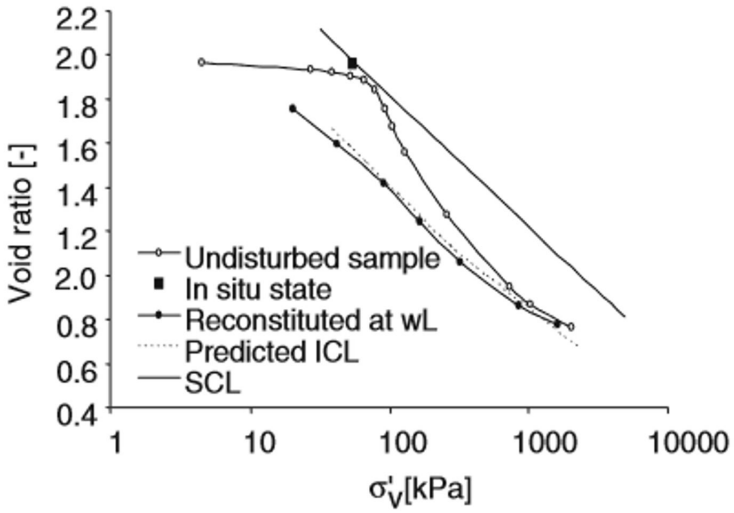

Figure 3.16: Effect of destructuration (Grimstad et al., 2010).

To model the bonding and the destructuration, Creep-SCLAY1S has three parameters: χ_0, ξ and ξ_d (Karstunen & Amavasai, 2017). χ_0 is the initial bonding and can be estimated with the sensitivity of the soil, see Equation (3.32).

$$\chi_0 = S_t - 1 \tag{3.32}$$

The destructuration (degradation of bonding) is calculated with Equation (3.33), where ξ and ξ_d are constants which need to be calibrated against laboratory tests (Karstunen & Amavasai, 2017). As can be seen in Equation (3.33), the destructuration is dependent on both volumetric and deviatoric strain. Further, the constant ξ represents the absolute rate of destructuration and ξ_d represents destructuration linked to the deviatoric viscoplastic strain (Sivasithamparam et al., 2015).

$$\Delta\chi = -\xi\chi\left[|\Delta\varepsilon_p^c| + \xi_d\left(\Delta\varepsilon_q^c\right)\right] \tag{3.33}$$

3.3.1.5 Creep Parameters

In order to model rate-dependency, Creep-SCLAY1S incorporates the parameters μ_i* and τ (Karstunen & Amavasai, 2017). The modified intrinsic creep index, μ_i*, is derived in the same way as the modified creep index, μ*, for the Soft Soil Creep model, i.e. from a particular stress increment stage in an IL Oedometer test, see Figure 3.17.

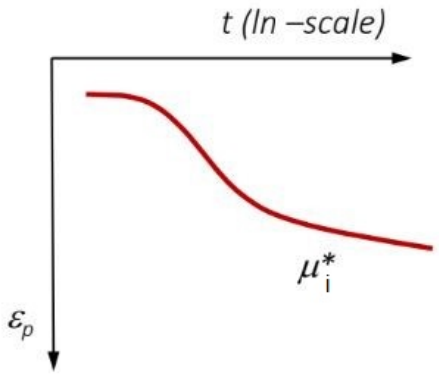

Figure 3.17: Definition of modified creep index (Karstunen & Amavasai, 2017).

μ_i* is related to "pure" creep as all bonding is destroyed by using either a reconstituted sample, or doing the test using a high enough stress level to destroy all bonding (Karstunen & Amavasai, 2017). A parameter that is related to μ_i* is the intrinsic time resistance number, r_{si}, which is a more common parameter in Swedish practice (Olsson, 2013). Equation (3.34) describes the relationship further.

$$r_{si} = \frac{1}{\mu_i^*} \tag{3.34}$$

Furthermore, the reference time, τ, is related to the duration of a load step in the IL Oedometer test, which gives the apparent preconsolidation pressure (Amavasai et al., 2018).

3.4 NGI-ADP Model

The Creep-SCLAY1S model is the main focus of this thesis, and therefore the NGI-ADP model is just briefly described. For more detailed information see Grimstad et al. (2012); Plaxis (2018a). The NGI-ADP model is a total stress based elasto-plastic constitutive model suited for undrained behaviour of clay and modelling undrained loading (Grimstad et al., 2012). There is a direct input of undrained shear strength as opposed to Creep-SCLAY1S that is effective stress based. The model also accounts for anisotropy of undrained shear strength and stiffness.

Within geotechnical engineering, isotropic undrained shear strength is represented by Tresca's yield criterion i.e. a hexagonal prism in 3D principal total stress space (Grimstad et al., 2012). To account for differences in undrained shear strength in compression and extension, the NGI-ADP model uses a modified Tresca criterion. More precise it uses the Tresca approximation after Billington (1988) in combination with von Mises plastic potential function (Mises, 1913), see Figure 3.18. This avoids possible corner problems for numerical calculations. The plastic potential and yield function in this model are independent of mean stress, and thus no volumetric strains develop. The plastic potential and yield functions in this model are not strictly isotropic hardening plasticity and thus increased mobilization changes the shape of the yield curve.

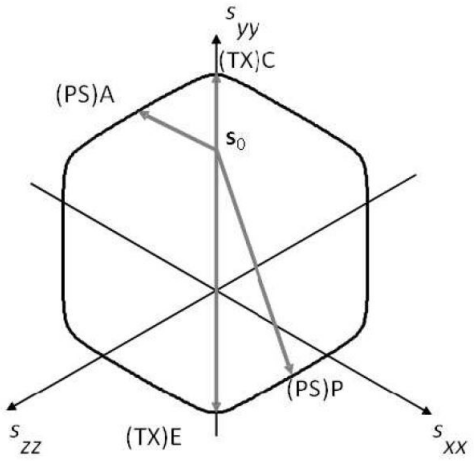

Figure 3.18: Failure criterion for the NGI-ADP model (Grimstad et al., 2012).

The NGI-ADP model accounts for differences in failure shear by using a non-linear stress path dependent relationship for hardening from direct input of failure strains in three directions of shearing: triaxial compression ($\alpha = 0°$), direct simple shear ($\alpha \approx 30°$) and triaxial extension ($\alpha = 90°$) (Grimstad et al., 2012). These are translated to the design profile of undrained shear strength, i.e. active (A), direct simple shear (D) and passive (P) modes of loading.

3.5 Sample Disturbance

In order to make a good prediction of soil stability and deformations, it is important to obtain reliable test data. However, when the soil is extracted from the ground, transported, stored and prepared for the test, the soil will be disturbed, which will give parameters differing from the in-situ soil conditions (DeGroot, Poirier, & Landon, 2005). The degree of disturbance will depend on which sampling method that is used and how the sample is handled, but will also depend on the characteristics of the soil. Soils that are extra sensitive to sample disturbance are clays with low plasticity, low OCR and a high level of structure (T. Wood, 2016). Examples of such soils are Scandinavian soft clays, where problems with sample disturbance have been noticed for a long time (T. Wood, 2016). The sample disturbance will affect important design parameters such as stiffness and strength, more specific, disturbance tends to reduce the preconsolidation pressure and the initial stiffness, while it tends to increase the post yield stiffness (T. Wood, 2016). A visualization of how a disturbed sample could differ from in-situ conditions can be seen in Figure 3.19.

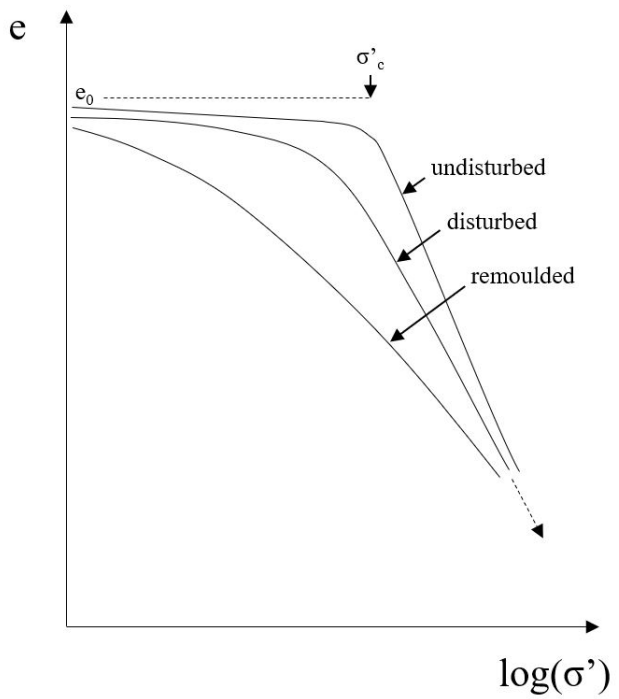

Figure 3.19: Effect of sample disturbance (Karstunen & Amavasai, 2017).

One major influence on sample quality is the sampling method. The sampling method which is considered to give least disturbance is block sampling. However, this is a time consuming and expensive method, and therefore the method most commonly used in Sweden for soft clays is piston sampling (STI & STII) (T. Wood, 2016). The accuracy with piston samplers, and other samplers as well, could be improved with larger diameter in order to reduce effects from friction and influence of small stones and shells etc (Lanzky & Palmquist, 2015). In Figure 3.20, two examples of the difference between block sampling and piston sampling can be seen.

Results from Karlsson et al. (2015) have shown that the largest disturbance due to sampling technique will occur at small strains, approximately around 0-2% axial strain, which can be distinguished in Figure 3.20.

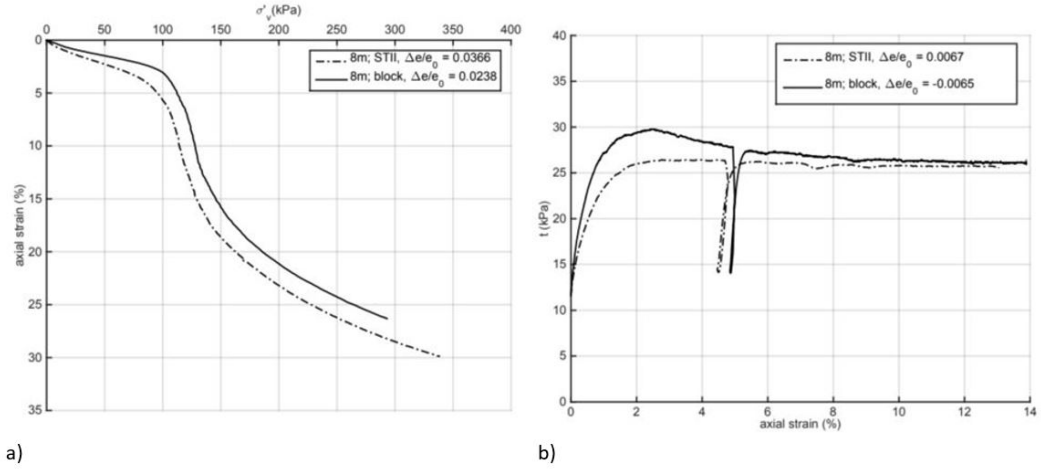

Figure 3.20: Example of comparison of block and piston sampling (Karlsson et al., 2015).
a) CRS **b)** CADC

Even though the sampling technique is an important factor for the quality, it is also important to consider the influence of the remaining disturbance chain, also known as secondary disturbance (T. Wood, 2016). For instance the humidity, temperature and storage time could affect the structure of the clay and hence the laboratory tests will produce unreliable stress-strain responses. Furthermore, depending on which test type or under which conditions the test is performed, the response will be different. In Figure 3.21, the effect of different strain rates and temperatures is illustrated.

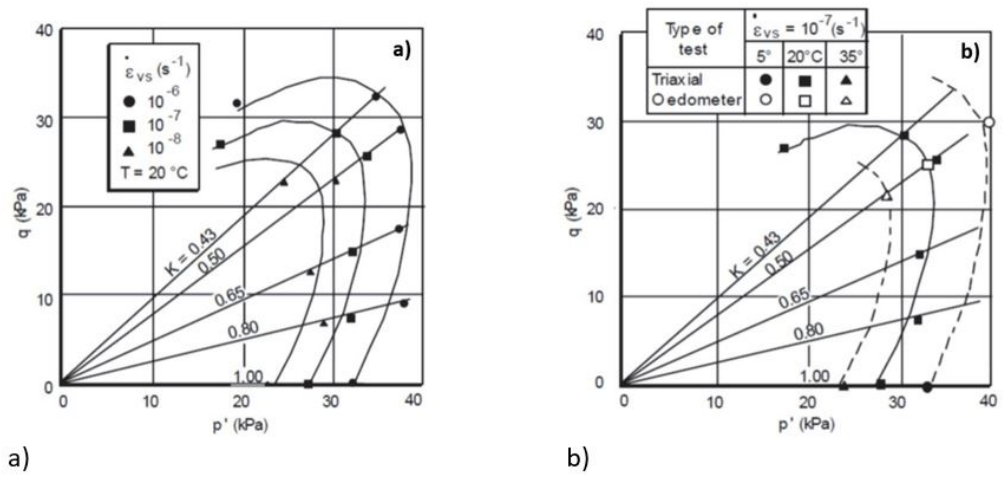

Figure 3.21: Effect of different test conditions (Leroueil, 2006).
a) Strain rate, **b)** Temperature

In order to decrease the influence of sample disturbance, and hence increase the accuracy of the predictions, there exist several methods to classify how disturbed a sample is. One method, introduced by Andresen and Kolstad (1979), is based on evaluating volumetric strain, ε_p, from laboratory tests. For the Oedometer test and the triaxial compression test, the volumetric strain is evaluated for the assumed σ'_{v0} (also σ'_{h0} for triaxial) (Terzaghi et al., 1996). The classification system is called Specimen quality designation, SQD, and the different classes/intervals can be seen in Table 3.3.

Another method, introduced by Lunne et al. (1997), is based on estimating the volume change from a relative void ratio. The relative void ratio, $\Delta e/e_0$, is calculated by dividing the void ratio change by the in-situ void ratio. The void ratio change, Δe, is determined from the change in void ratio during consolidation/compression until σ'_{v0} is reached, while e_0 is determined from the natural water content in the sample. The rating for the relative void ratios can be found in Table 3.3.

Table 3.3: Assessment of sample quality using volumetric strain and void ratio change (Lunne et al., 1997; Terzaghi et al., 1996).

Sample quality assessment with volumetric strain		**Sample quality assessment with normalized void ratio change**	
ε_p [%]	**SQD**	$\mathbf{\Delta e/e_0}$ **for** $OCR =$ **1-2**	**Rating**
< 1	A	< 0.04	Very good to excellent
1 - 2	B	0.04 - 0.07	Good to fair
2 - 4	C	0.07 - 0.14	Poor
4 - 8	D	> 0.14	Very poor

Further, there is another method introduced by Larsson et al. (2007) based on the work done by Lunne et al. (1997). This method uses the value of volumetric strain, ε_p, together with the natural water content, w_N. The sample quality is retrieved according to Figure 3.22.

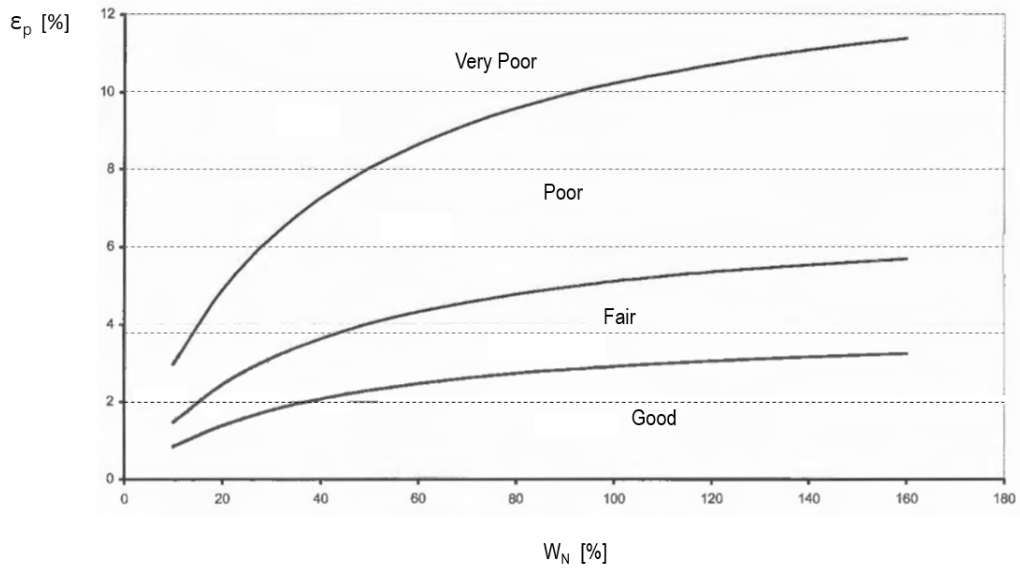

Figure 3.22: Assessment of sample quality using volumetric strain change and natural water content (Larsson et al., 2007).

4

Technical Specifications

In this chapter, more specific information concerning the excavation, soil conditions, retaining structure and the used numerical model design are presented. In Figure 4.1 the geometry of the excavation and the analyzed section is shown. In total, the excavation occupies an area of around 1000 m^2 and is as deepest 7 m in the south part and as shallowest 2 m in the northern part. The studied section is appropriate for analysis in Plaxis 2D since plane strain can be used for approximation. Figure 4.1 also shows the main boreholes used for the parameter extraction, presented in Section 4.1.

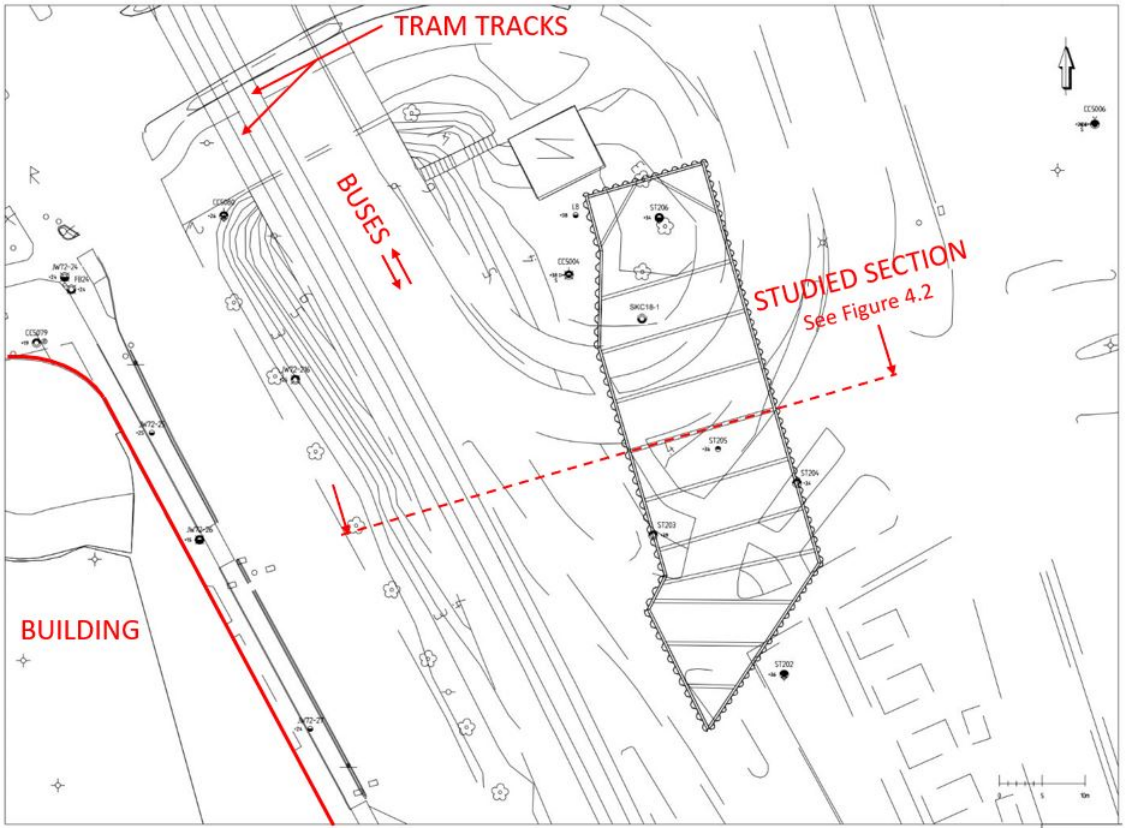

Figure 4.1: Overview of the studied section and main boreholes.

As stated before, the excavation is located in an urban area which means that the existing structures and the excavation could affect each other. The surrounding structures which are in close connection to the excavation are road embankments on both sides of the excavation and wooden piles beneath the road embankment which

is used for trams and buses, see Figure 4.1. Due to the closeness of these structures they are included in the numerical model. For clarity, the analyzed section with these structures together with the finalized excavation and ramp can be seen in Figure 4.2.

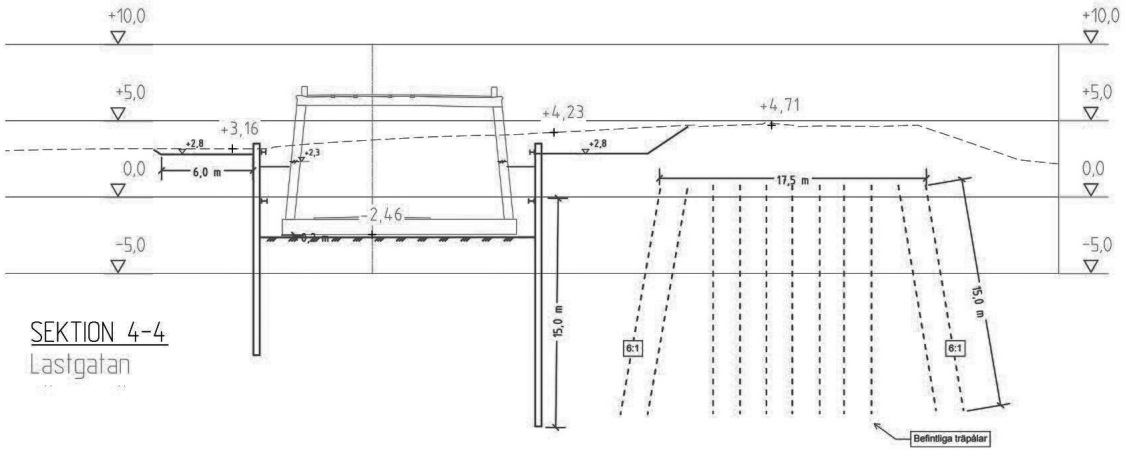

Figure 4.2: The studied section showing the finished construction as well as a road embankment with existing wooden piles beneath.

The piles beneath the embankment (to the right in Figure 4.2) are approximately 15 m long, starting from level +0 or -1 m. Further, the embankment consists of gravel and there are no indications of load distributing layers in connection to the piles.

4.1 Soil Profile and Properties

Since the input data is crucial in order to get reliable results, a lot of effort was put into retrieving the soil profile and the soil properties. In this section this iterative process is described. Figure 4.3 presents the methodology for obtaining the soil profile and the soil properties which are used as input to the numerical model.

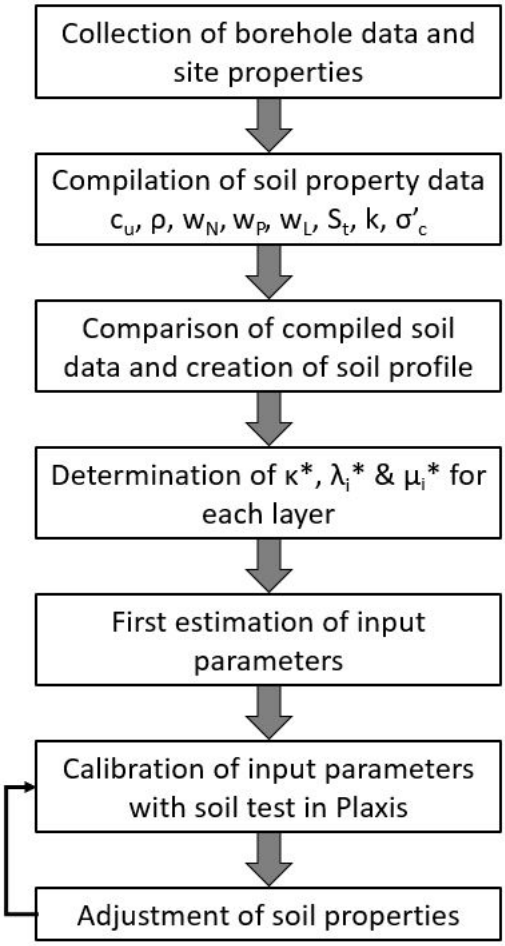

Figure 4.3: Methodology for retrieving soil profile and parameters.

The data about the site properties (thickness of clay deposit, depth to bedrock, ground level and level of water table) was retrieved from site investigations for the Hisings bridge project, provided by Skanska Teknik. As mentioned before, the Hisings bridge project is the project which includes the studied excavation. Data related to the properties of the soil was also retrieved from borehole data for the Hisings bridge project. In order to get a wider perspective and to retrieve values for the deeper parts of the soil deposit, borehole data from the West Link project and Regionens hus project were also used. In total 25 boreholes were used for analysis. The data compiled was c_u, ρ, w_N, w_P, w_L, S_t, k and σ'_c. The compiled data was then compared in order to determine the soil layering and then parameters for every layer were determined. The data from boreholes closer to the excavation were weighted higher. As the OCR is a very important input parameter for the Creep-SCLAY1S

model it was also considered when creating the soil layering. The parameters which were most influential when creating the soil profile were c_u, ρ, w_N and σ'_c, while w_P, w_L, S_t and k were used to verify the position of the assumed soil layers. The plots for all these parameters, including test type, can be found in Figure B.1-B.7 in Appendix B. The chosen soil profile along with the selected parameters is presented in Figure 4.4.

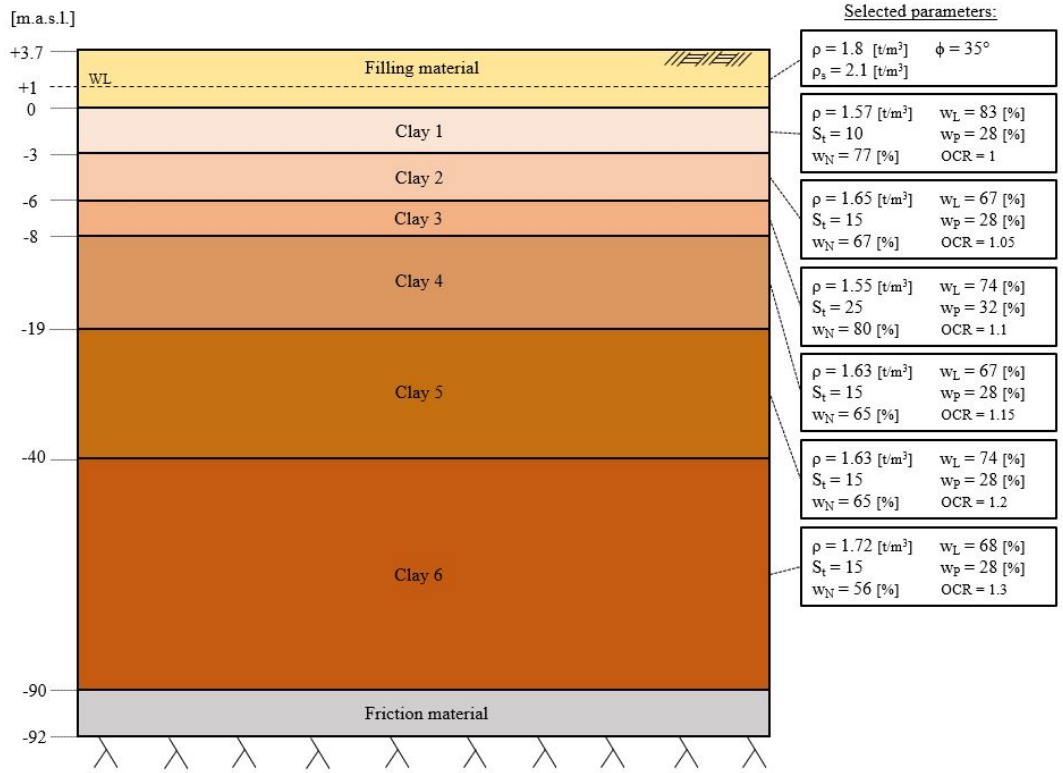

Figure 4.4: Soil profile with properties.

After determining the layering, the "model-specific" parameters κ^*, λ_i^*, μ_i^* and ϕ'_{cv} were determined for each layer. The parameters κ^*, λ_i^* were determined by evaluating 15 CRS and 6 IL Oedometer tests. The CRS tests used were retrieved from 6-20 m depth while the IL Oedometer tests were retrieved from 7-20 m depth. The parameter μ_i^* was determined solely from the IL Oedometer tests. The methodology used for retrieval of κ^*, λ_i^*, μ_i^* is presented in Section 3.3.1. The parameter ϕ'_{cv} was determined from the triaxial tests, both for compression (4 tests) and extension (3 tests). All tests used for determination of κ^*, λ_i^*, μ_i^* and ϕ'_{cv} were performed by Skanska in the laboratory at Chalmers. Further, all tests were executed on clay from borehole SKC18-1, which is located in the studied section. Before assigning each layer these "model-specific" parameters, an estimation of the sample quality was done. The assessment was done according to the methods presented in Section 3.5. For the CRS tests the methods according to Andresen and Kolstad (1979) and Larsson et al. (2007) were used and for the IL Oedometer tests, the method according to Lunne et al. (1997) was used. The sample quality assessment for the IL Oedometer tests and CRS tests can be seen in Table C.2-C.3 in Appendix C. The sample quality assessment shows that the IL Oedometer tests are of better

quality than the CRS tests. The IL Oedometer tests were therefore weighted higher when choosing parameters for the layers. The triaxial tests were, based on measured axial strain during consolidation stage, assumed to be of good enough quality as well.

When all parameters from laboratory tests were assigned to each layer, the rest of the parameters needed for using the Creep-SCLAY1S model were calculated according to the equations presented in Section 3.3. The first setup of input parameters can be seen in Table C.1 in Appendix C. This setup was then used as input in the soil test function in Plaxis 2D. The calibration was done with triaxial compression and extension tests (level -5.2, -8.2 and -16.1 m), IL Oedometer tests (level -4.1, -7.1 and -17 m) and CRS tests (level -4.1, -7.1 and -16 m). When changing parameters to match the behaviour in the real laboratory tests, certain parameters were changed more than others.

One of the most significant changes from the initial parameter setup is the increase of κ^*, which is motivated by the effect of sample disturbance (discussed in Section 3.5). With other words, κ^* is usually underestimated as small strain stiffness is difficult to estimate due to sample disturbance. λ_i^* was also increased for all layers and set to the same value, as the clay is assumed to have the same mineralogy. It might be contradictory to change the intrinsic parameters since sample disturbance does not have much impact on remoulded tests, although it was evident that the λ_i^* needed to be increased. However, μ_i^* was not changed. Parameters dependent on ϕ'_{cv} (K_0^{NC}, ω_d, M_e and M_c) were not altered or just altered slightly. Also, χ_0 and the OCR were not changed when calibrating. Other parameters which were changed are ω, ξ and ξ_d. ω is stated to only be an estimate which might need calibration while ξ and ξ_d are parameters that are supposed to be calibrated to fit the laboratory tests as good as possible, and are therefore expected to be changed. All final results from soil tests can be seen in Figure D.1-D.9 in Appendix D. The parameter calibration against laboratory tests was only done for depths in Clay 2 - Clay 4. Therefore, Clay 1 is assumed to have similar properties as Clay 2 based on the borehole data, except γ, OCR, k and S_t. In the same way Clay 5 and Clay 6, have similar properties as Clay 4, except γ, OCR and k. The final chosen input parameters can be seen in Table 4.1.

Table 4.1: Chosen parameters.

Parameter	Unit	Clay 1	Clay 2	Clay 3	Clay 4	Clay 5	Clay 6
γ	kN/m^3	15.4	16.2	15.2	16	16	16.9
k	m/s	1.2E-9	0.7E-9	2.1E-9	1.2E-9	0.8E-9	0.5E-9
ϕ'_c	°	35	35	34.3	34.5	34.5	34.5
K_0	-	0.5	0.5	0.5	0.5	0.5	0.5
K_0^{NC}	-	0.43	0.43	0.44	0.44	0.44	0.44
OCR	-	1	1.05	1.1	1.15	1.2	1.3
ν'	-	0.15	0.15	0.15	0.15	0.15	0.15
κ^*	-	0.019	0.019	0.014	0.014	0.014	0.014
λ_i^*	-	0.072	0.072	0.072	0.072	0.072	0.072
M_c	-	1.42	1.42	1.39	1.4	1.4	1.4
M_e	-	1.1	1.1	0.96	1.06	1.06	1.06
α_0	-	0.55	0.55	0.53	0.53	0.53	0.53
ω	-	55	55	55	60	60	60
ω_d	-	0.96	0.96	0.94	0.94	0.94	0.94
χ_0	-	9	14	24	14	14	14
ξ	-	12	12	11	11.5	11.5	11.5
ξ_d	-	0.25	0.25	0.3	0.35	0.35	0.35
μ_i*	-	1.9E-3	1.9E-3	2E-3	1.5E-3	1.5E-3	1.5E-3
τ	days	1	1	1	1	1	1

It should also be mentioned that K_0 was taken from the automatic calculation in Plaxis 2D based on the input of K_0^{NC} into the software, and automatically no K_0 value beneath 0.5 was used. However these values (which are estimated with Jaky's formula) seem to be a bit low for Gothenburg clay. Therefore, the sensitivity of changes in K_0 has been investigated through comparison with values obtained with the method presented by Larsson et al. (2007), see Section 3.3.1.1. For the results from the sensitivity analysis, see Section 5.3.

4.2 Numerical Modelling of Excavation

The numerical modelling of the excavation is done with Plaxis 2D (FEM analysis) assuming plane strain conditions. In this section the model design properties are presented. Since the model design using Creep-SCLAY1S is based on the NGI-ADP model design created by Skanska Teknik, both model set-ups are presented here.

4.2.1 Existing Contractor Design with NGI-ADP

Originally, the NGI-ADP model design created by Skanska Teknik was 100 m wide and 45 m thick. As the NGI-ADP model does not incorporate consolidation nor rate-effects, the full thickness of the clay deposit was not necessary to include. However, in order to make comparisons with the predictions from the Creep-SCLAY1S model (which includes consolidation and rate-effects) the original geometry of the NGI-

ADP model design was altered. The whole model was therefore expanded to be 180 m wide and 95 m thick (before the construction of the existing embankment), to include the entire clay deposit. Figure 4.5 shows the geometry and included elements of the modified contractor's NGI-ADP model design. Further, the soil profile in this model consists of three clay layers. The first ranging from level 0 m to -3 m, the second from level -3 m to -25 m, and the third from level -25 m down to the friction material (-90 m). More specific information about the properties of the clay layers can be found in Table C.4 in Appendix C. On top of the clay deposit, there is filling material ranging from level +3.7 m to 0 m. The embankment lies on the filling material and has a maximum height at level +4.8 m. Both the filling material and the embankment are modelled as Mohr-Coulomb materials. For more information about the filling material and the embankment, see Table C.5 in Appendix C.

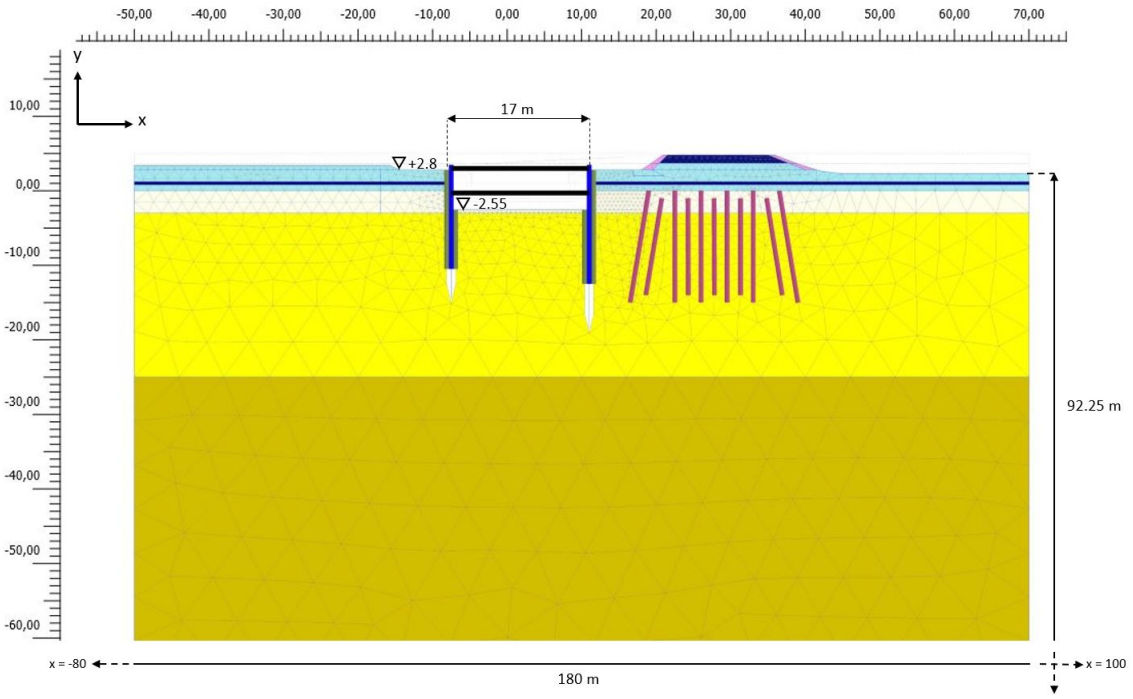

Figure 4.5: Section of NGI-ADP model design in Plaxis 2D.

The wooden piles are modelled as embedded piles, and are approximately 15m long, while the sheet pile walls, SPW, are modelled as elasto-plastic. The SPW on the east side of the excavation has a PU12 profile and is 14 m long. As deformations were crucial to minimize, considering the embankment, the SPW on the west side has an AU23 profile and is 16 m long. The struts are modelled as an elastic material and have circular hollow section, CHS, profiles on both levels (y=+3 m and y=-0.3 m, respectively). For more detailed information about the structural entities, see Table C.6-C.7 in Appendix C. More specific details about the design can be retrieved from Skanska Teknik (2018a). The slightly modified construction sequence with the NGI-ADP model, which matches the Creep-SCLAY1S model, is presented in Table E.1 in Appendix E.

4.2.2 Modified Design with Creep-SCLAY1S

To be able to use Creep-SCLAY1S for modelling the excavation, some additional modifications were done to the existing NGI-ADP model design. The changes (except changing constitutive model for the soil) were to divide the soil into new layers, which is described in Section 4.1, and to change the interface of the SPWs to facilitate the calculations. The interfaces were modelled with the Soft Soil model, where the used parameters can be found in Table C.8 in Appendix C. The filling material, embankment, piles and all structural entities were left the same as in the NGI-ADP model design. The geometry of the Creep-SCLAY1S model design can be seen in Figure 4.6.

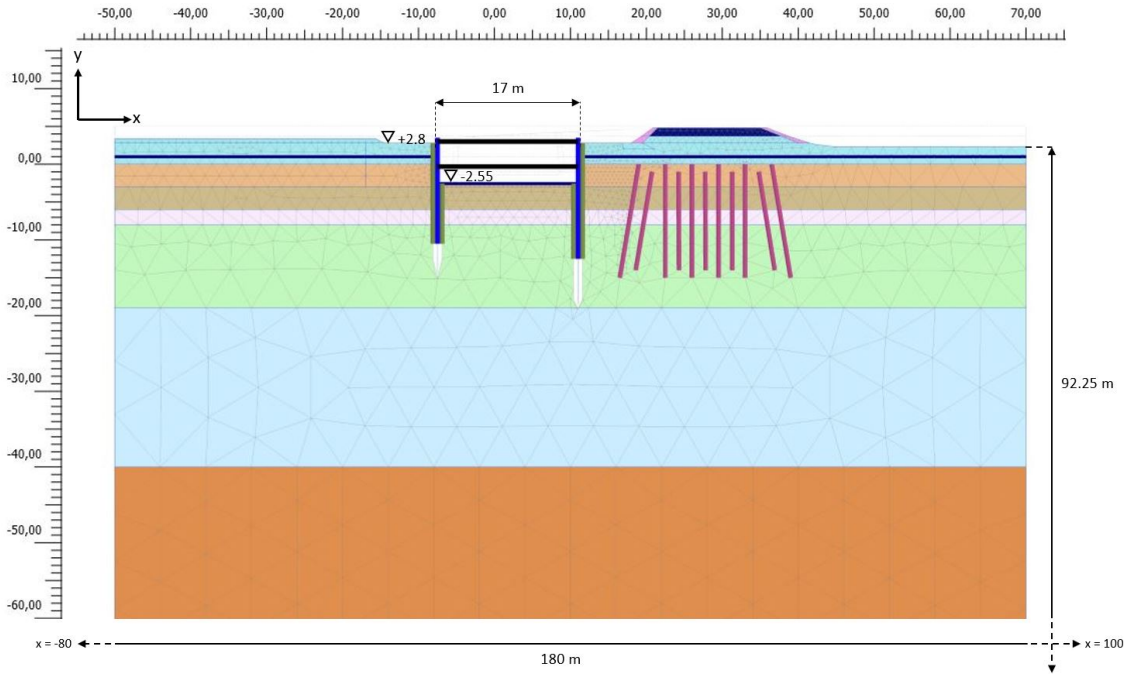

Figure 4.6: Section of Creep-SCLAY1S model design in Plaxis 2D.

Since the Creep-SCLAY1S model is time-dependent, duration of each construction phase was added. Further, "pure" consolidation phases were also added to the construction sequence. The first "pure" consolidation phase was added after construction of the embankment (which was in the 1930's) and is 80 years long, to incorporate the effect that the embankment has on the stress history. Also, three separate consolidation phases of 1 month, 3 months and 1 year respectively were added after the final excavation was completed. This was done to see the effect of time if the excavation is left open. The construction sequence for the Creep-SCLAY1S model can be seen in Table 4.2.

Table 4.2: Construction sequence with Creep-SCLAY1S in Plaxis 2D.

Phase	Description	Type of procedure	Time [days]
Initial phase	Soil activation and calculation of initial stresses	K_0-procedure	-
Phase 1	Installation of existing wooden piles	Consolidation	30
Phase 2	Construction of existing embankment	Consolidation	30
Phase 3	Consolidation to current conditions	Consolidation	29.2E3
Phase 4	Excavation for unloading down to +2.8m	Consolidation	120
Phase 5	Installation of SPW	Consolidation	26
Phase 6	Excavation for first level waling beam down to +1m	Consolidation	14
Phase 7	Installation of first strut level	Consolidation	28
Phase 8	Excavation for second level waling beam down to -1m	Consolidation	14
Phase 9	Installation of second strut level	Consolidation	28
Phase 10	Final excavation down to -2.55m	Consolidation	28
Phase 11	Consolidation for 1 month	Consolidation	30
Phase 12	Consolidation for 3 months	Consolidation	90
Phase 13	Consolidation for 1 year	Consolidation	365

5
Results

In this chapter the main findings from the study are presented. The results include analysis of both the soil displacements, Section 5.1, and the retaining structure (normal forces and bending moments), Section 5.2. In Figure 5.1 the chosen points, sections and structures of interest are presented. Point A is located in the middle of the excavation bottom and is where most bottom heave is expected. Point B is located on ground level, 1.5 m from the excavation and is the location where an inclinometer is installed. Point C is the location of the center of the closest tram tracks. This point is studied since the tram tracks are sensitive to deformations. Section A and B are selected for study of displacement with depth. For the structures, both of the struts and the right-hand SPW are chosen for analysis, see Figure 5.1. The right-hand SPW is expected to be more critical than the one to the left due to the road embankment. Therefore, the left SPW is not studied.

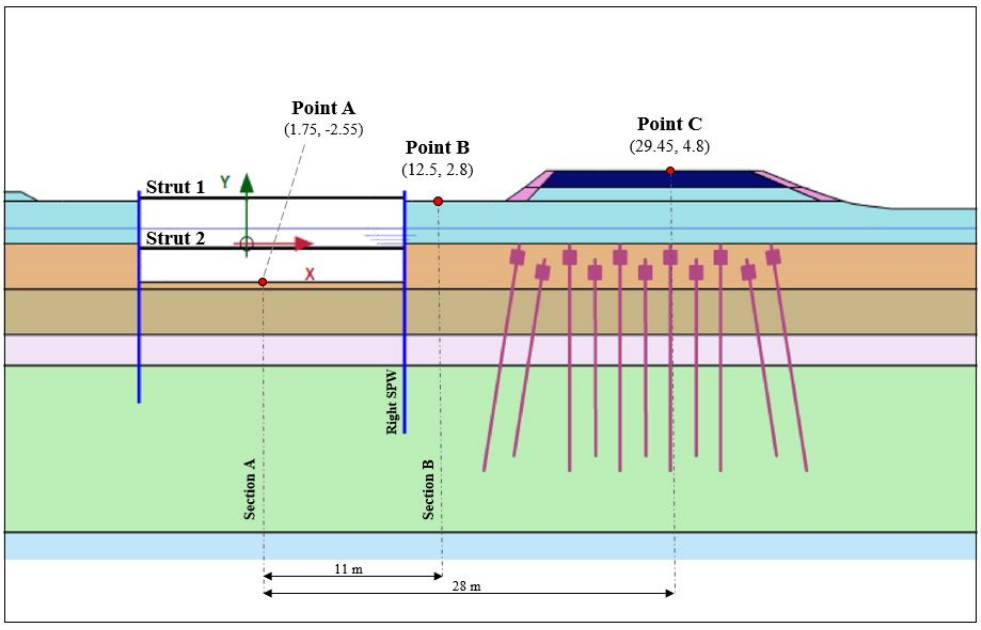

Figure 5.1: Chosen points, sections and structures for analysis.

The results will mainly focus on comparing the predictions with Creep-SCLAY1S and NGI-ADP, but also include a sensitivity analysis and an improved prognosis with piles for the Creep-SCLAY1S model. Finally, a brief comparison of the numerical predictions and the, so far, measured heave in the excavation is presented.

5.1 Soil Displacements

In this section the predicted soil displacements with the Creep-SCLAY1S and NGI-ADP models are presented. The focus here will be close to the excavation, especially at the excavation bottom, and also on the road embankment. More specific, the analyzed displacements are u_y in point A, u_x in point B and u_y in point C (from Figure 5.1). The overall formation of deformations in the models is, as expected, that the large embankment will settle and that the bottom of the excavation will heave. For an overview of the total displacements in the whole model, see Figure F.1 and Figure F.2 in Section F.1 in Appendix F. Further, the result only considers the construction of the studied excavation (from phase 4 and forward) and the previous phases are therefore not shown. To clarify, phase 4 represents construction of the unloading excavation and phase 10 represents the final excavation. Phase 11, 12 and 13 are consolidation phases and therefore the NGI-ADP curves do not change values in these phases. For the complete outline of phases see Table 4.2 in Section 4.2.2.

5.1.1 Distribution of Bottom Heave

In Figure 5.2 the predicted bottom heave profile for the final excavation depth is presented. It can be seen that the predicted maximum heave differs with 4 cm between the models, which is considered a rather large difference. Further, it can be seen that the variation of heave is not as large for Creep-SCLAY1S (between 14-15 cm) as for NGI-ADP (between 7-11 cm). For Creep-SCLAY1S the heave is largest near the right-hand SPW, where the large embankment likely causes more rotational movement in the soil. For NGI-ADP the distribution of heave is slightly more symmetrical with the maximum heave in the center of the excavation.

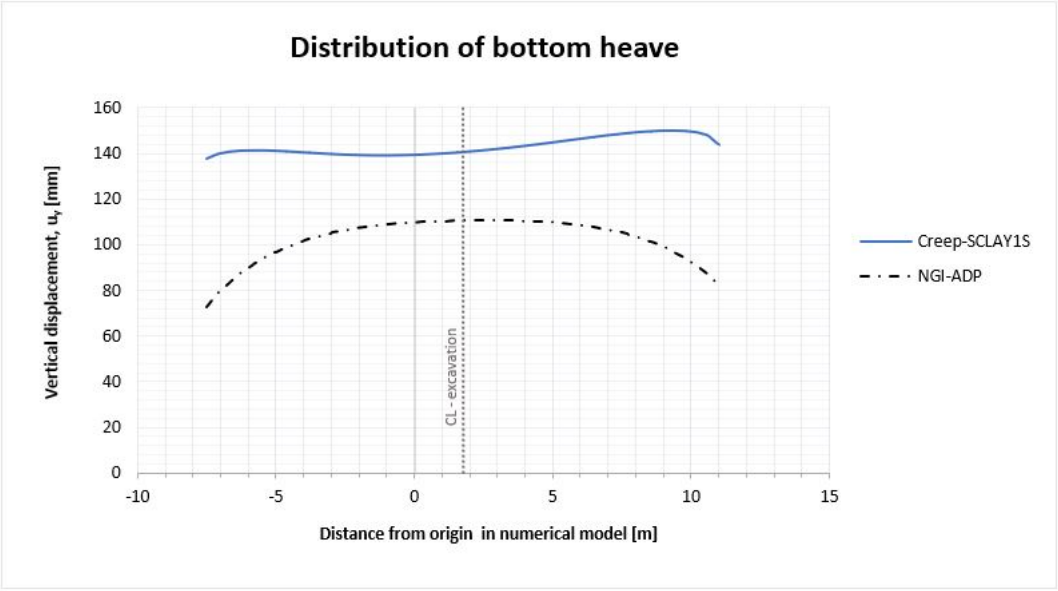

Figure 5.2: Distribution of bottom heave for final excavation depth (phase 10).

A possible reason for the difference between the heave profiles may be due to the differences in stiffness formulations in the models, as the NGI-ADP model uses undrained shear strength, c_u, and the Creep-SCLAY1S model uses the modified swelling index, κ^*. Figure 5.3 shows the variation in unloading/reloading shear modulus, G_{ur}, beneath the excavation bottom (level -2.55 m) to the toe of the SPW (level -12.5 m). It is evident that the NGI-ADP model uses larger values G_{ur} than the Creep-SCLAY1S model, which may be one factor adding to the larger heave in the Creep-SCLAY1S model. However, this only incorporates the elastic behaviour of the soil in the models, and thus does not take the effect of creep into account in the Creep-SCLAY1S model.

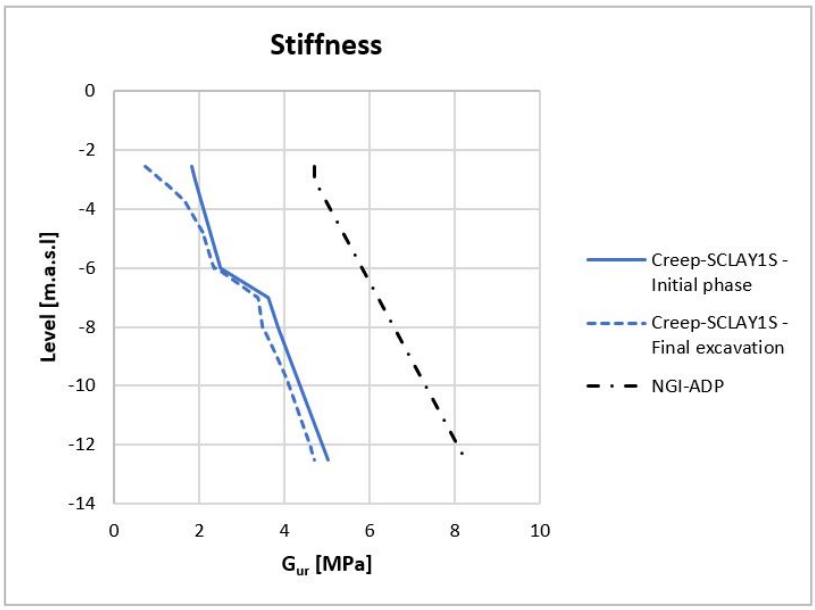

Figure 5.3: Difference in stiffness between Creep-SCLAY1S and NGI-ADP.

5.1.2 Point A - Center of Excavation Bottom

In Figure 5.4 a prediction of the vertical displacement, u_y, for point A is illustrated for the different construction phases. Further, the figure shows predictions with Creep-SCLAY1S and NGI-ADP. It can be seen in Figure 5.4 that Creep-SCLAY1S predicts larger displacements, especially for the consolidation phases at the end. Thus, the difference is more noticeable for the construction phases that stretch over many days, which can be seen as an effect of the consolidation process and creep strains. When the final excavation is reached, the predicted bottom heave will approximately be 14 cm and 11 cm for Creep-SCLAY1S and NGI-ADP, respectively. Thus, the Creep-SCLAY1S model predicts approximately 20% larger values. Although, if the excavation would stay open for a year, the bottom heave would be around 20 cm with Creep-SCLAY1S (100% larger than with NGI-ADP). For more detailed values see Table F.1 in Section F.1 in Appendix F.

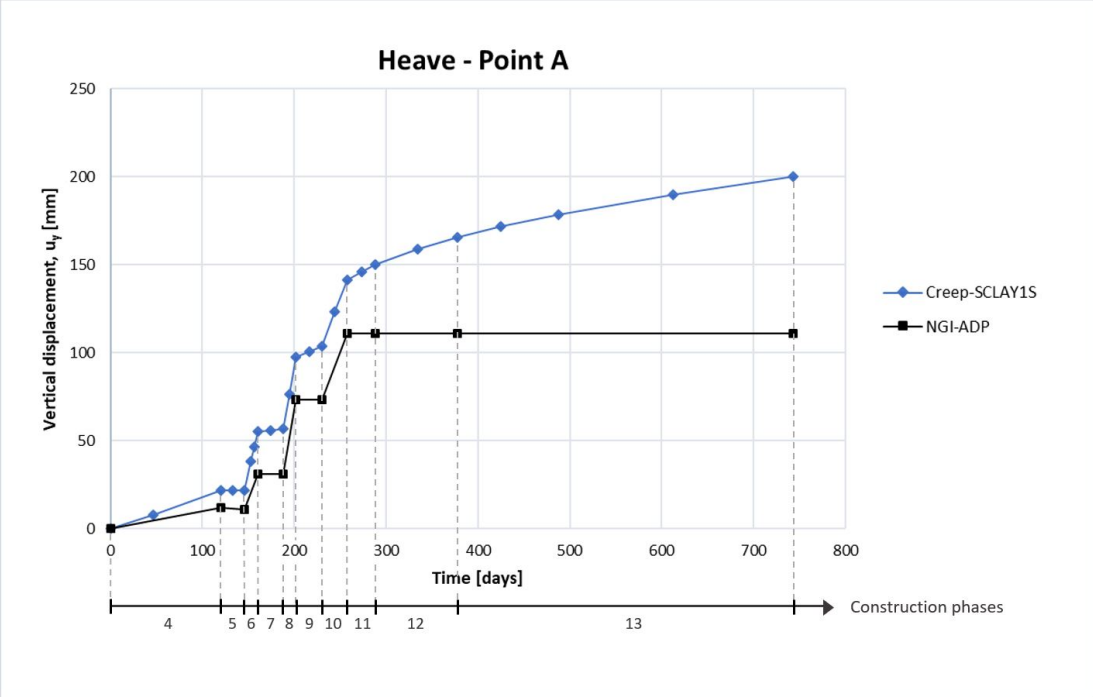

Figure 5.4: Comparison of heave in point A with Creep-SCLAY1S and NGI-ADP.

In Figure 5.5 the variation of vertical displacements with depth is presented. It can be seen that Creep-SCLAY1S predicts larger displacement for all depths and construction phases. Further, the results from Creep-SCLAY1S show that the heave will increase with time. It should also be noted that heave is predicted through the whole clay profile (over 90 m) with both models.

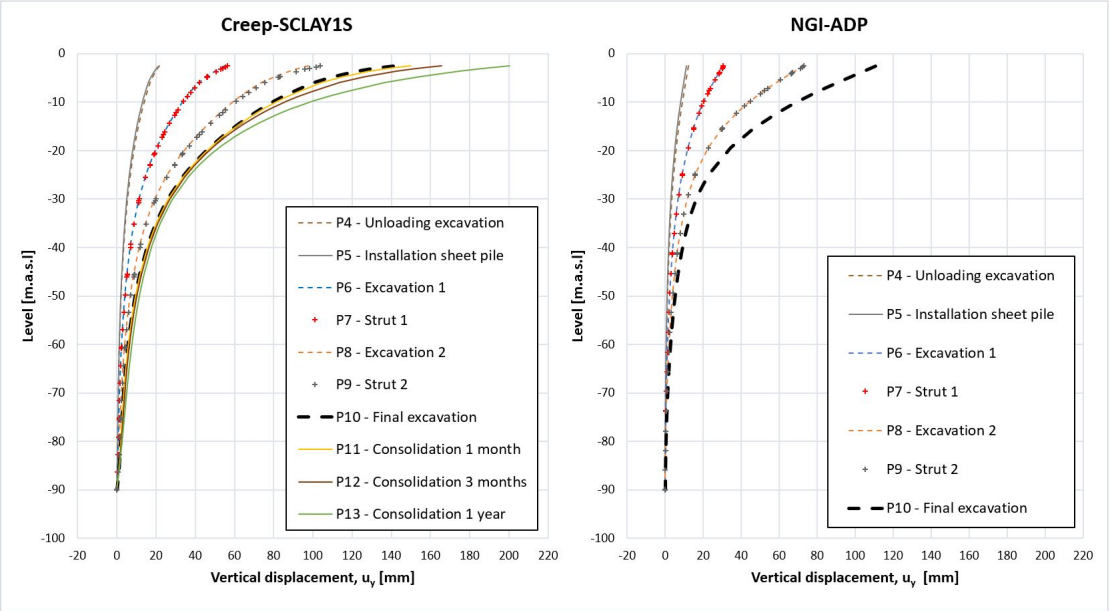

Figure 5.5: Prediction of vertical displacement in section A for all construction phases, with Creep-SCLAY1S and NGI-ADP.

Figure 5.6 shows a comparison of how the different models predict heave with depth. The comparison is made for the final excavation. Except that Creep-SCLAY1S predicts larger displacements, the heave does not decrease as fast with depth as for the NGI-ADP model. The difference is largest at the bottom of the excavation (level -2.55 m) and between level -10 m and -40 m.

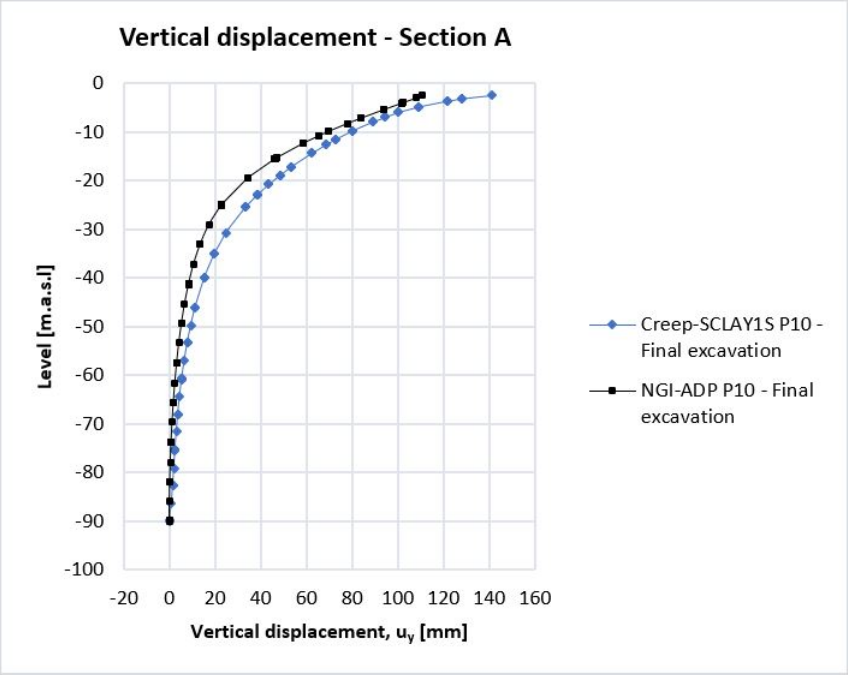

Figure 5.6: Comparison of vertical displacement in section A.

Further, Figure 5.7 also includes numerical and analytical predictions for heave with depth. The analytical estimation for the heave for Section A was calculated with Equation F.2 in Appendix F.1. Thus, the analytical estimation is based on calculations with M_{ul} according to Persson (2004), see Section 3.1.2.1, in combination with the 2:1 method for 2D plane strain, see Equation (F.1) in Appendix F.1. It can be seen that the NGI-ADP prediction is very similar to the analytical prediction. It can also be seen that in the excavation bottom, the analytical prediction of heave lies between the numerical predictions.

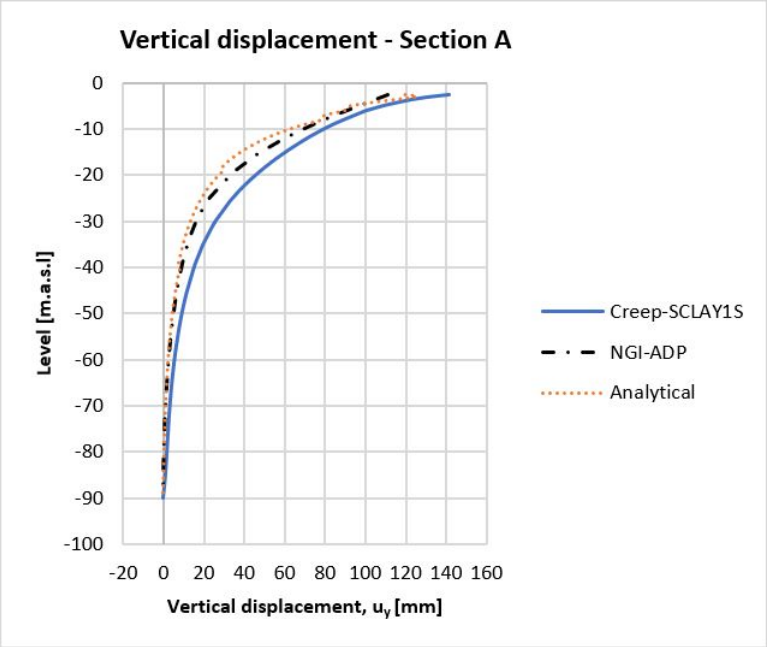

Figure 5.7: Comparison of heave in section A between Creep-SCLAY1S, NGI-ADP and analytical estimation using M_{ul}.

5.1.3 Point B - 1.5 m Beside Excavation

In Figure 5.8 a prediction of the horizontal displacement, u_x, for point B is illustrated for the different construction phases. Further, the figure shows predictions with Creep-SCLAY1S and NGI-ADP. In similarity with the vertical displacement in point A, the horizontal displacements in point B are larger with Creep-SCLAY1S than with NGI-ADP. In contrast to the vertical deformations in point A, the horizontal displacements in point B differ quite much between the models at final excavation (phase 10), which depends on phase 6 (excavation 1) where the Creep-SCLAY1S model predicts significantly larger displacements. This may seem strange since only filling material is removed in the 1st excavation phase. Although, the consolidation and destructuration effects incorporated in the Creep-SCLAY1S model could lead to that the top clay layer is more prone to deform than the top clay layer in the NGI-ADP model.

For Creep-SCLAY1S, the predicted displacement of point B (at final excavation) is around 5.5 cm, while for the NGI-ADP the predicted displacement is around 2 cm. Thus, Creep-SCLAY1S predicts over 2.5 times (150%) larger values of u_x than NGI-ADP. The horizontal displacements are most prominent in the excavation phases, which also is where the large difference between the predictions of the models are observed. It can also be noticed that time does not have a large influence on the horizontal displacements in point B, as displacements barely change during the last consolidation phases. For more detailed values see Table F.2 in Section F.1 in Appendix F.

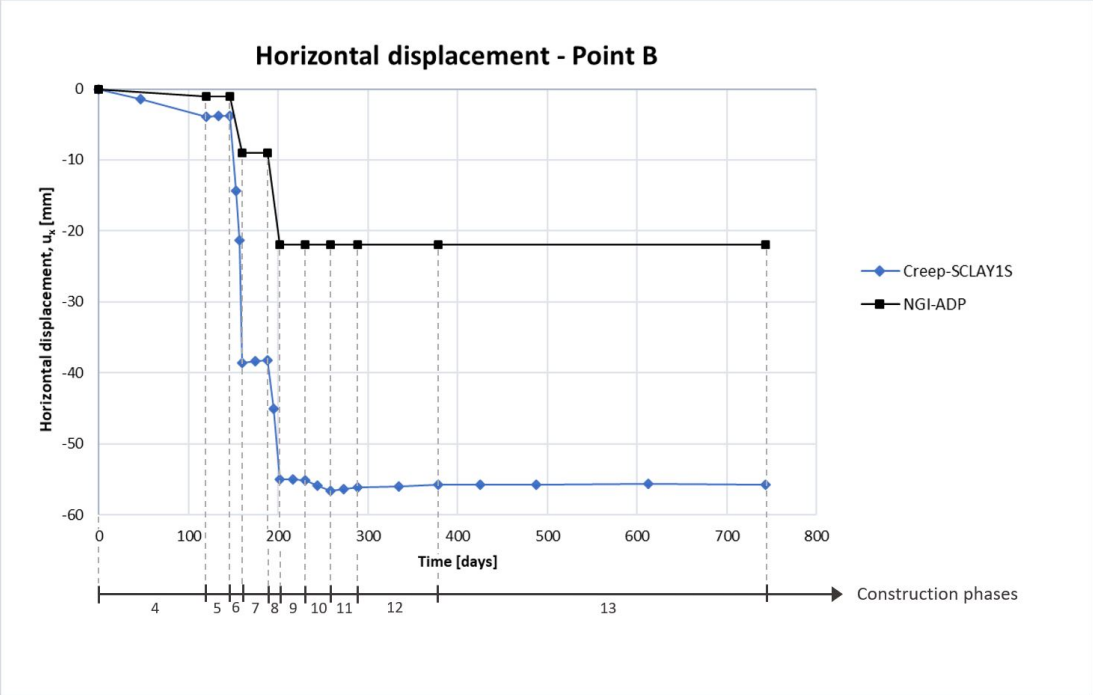

Figure 5.8: Comparison of horizontal displacements in point B with Creep-SCLAY1S and NGI-ADP.

In Figure 5.9 the variation in horizontal displacements with depth is studied with Creep-SCLAY1S and NGI-ADP. Except the difference in magnitude, a slight difference in shape when comparing the figures can also be seen. The curves from Creep-SCLAY1S have a more prominent notch where the SPW ends (about level -12.5 m) in comparison to the curves from NGI-ADP. It can also be distinguished that the horizontal displacements with Creep-SCLAY1S do not decrease as fast with depth as with NGI-ADP. The maximum deformation for both models seem to occur around the depth of the excavation bottom (-2.55 m), or slightly above.

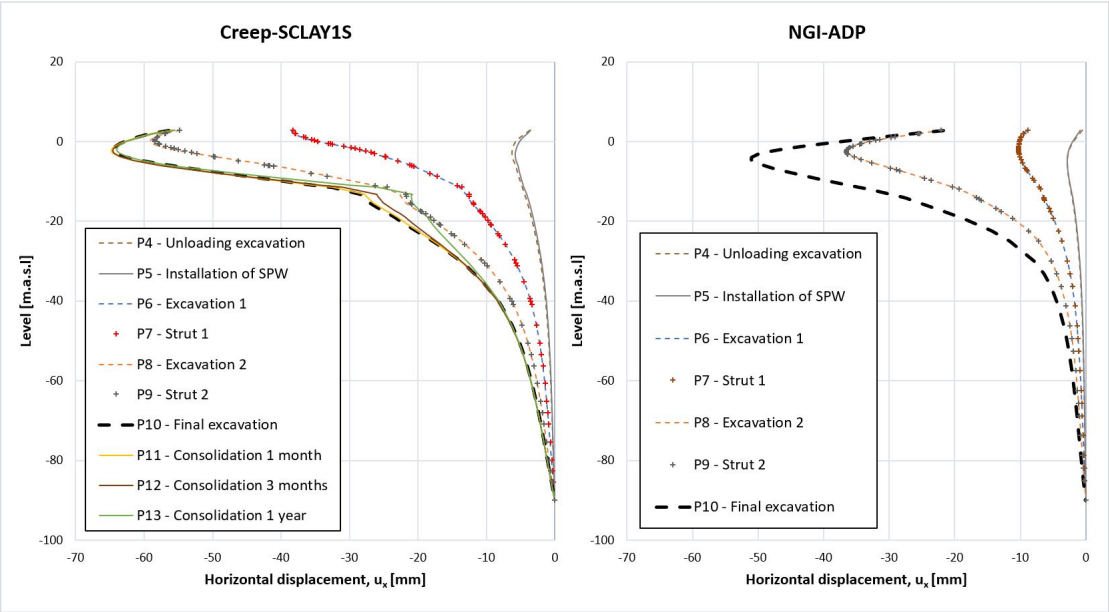

Figure 5.9: Horizontal displacement of section B for all construction phases, with Creep-SCLAY1S and NGI-ADP.

Figure 5.10 shows a comparison of the different model predictions of horizontal displacement with depth. The comparison is made for the final excavation. The largest difference is obtained at ground surface level. There also is a notable difference between level -20 m to -50 m.

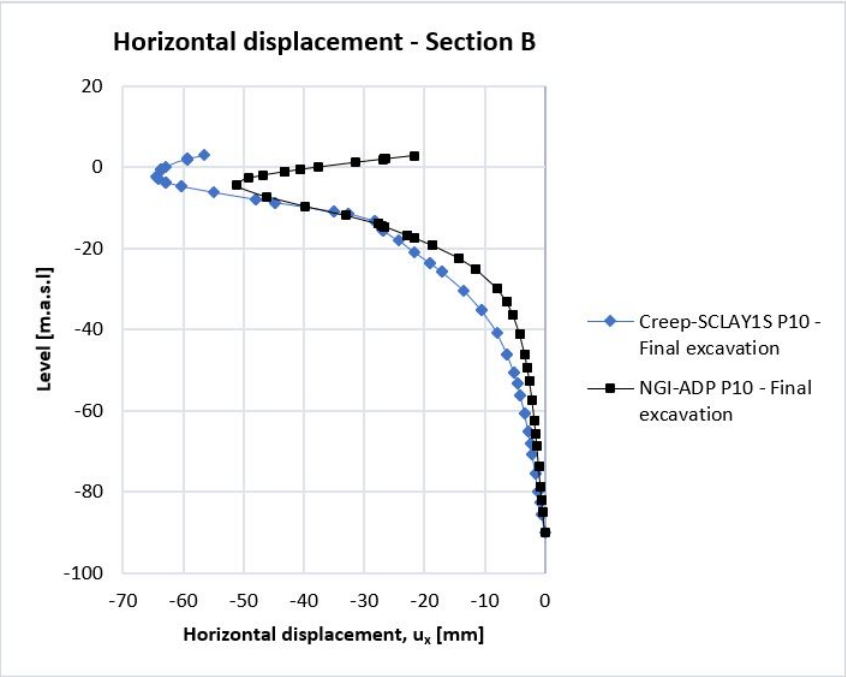

Figure 5.10: Comparison of horizontal displacement in section B.

5.1.4 Point C - Left Tram Lane on Embankment

In Figure 5.11 a prediction of the vertical displacement, u_y, for point C is illustrated for the different construction phases. Further, the figure shows predictions with Creep-SCLAY1S and NGI-ADP. Also in point C, Creep-SCLAY1S predicts larger displacements than NGI-ADP except when the final excavation depth is reached (phase 10). For the final excavation, Creep-SCLAY1S predicts a settlement of 1.4 cm while NGI-ADP predicts a settlement of 1.8 cm. Creep-SCLAY1S gives larger displacement in the earlier excavation steps (phase 4 and 6) while NGI-ADP "catches up" and gives larger displacements for the last excavations (phase 8 and 10, from level +2.8 m to level -2.55 m). Even though the predicted settlement at final excavation is similar, the time-effects modelled with the Creep-SCLAY1S model in the succeeding consolidation phases (11-13) are distinct. For more detailed values see Table F.3 in Section F.1 in Appendix F.

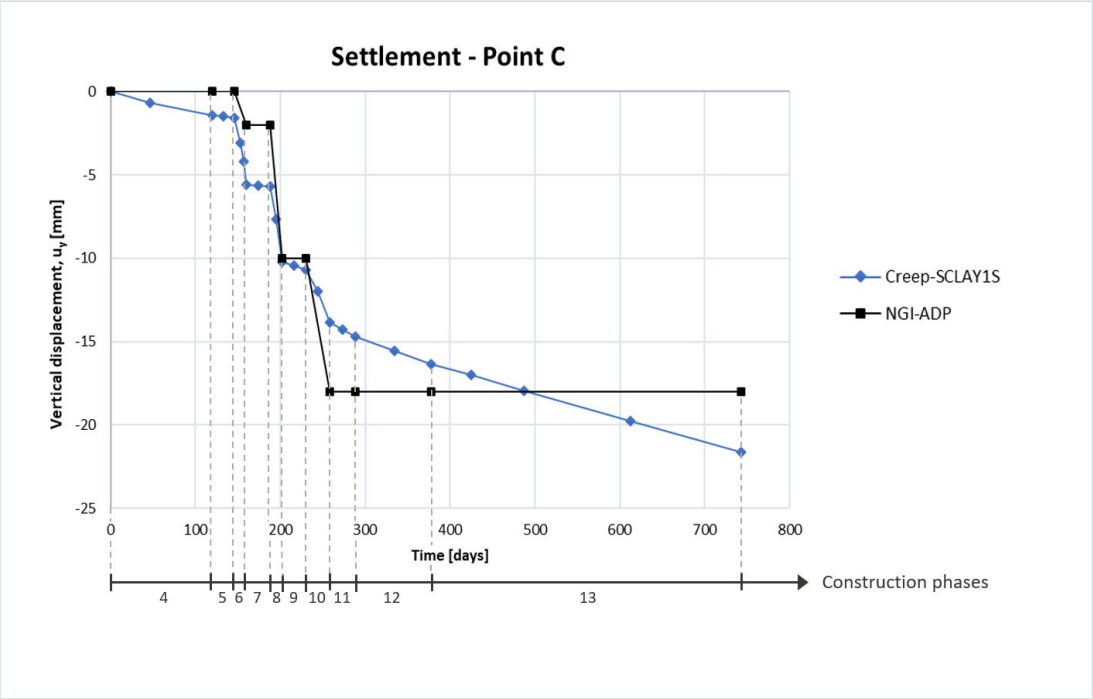

Figure 5.11: Comparison of settlements in point C with Creep-SCLAY1S and NGI-ADP.

5.2 Structural Entities

In this section the result for horizontal displacements and bending moment of the right-hand SPW, as well as the normal forces in the struts are presented.

5.2.1 Sheet Pile Wall

In Figure 5.12, the horizontal displacement of the wall is illustrated against depth for the Creep-SCLAY1S and NGI-ADP model, respectively. The excavation bottom and the strut levels are marked with a line and red arrows, respectively. The horizontal displacement of the SPW for each phase seems to increase down to level ca -3 to -5 m for both models. It can also be seen that the Creep-SCLAY1S model predicts larger displacements than the NGI-ADP model in each phase. The maximum value for the NGI-ADP model can be seen in phase 10 (final excavation), with a maximum displacement of approximately 5.5 cm. In comparison, the Creep-SCLAY1S model predicts a displacement of approximately 7 cm for the same phase. It can also be seen that the Creep-SCLAY1S model predicts notable displacements already in phase 5 (installation of SPW), which may be due to the low stiffness in the top layers of the clay deposit. It is evident that the most critical phase is phase 10 (final excavation). However, for the Creep-SCLAY1S model, also a slight increase in displacement is occurring for the succeeding consolidation phases. It can also be seen that for the Creep-SCLAY1S model, the largest displacement occurs around the excavation bottom (level -2.55 m). For the NGI-ADP model, the largest displacement seems to occur around 2 m beneath the excavation bottom instead (level -4 m to -5 m). More exact values can be found in Table F.4 in Section F.2 in Appendix F.

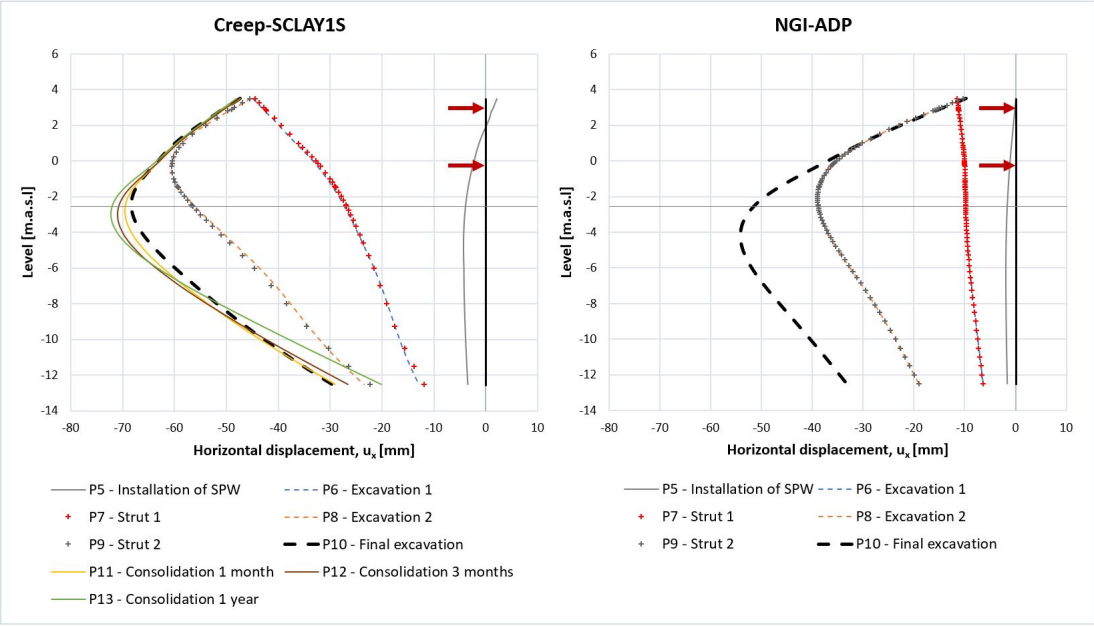

Figure 5.12: Horizontal displacement of right-hand SPW with Creep-SCLAY1S and NGI-ADP.

In Figure 5.13 a comparison of the model predictions of horizontal displacement for the most critical phase is shown (phase 10). The excavation bottom and the strut levels are marked with a line and red arrows, respectively. It is evident that the Creep-SCLAY1S model gives larger displacements overall, except for at the bottom of the SPW (level -12.5 m).

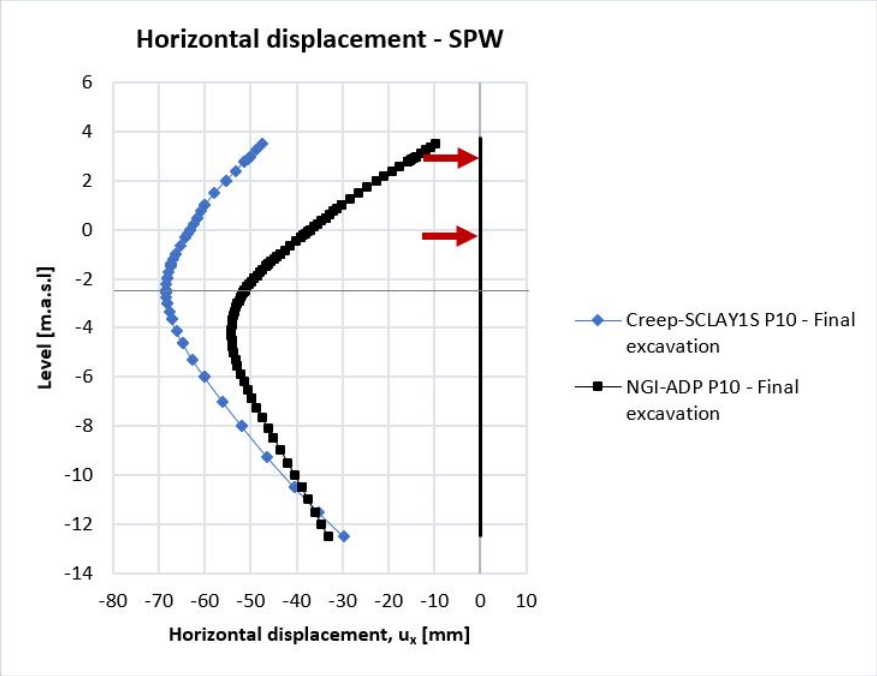

Figure 5.13: Comparison of horizontal displacement for critical phase.

Figure 5.14 shows the bending moment of the wall for each phase against depth for the Creep-SCLAY1S and NGI-ADP model, respectively. The excavation bottom and the strut levels are marked with a line and red arrows, respectively. For both models, phase 8 (excavation for second waling beam) shows that the bending moment peaks around level -0 m where the second strut level is installed (level -0.3 m). In phase 10 (final excavation), around the excavation bottom (level -2.55 m), the bending moment peaks again for both models. An increase in bending moment with time is predicted for the Creep-SCLAY1S model. The maximum bending moment for the NGI-ADP model can be seen in phase 10, with a value of approximately -65 kNm/m. In comparison, the Creep-SCLAY1S model gives a bending moment of approximately -50 kNm/m for the same phase. The effect of time gives a slight increase in bending moment, going from -50 to -64 kNm/m, between phase 10 and phase 13. More exact values can be found in Table F.5 in Section F.2 Appendix F.

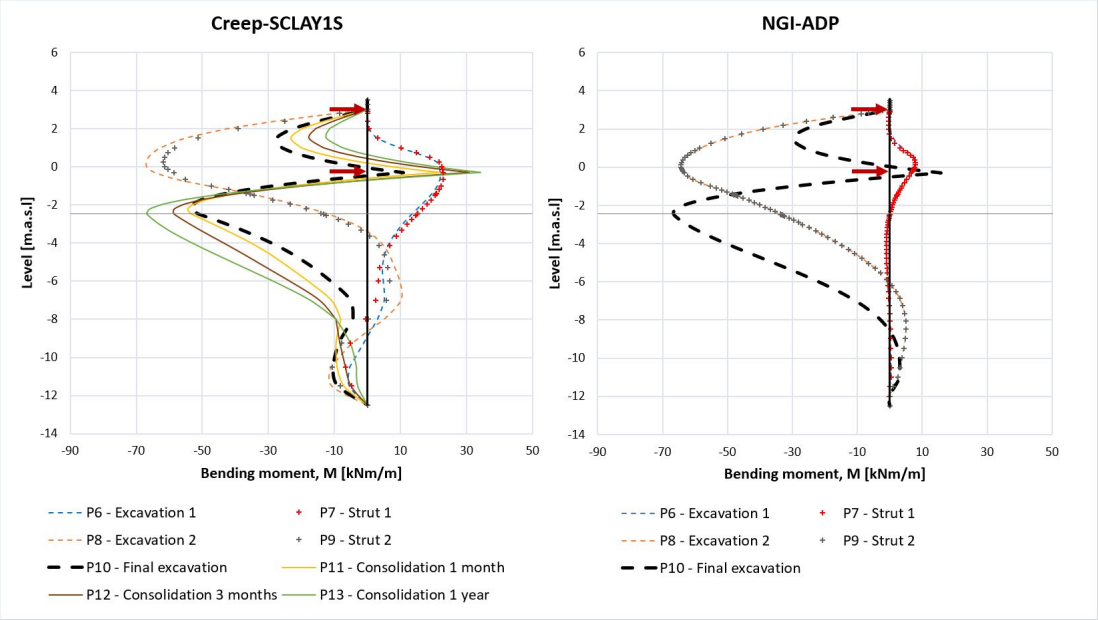

Figure 5.14: Bending moment of right-hand SPW using Creep-SCLAY1S and NGI-ADP.

In Figure 5.15 a comparison of the bending moment with the two models for the final excavation (phase 10) is illustrated. The two models predict similar values down to approximately 1 m above excavation bottom (level - 1.55 m), where the values for the NGI-ADP model are larger down to level -8 m. This may be correlated to the large horizontal displacements of the SPW for Creep-SCLAY1S, that "pushes" the whole SPW towards the excavation. Thus, larger horizontal displacement gives smaller bending moment. In addition to this, the Creep-SCLAY1S model does not get the same resistance at the bottom of the SPW, which also may be an effect of the large embankment on the right side of the excavation.

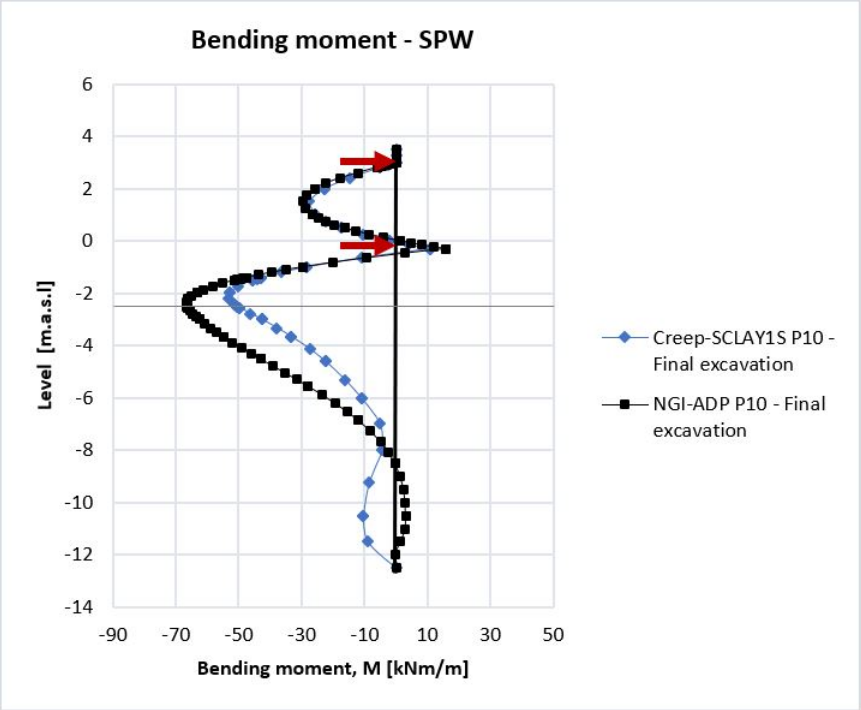

Figure 5.15: Comparison of bending moment for critical phase (phase 10).

5.2.2 Struts

Table 5.1 shows the normal forces in the struts for the Creep-SCLAY1S and NGI-ADP model predictions. The forces are larger in phase 10 (final excavation) for the NGI-ADP model, approximately 180 and 785 kN, compared to 150 and 710 kN for the Creep-SCLAY1S model. It is also evident that the time and viscous effects in the Creep-SCLAY1S model, seem to lower the forces of the first strut level, and increase the forces of the second strut level, reaching values of approximately 75 and 855 kN, respectively, in phase 13. This is likely due to that the sheet pile wall will continue to "rotate" if the excavation is left open after final excavation. The forces in the first strut level therefore decrease simultaneously as the force in the lower strut level increases. The value for the NGI-ADP will remain unchanged due to the lack of not taking consolidation and rate-dependency into account.

Table 5.1: Comparison of predicted strut forces.

Phase	Force - Strut 1 [kN] Creep-SCLAY1S	Force - Strut 2 [kN] Creep-SCLAY1S	Force - Strut 1 [kN] NGI-ADP	Force - Strut 2 [kN] NGI-ADP
Phase 7 - Installation of first strut level	1	-	4.5	-
Phase 8 - Excavation for second level waling beam down to -1m	277.4	-	264.4	-
Phase 9 - Installation of second strut level	254.0	62.0	264.1	1.1
Phase 10 - Final excavation down to -2.55m	149.9	708.2	181.5	786.9
Phase 11 - Consolidation for 1 month	129.3	777.3	-	-
Phase 12 - Consolidation for 3 months	102.6	836.7	-	-
Phase 13 - Consolidation for 1 year	74.7	855.3	-	-

5.3 Sensitivity Analysis Creep-SCLAY1S

In this section a sensitivity analysis for some of the input parameters to the Creep-SCLAY1S model are presented. The parameters that are analyzed are OCR, k, κ^* K_0^{NC} and K_0. For the soil, the vertical displacement, u_y, in point A and C for phase 8, 10 and 13 are studied. This is done to see the development of displacements with time in the most critical phases. For the structures, the maximum bending moment, M_{max}, for the SPW and the normal forces, N, in the struts are studied in phase 8 and 10. The purpose of this sensitivity analysis is to change the input parameters within realistic ranges and estimate their effect on the result.

5.3.1 Sensitivity of OCR

The OCR was both increased and decreased with 10% for every clay layer. For the decrease, the OCR for the different layers lies in a span of 1-1.17 and for the increase, the OCR lies in a span of 1.1-1.43. The OCR is of interest since the Creep-SCLAY1S model is expected to be very sensitive to this parameter. In Table 5.2 and Table 5.3 the result from the sensitivity analysis of the OCR can be seen.

From Table 5.2 it is evident that a lower OCR will result in more heave in the excavation bottom (point A) and more settlement of the tram tracks on the embankment (point C). This is due to the increased compressibility of the clay deposit for lower $OCRs$. An increase of OCR will give the opposite effect, that is, a decrease in bottom heave and settlement. From Table 5.2 it can be seen that the model seems to be more sensitive to a decrease in OCR rather than an increase (both in point A and C). In point A the largest change of the original u_y is 6.5% (phase 10) and in point C the largest change of the predicted u_y is 50% (phase 13). This implies that the predictions of settlement in point C are more sensitive to changes in OCR than the predictions of heave in point A.

Table 5.2: Sensitivity analysis of OCR on u_y in point A and C.

Point & Phase	u_y [m] $0.9 \cdot OCR$	u_y [m] Original OCR	u_y [m] $1.1 \cdot OCR$	Change [%]
Point A - P8: Excavation for 2nd level waling beam	0.102	0.098	0.094	+4/-4
Point A - P10: Final excavation	0.150	0.141	0.134	+6.5/-5
Point A - P13: Consolidation for 1 year	0.209	0.200	0.193	+4.5/-3.5
Point C - P8: Excavation for 2nd level waling beam	-0.013	-0.010	-0.008	+30/-20
Point C - P10 Final excavation	-0.018	-0.014	-0.011	+28.5/+21.5
Point C - P13 Consolidation for 1 year	-0.033	-0.022	-0.014	+50/-36.5

In Table 5.3 it can be seen that for phase 8, a decrease of OCR gives a slight increase in maximum bending moment, M_{max}, whereas an increase does not give any significant change. For phase 10, the opposite seems to occur. There is no distinct result that indicates that the degree of sensitivity depends on whether the OCR is increased or decreased. The large changes of the original prediction rather seem to depend on the construction phase/the depth of the excavation. For the struts, the normal forces, N, seem to increase with decreased OCR and vice versa. If looking at the percentual change of the original u_y, it can be seen that the struts are almost equally sensitive to increases and decreases of OCR. Further, the second strut level seems to be more sensitive to changes in OCR than the first strut level, around 8% compared to 2% change.

Table 5.3: Sensitivity analysis of OCR on M_{max} and N.

Quantity	$0.9 \cdot OCR$	Original OCR	$1.1 \cdot OCR$	Change [%]
M_{max} - P8: Excavation for 2nd level waling beam [kNm/m]	-67.8	-67.0	-66.9	+1/0
M_{max} - P10: Final excavation [kNm/m]	-52.9	-53.3	-58.6	-1/+10
N - P8: Excavation for 2nd level waling beam Strut 1 [kN]	282.5	277.4	272.8	+2/-1.5
N - P10: Final excavation Strut 2 [kN]	763.8	708.2	656.0	+8/-7.5

5.3.2 Sensitivity of Permeability, k

In Table 5.4 and Table 5.5 the result from the sensitivity analysis of the permeability, k, can be seen. The permeability was increased with a factor of 10, as k values retrieved from laboratory tests in general are expected to be lower than the in-situ k. The higher values of in-situ k could for instance be explained by thin layers of silt or scaling effects (micro in laboratory vs macro in-situ). The increased values of k in the sensitivity analysis lie in a span of $0.5 \cdot 10^{-8} - 2.1 \cdot 10^{-8}$.

In Table 5.4 it can be seen that an increase of k gives an increase in heave and decrease in settlements. Both point A and point C seem to heave in the studied phases, which could be explained by the faster consolidation process, as when using increased k the excess pore pressure below the existing road embankment has already dissipated before starting the excavation. The largest change for the studied points can be seen in phase 13 for both point A (approximately 50%) and for point C (approximately 160%).

Table 5.4: Sensitivity analysis of k on u_y in point A and C.

Point & Phase	u_y [m] Original k	u_y [m] $k \cdot 10$	Change [%]
Point A - P8: Excavation for second level waling beam	0.098	0.127	+29.5
Point A - P10: Final excavation	0.141	0.199	+41
Point A - P13: Consolidation for 1 year	0.200	0.306	+53
Point C - P8 Excavation for second level waling beam	-0.01	-0.001	-90
Point C - P10 Final excavation	-0.014	-0.001	-93
Point C - P13 Consolidation for 1 year	-0.022	0.013	-159

Table 5.5 shows that an increase in k, increases M_{max} in phase 10, while for phase 8 it does not change significantly. N decreases for both strut levels (approximately 6% versus 12%). Overall, the percentual change of M_{max} and N are not as large in comparison to the change of u_y when increasing k.

Table 5.5: Sensitivity analysis of k on M_{max} and N.

Quantity & Phase	Original k	$k \cdot 10^1$	Change [%]
M_{max} - P8: Excavation for 2nd level waling beam [kNm/m]	-67.0	-66.5	-1
M_{max} - P10: Final excavation [kNm/m]	-53.3	-63.5	+19
N - P8: Excavation for 2nd level waling beam Strut 1 [kN]	277.4	261.1	-6
N - P10: Final excavation Strut 2 [kN]	708.2	627	-11.5

5.3.3 Sensitivity of Modified Swelling Index, κ*

In Table 5.6 and Table 5.7 the result from the sensitivity analysis of κ^* can be seen. It was decided to decrease κ^* with 25 % with guidance from the results of (Karlsson et al., 2015), that studied the results from laboratory tests taken from Swedish standard piston sampler and mini-block sampler. The decreased values for κ^* in the sensitivity analysis lie in a span of 0.011-0.014.

It is evident that a decrease in κ^*, decreases heave in point A and settlements in point C. This can be explained by the increased stiffness of the clay deposit. It seems like the change in vertical displacements is lowered with time, where the time effect is more prominent in point C. The settlement in point C decreases from approximately 10% in phase 8, to 5% in phase 13.

Table 5.6: Sensitivity analysis of κ^* on u_y.

Phase	u_y [m] $0.75 \cdot \kappa^*$	u_y [m] Original κ^*	Change [%]
Point A - P8: Excavation for second level waling beam	0.078	0.098	-20.5
Point A - P10: Phase 10 - Final excavation	0.115	0.141	-18.5
Point A - P13: Consolidation for 1 year	0.167	0.200	-16.5
Point C - P8: Excavation for second level waling beam	-0.009	-0.010	-10
Point C - P10: Final excavation	-0.013	-0.014	-7.1
Point C - P13: Consolidation for 1 year	-0.021	-0.022	-4.5

In Table 5.7 it can be seen that a decrease in κ^* decreases M_{max} roughly the same for both phase 8 and 10. For N a decrease can be seen for the first strut level in phase 8, while an increase can be seen for the second strut level in phase 10.

Table 5.7: Sensitivity analysis of κ^* on M_{max} and N.

Quantity & Phase	$0.75 \cdot \kappa^*$	Original κ^*	Change [%]
M_{max} - P8: Excavation for 2nd level waling beam [kNm/m]	-62.8	-67.0	-6.5
M_{max} - P10: Final excavation [kNm/m]	-50	-53.3	-6
N - P8: Excavation for 2nd level waling beam Strut 1 [kN]	267.8	277.4	-3.5
N - P10: Final excavation Strut 2 [kN]	745.2	708.2	+5

5.3.4 Sensitivity of K_0^{NC} and K_0

In Table 5.8 and Table 5.9 the result from the sensitivity analysis of K_0^{NC} and K_0 can be seen. K_0^{NC} and K_0 were recalculated with the formula for K_0^{NC} and K_0 according to Larsson et al. (2007) presented in Section 3.3.1.1. The increased K_0^{NC} and K_0 can be found in Table F.6 in Section F.3 in Appendix F.

It can be seen that an increase in K_0^{NC} and K_0, decreases vertical displacements in both point A and C. It seems like the simulation is more sensitive to an increase in those parameters in point C, i.e settlements. The largest change in point C can be seen in phase 8 (58%), while for point A the change is roughly the same for all studied phases (around 10% increase).

Table 5.8: Sensitivity analysis of K_0^{NC} and K_0 on u_y in point A and C.

Phase	u_y [m] increase of K_0^{NC} & K_0	u_y [m] Original K_0^{NC} & K_0	Change [%]
Point A - P8: Excavation for second level waling beam	0.089	0.098	-9
Point A - P10: Final excavation	0.127	0.141	-10
Point A - P13: Consolidation for 1 year	0.185	0.200	-7.5
Point C - P8: Excavation for second level waling beam	-0.008	-0.019	-58
Point C - P10: Final excavation	-0.010	-0.014	-28.5
Point C - P13: Consolidation for 1 year	-0.011	-0.022	-50

Table 5.9 shows that an increase in K_0^{NC} and K_0 does not affect he structural entities noticeably, except for in phase 10 (final excavation), where a decrease (10%) in N can be seen for the second strut level.

Table 5.9: Sensitivity analysis of K_0^{NC} and K_0 on M_{max} and N.

Quantity & Phase	Increase of K_0^{NC} & K_0	Original K_0^{NC} & K_0	Change [%]
M_{max} - P8: Excavation for 2nd level waling beam [kNm/m]	-66.7	-67.0	-0.5
M_{max} - P10: Final excavation [kNm/m]	-55	-53.3	+3
N - P8: Excavation for 2nd level waling beam Strut 1 [kN]	274.1	277.4	-1
N - P10: Final excavation Strut 2 [kN]	635.3	708.2	-10.5

5.4 Validation of Simulation

In order to estimate if the simulation with Creep-SCLAY1S gives reasonable output, some controls were done. One of them was to make sure that the model accounts for the extra pressure from a water column behind the SPW. It was therefore checked that the total pressure on the SPW always was equal to or larger than the water pressure.

Also, measured settlements from satellite data were compared with modelled settlement. Satellite data showed a settlement rate of 2-9 mm/year in the area (Tornborg, 2019). In the center of the excavation the trend line of satellite measurements indicates on a settlement rate of 7.4 mm/year. The value obtained with Creep-SCLAY1S was 7.5 mm/year, thus in the measured range. Figure 5.16 shows the measured settlements in the studied area.

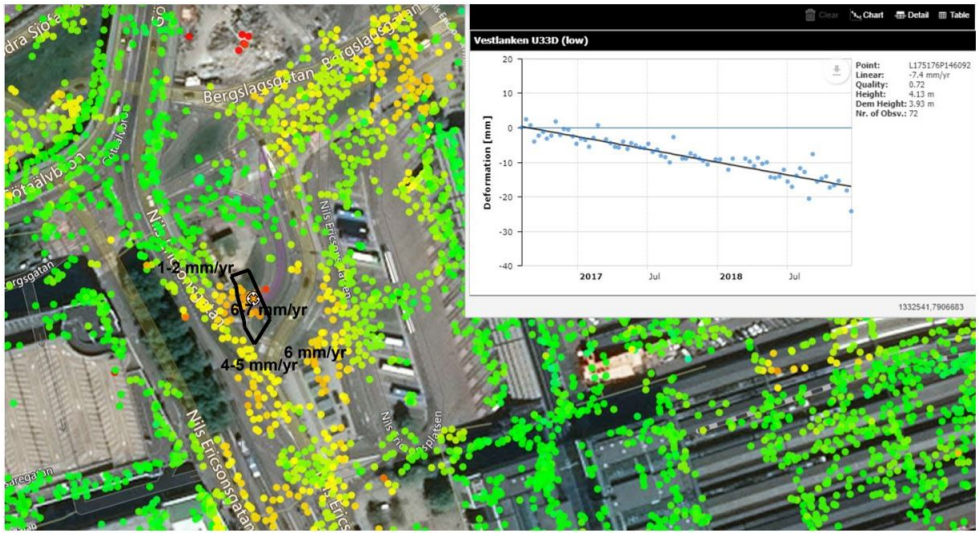

Figure 5.16: Satellite measurement of settlements in studied area with studied excavation marked in black (courtesy to Trafikverket).

Although the rate of settlement seems satisfactory, correct values can be obtained in the wrong way. One of the simplifications in this study is the setup of construction phases. In order to account for the effects of the large embankment next to the excavation and still use the K_0-procedure for generation of the in-situ stresses, the initial phase starts with a horizontal ground surface before the construction of the large embankment. The difficulty lies in that the construction of the embankment took place approximately 80 years ago, while the used input data was received from measurements and laboratory tests performed in the last 5 years. Thus, the input values (based on recent laboratory tests) will be altered during construction of the embankment and the 80 year long consolidation, and there will be a risk of not obtaining representative/desired behaviour of the soil model, due to the evolution of input parameters with time/modelling stages. Other options were considered, for example using the gravity-load function instead of K_0-procedure or start modelling from year 1600 with "untouched soil" and altering input parameters until reaching

current conditions (before the modelling of excavation starts). However, the uncertainty of using such a methodology was in this thesis considered to be larger.

In order to estimate how much the input OCR (as mentioned, based on recent laboratory tests) has changed during consolidation following construction of the existing embankment, and get a sense of the magnitude of uncertainty, the stress parameters p'_m and p'_{eq} were studied. p'_m is the relative preconsolidation pressure and describes the size of the Normal compression surface, NCS. p'_{eq} describes the size of the Current state surface, CSS. By comparing how much the relation between these parameters changes from phase 1 and phase 3, a measure of the modelling error can be estimated, see Table 5.10. For clarity, the points which are studied in Table 5.10 are presented in Figure 5.17. These points are selected since they are close to the excavation and are predicted to have large total deformations (from Figure F.1 in Section F.1 in Appendix F).

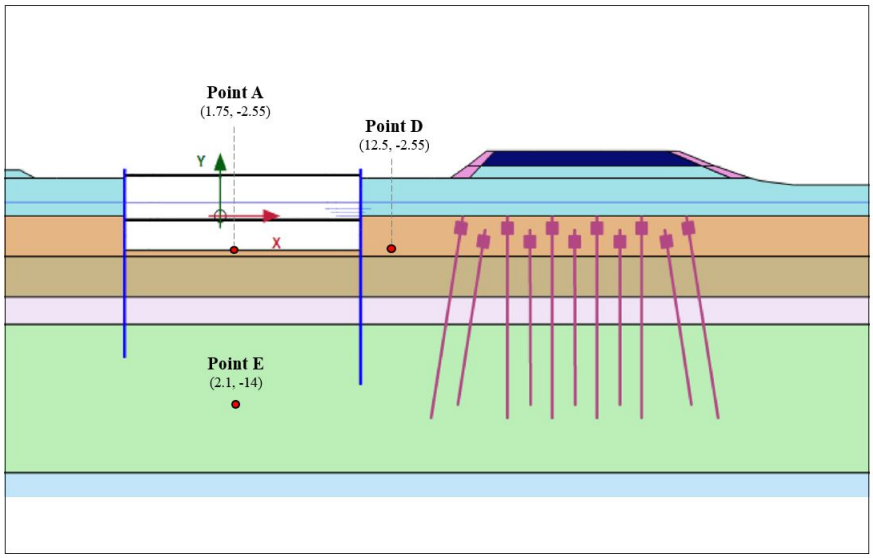

Figure 5.17: Points for comparison of p'_m and p'_{eq}.

Table 5.10, shows that the isotropic degree of overconsolidation increases after the consolidation for 80 years. However, it would instead be expected to decrease as consolidation would make the soil more NC. This could be an effect of creep and destructuration which instead gives the opposite effect. It is also evident that the values for point E differ less than for point A and D. This implies that the soil further down in the deposit is not affected to the same extent as the soil in the top layers.

Table 5.10: Change of reference surface between phase 1 and phase 3.

Point & phase	p'_m	p'_{eq}	Isotropic degree of over-consolidation (p'_m/p'_{eq})
Point A - P1: Before embankment fill	39.7	34.4	1.15
Point A - P3: Consolidation for 80 years	69.3	50.8	1.36
Point D - P1: Before embankment fill	39.2	33.8	1.16
Point D - P3: Consolidation for 80 years	67.9	49.8	1.36
Point E - P1: Before embankment fill	97.6	84.2	1.16
Point E - P3: Consolidation for 80 years	105.3	86.1	1.22

5.5 Effect of Piles

Something that was not originally considered in the modelled construction sequence (both NGI-ADP and Creep-SCLAY1S) was the piles within the excavation. In reality, these piles were installed just before the installation of the SPW and took 24 days. In this section a modified prediction of the Creep-SCLAY1S model with added piles is presented. There are 5 pile rows in the studied section, see Figure 5.18. The piles are in total 57 m long, where the top 11.5 m are made of circular steel piles, while the rest of the pile element consists of reinforced square concrete piles. The piles closest to the SPWs have an out-of-plane spacing of 3.6 m, while the remaining piles have an out-of-plane spacing of 4.9 m. All piles are modelled as elastic. More specific details about the used parameters for the piles can be found in Table F.7 and Table F.8 in Section F.4 in Appendix F. Installation effects such as pre-augering down to ca 18 m depth and installation of the displacement piles are not considered. Further, only the vertical displacement (heave) in the excavation is studied.

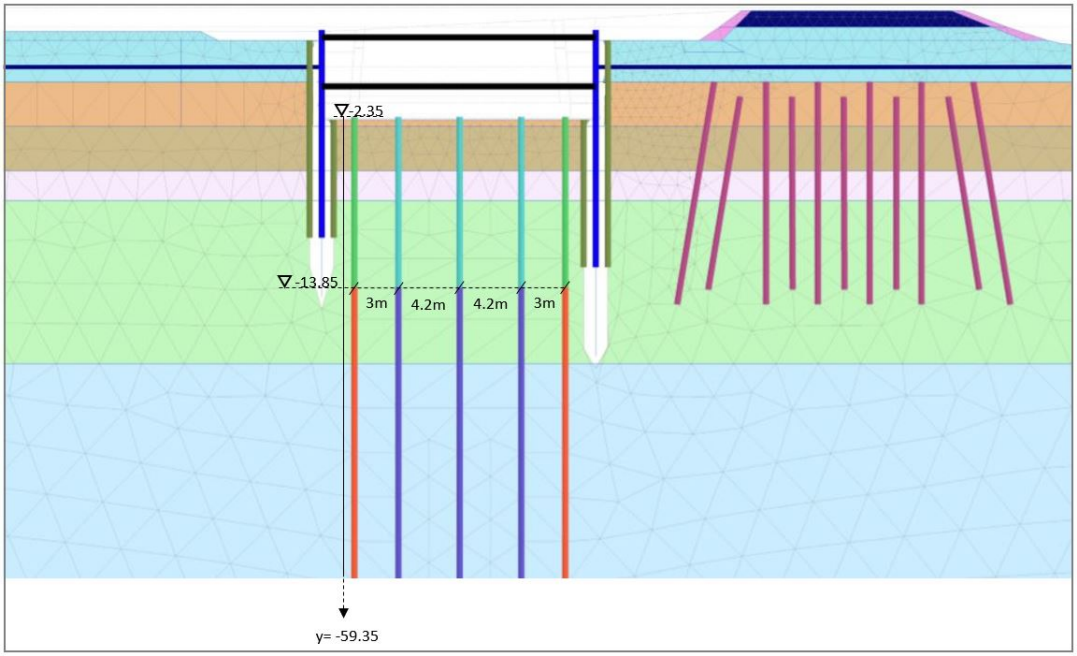

Figure 5.18: Position of piles in studied excavation.

In Figure 5.19 the predicted bottom heave profile, with and without the effect of the piles, is presented for the final excavation depth. It can be seen that the predicted maximum heave differs with approximately 1.5 cm between the simulations. Thus, the piles will reduce the heave in the excavation bottom with around 10%. The distribution of heave looks similar, except for the area closest to the piles, where the reduction of heave is more prominent (due to skin resistance).

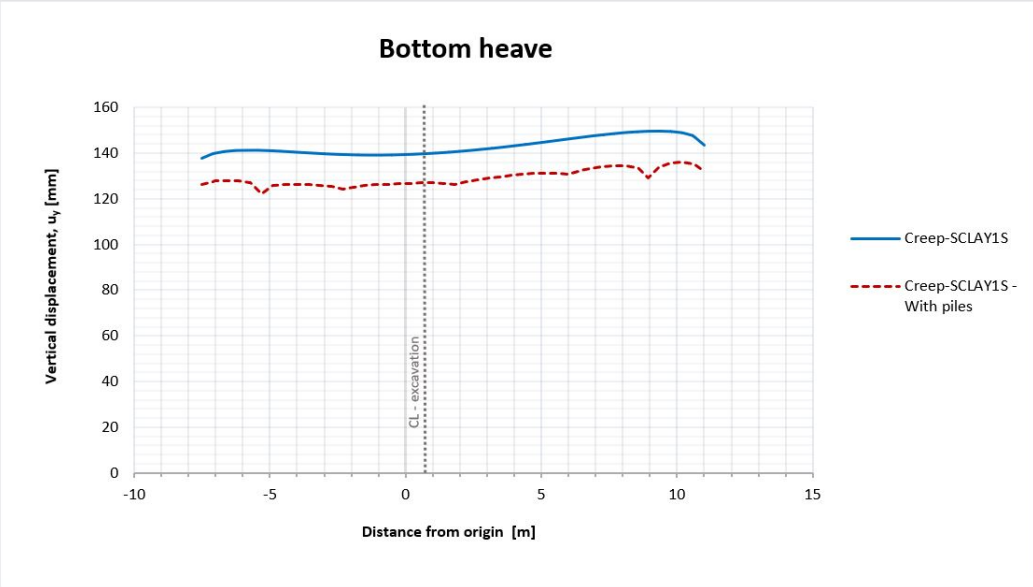

Figure 5.19: Bottom heave for the final excavation depth (phase 10).

In Figure 5.20 a prediction of the vertical displacement, u_y, for point A (center of excavation bottom) is illustrated throughout the whole construction process. This figure allows to see the effect of the piles with time. It should be noted that the construction process is 24 days longer for the modified model, which is clear from the horizontal offset between the curves. In Figure 5.20, no noticeable change in heave-rate can be seen throughout the construction process. Although if looking at Table F.9 in Section F.4 in Appendix F, it can be seen that the difference in heave will increase slightly with time. When the final excavation is reached, the predicted bottom heave will approximately be 14 cm and 13 cm for Creep-SCLAY1S and the Creep-SCLAY1S with piles, respectively. For more detailed values see Table F.9 in Section F.4 in Appendix F.

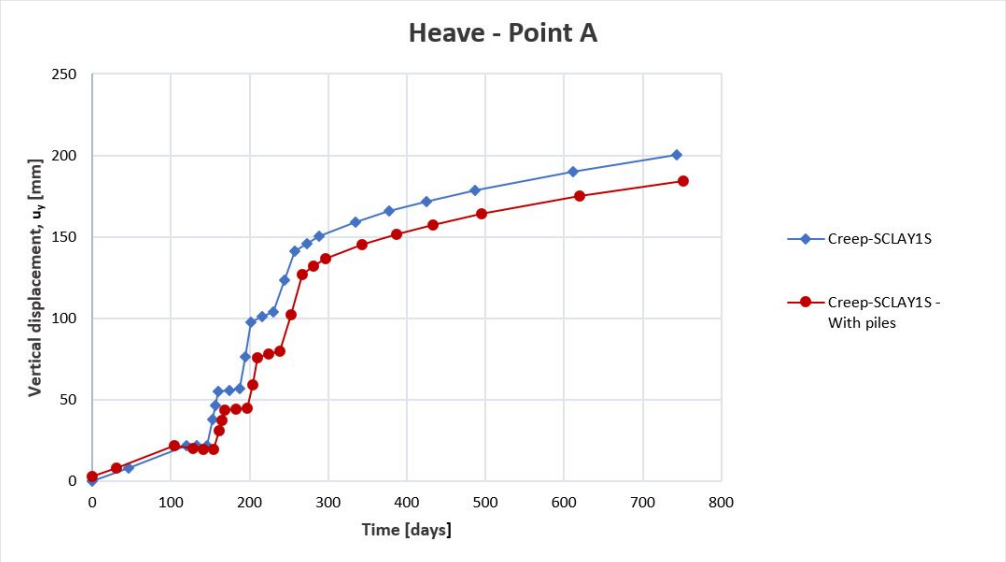

Figure 5.20: Comparison of heave in point A with Creep-SCLAY1S and Modified Creep-SCLAY1S.

Figure 5.21 shows how the piles affect the prediction of heave with depth in the section from the center of the excavation bottom. The comparison is made for the final excavation. The two simulations give similar heave profiles with depth, and do not seem to differ noticeably from level -40 m. The difference is largest at the bottom of the excavation (level -2.55 m). Further, no difference in heave where the change from steel pile to concrete pile (level -14 m) can be distinguished.

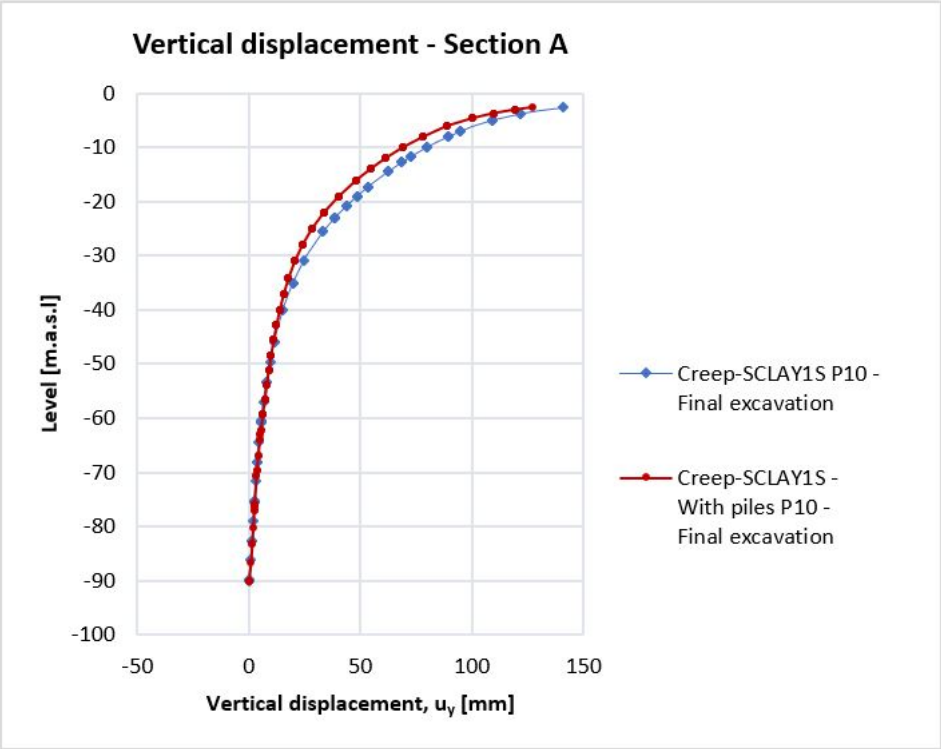

Figure 5.21: Comparison of vertical displacement in section A.

5.6 Comparison with Measured Values

Since the excavation is not yet finalized it is not possible to compare the predictions with measured values throughout the whole construction process. Also, this has not been the main focus of this thesis. Although, the excavation for the second level wailing beam has been performed in the time of finalizing this thesis and thus, measurements until this construction phase are available. In Figure 5.22, a compilation of the heave predictions for section A (from center of excavation bottom) is presented together with the measured values.

The heave measurements are obtained from a bellow hose in the center of the studied section. In order to construct the green line (measurements without installation effects), the heave created during installation of SPW and piles was removed. Thus, all predictions and the measured values without installation effects (green line) show the heave after installation of the SPW.

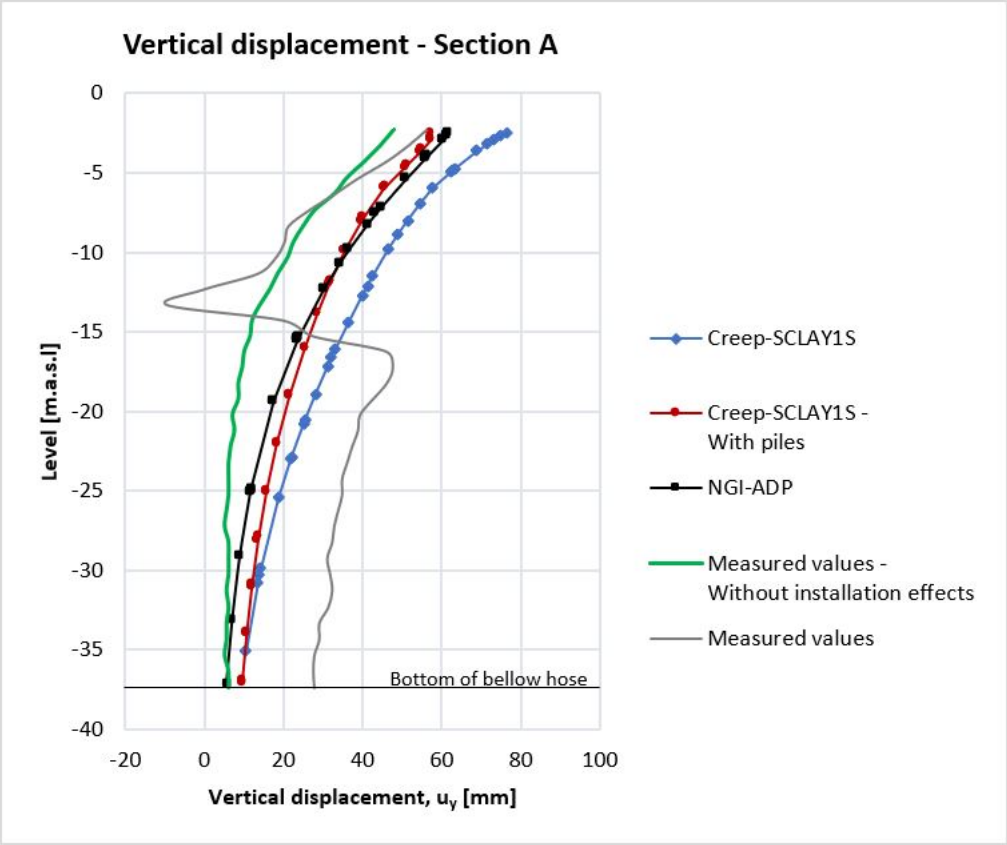

Figure 5.22: Comparison of heave predictions in section A for phase 8 (heave = positive).

6
Discussion

Overall, the Creep-SCLAY1S and NGI-ADP models predict similar behaviour of the soil and the retaining structure, and when comparing with the measured values it seems like both models have been able to capture the real behaviour (see Figure 5.22). However the size of soil displacements and structural forces differ between the models, and also from the measured values. In comparison with the measured values, both NGI-ADP and Creep-SCLAY1S overestimate the vertical displacements. If comparing the models, Creep-SCLAY1S generally predicts larger displacements in the soil and lower structural forces/bending moments (since the movements reduce the mobilized earth pressure on the retaining system). Although the predictions of soil displacements with the Creep-SCLAY1S model are larger than with the NGI-ADP model, it is evident that Creep-SCLAY1S predicts the development of deformations/stresses with time in a more realistic way.

When studying the soil displacements further, it can be seen that the model predictions differ more in horizontal displacements than in vertical displacements. For instance, the Creep-SCLAY1S model predicts a heave that is 30% larger than with NGI-ADP in point A, and a horizontal displacement that is 150% larger than with NGI-ADP in point B (for final excavation). Although, for the Creep-SCLAY1S model, the effect of time (after the finalized excavation), is prominent when studying vertical displacements, while they are negligible for the horizontal displacements. This could be an effect of low K_0-values. Also, the different ways of modelling anisotropy in the studied models, could affect this as well. Both K_0 and α_0 (parameters for Creep-SCLAY1S) in this study depend on Jaky's formula, which is only valid for clays with horizontal layering, which may differ slightly from the clay in this study.

Another explanation of the large difference in horizontal displacement (both of soil and SPW), is that the Creep-SCLAY1S model is more affected by an on-going stability mechanism induced by the weight of the road embankment. This mechanism could also explain the displacements of the sheet pile wall during the installation and also the difference in distribution of bottom heave between the models. Thus, it seems like the existing road embankment affects the overall stability more in the Creep-SCLAY1S model. From the results, it is also clear that the largest difference between the models is in the soil closest to the ground surface. This may be explained by the fact that the consolidation effects (in Creep-SCLAY1S) induced by the road embankment affect the top clay layers more, especially since they were already normally consolidated before the 80 year consolidation phase after the con-

struction of the road embankment. The effect of rate-dependency incorporated in the Creep-SCLAY1S model is noticeable on the structural entities as well, meaning that the design values for the structures can be important to consider further depending on the time-span that the excavation is expected to stay open.

These rather large differences between the models could partially be explained by the different initial stiffness formulations for the models (discussed in Section 5.1.1). Thus, the higher stiffness of NGI-ADP creates less soil displacements in comparison with Creep-SCLAY1S. It should also be pointed out that the Creep-SCLAY1S model uses drained analysis (in this study), and takes rate-dependency into consideration as well as bonding and destructuration, which also leads to larger deformations in comparison to the NGI-ADP model.

Something prominent in the result is that soil displacements occur in the whole clay deposit, which is not that likely. This could be due to the lack of small strain stiffness in both models. Also, as 2D plane strain analysis has been used in this study, it could overestimate deformations since the clay deposit is very thick (90 m, while the excavation length is 60 m). Another effect on the predicted deformations is the incorporation of piles within the excavation, which reduces the heave. This may be due to the skin interface interaction between the soil and the piles that is delayed in time, due to the time-dependent behaviour of the clay deposit. The deficiencies related to the numerical models is further discussed in Section 6.1.

The sensitivity analysis of the Creep-SCLAY1S simulation shows that the uncertainty in permeability, k, is likely to affect the result most. For instance, a tenfold increase in k changes the displacement by a maximum of 160% (point C). The fact that the permeability is difficult to derive in laboratory versus field also adds to the uncertainty of the parameter in this study. When studying the settlements it was also noted that the model was relatively sensitive to changes in OCR. For instance, an estimation error of 10% in the OCR changes the settlements by maximum 50% in point C. Also, a decrease in OCR affects the results more than an increase, but since the used OCR probably was a bit too low (considering the 80 year consolidation before the excavation work began) this might not be of much concern.

Further findings from the sensitivity analysis is that the bottom heave is sensitive to a decrease in κ^*, where a decrease in heave of around 20% is predicted. This may be due to the increased stiffness of the clay deposit. The increase of K_0^{NC} and K_0 gives largest effect on the settlement of the road embankment, where a decrease in settlement up to 50% is predicted. This may be due to the increased initial mobilization in strength of the soil when higher K_0 values are used. In comparison, the structural entities were not affected notably by changes in the analyzed parameters as much as the soil. Roughly, an increase in k seemed to give the largest effect in phase 10 (final excavation), where an increase of 20% for M_{max} and decrease of 10% for N can be seen.

Both numerical models that have been used in this study have their advantages and drawbacks. The Creep-SCLAY1S model incorporates many aspects of Scandinavian clay behaviour that the NGI-ADP model does not (such as consolidation and creep). However, the complexity of the Creep-SCLAY1S model is time consuming, both for sampling and for derivation of input parameters to the model. Therefore, this is a crucial step to be able to obtain reasonable predictions with the Creep-SCLAY1S model. As the sensitivity analysis has shown, there are parameters that the model is more sensitive in, and this also adds to its importance. Another thing that is important to have in mind when using the different numerical models, is what purpose the study has. The rate-dependency, for instance, is a very important behaviour that is crucial to capture if the long-term aspect of excavations (or other underground structures) and their surroundings is of importance.

6.1 Sources of Error

Since the interaction of structure and soil is too complex to predict with certainty, simplifications are necessary, and with that sources of error arise. Some of the most evident simplifications in this thesis is the geometry and properties of the soil and its ambient structures. In reality the soil is not divided into strictly delimiting homogeneous layers, and the surfaces are most likely not horizontal. Also, there exist several structures in the surrounding that are not accounted for. A considerable simplification of the soil profile is that a constant OCR is used in the soil layers, which is especially significant due to the large influence of that parameter in Creep-SCLAY1S. This simplified distribution of OCR does not reflect reality since it can not fully capture the complexity of the clay deposit and the stress history in the area.

Further, the input data itself also contributes to a large source of error if retrieved incorrectly. For instance, the soil samples in this project were retrieved with piston samplers (Swedish STI & STII samplers), which in comparison to block sampling may give less accurate values according to studies that have been done on that subject. However, it should also be stressed that the sample quality also depends on whom has done the sampling, laboratory tests and the interpretation of the results. Also the conditions during laboratory tests could give misleading input parameters. For instance the strain rates used in laboratory testing are much higher than in reality. This is extra problematic for the NGI-ADP model, since the model formulation does not allow calibration against the strain rate in the laboratory tests, but it also creates uncertainty for the Creep-SCLAY1S model. The higher strain rate in the laboratory might lead to an overestimation of the soil strength. Even though the temperature in the laboratory was the same as the in-situ temperature, the variation of temperature during the year is not considered when deriving the input parameters nor during the simulations.

Even though numerical modelling is a useful tool, it is also important to understand the simplifications that come with the modelling (both the constitutive relationships and the design of the system). One of the major issues in the numerical models is the difficulty to capture the current stress state in a reliable way. Already since the

1600's there has been human exploitation in the studied area. This means that to capture all the stresses that the soil has been exposed to since then, the numerical model simulation would need to incorporate a longer time period than that has been used in this thesis. Also, this implies that the input values to the numerical model would need to correspond to the in-situ conditions at that time, which is nearly impossible to know accurately without speculations. As has been shown in Section 5.4 (validation) this source of error seems to be significant, since the stress state changes quite much during consolidation to current conditions (where the input parameters are valid).

Another source of error related to the numerical models, is the use of 2D plane strain. By using the assumption of 2D plane strain, 3D effects are not accounted for. Thus, the used models do not account for effects such as length of excavation, step-wise excavation, corner effects etc. In order to get a picture of how this could affect the result, a rough comparison of the stress distribution for 2D plane strain and 3D was performed with the analytical 2:1 method. Figure 6.1 shows the estimated differences in the excavation bottom that occur when using 2D respectively 3D modelling. It is clear that by using 2D plane strain, stresses are larger with depth than with 3D calculations. This would imply that the predicted deformations are overestimated when using 2D plane strain.

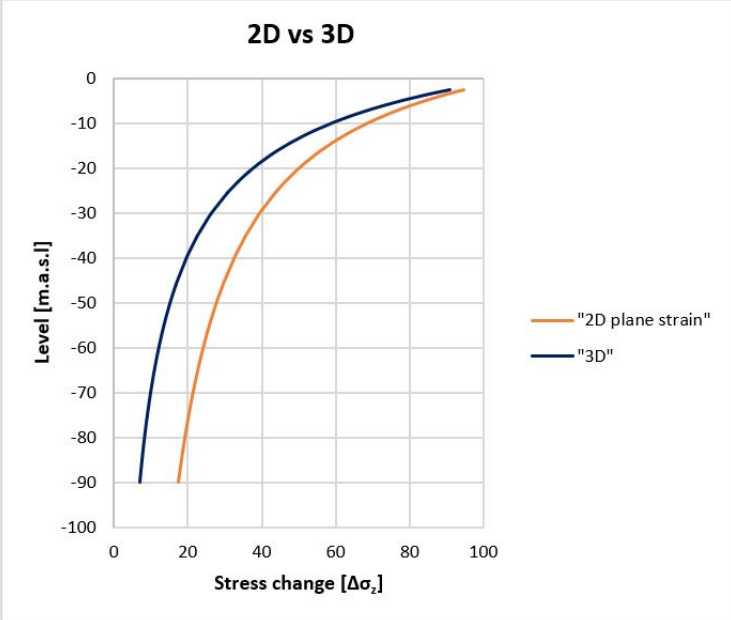

Figure 6.1: Comparison of stress in 2D and 3D using the analytical 2:1 method.

As already discussed, the lack of small strain stiffness in the numerical models is also a likely source of error, that could explain the occurrence of soil displacements in the whole clay deposit. If small strain stiffness was to be implemented in the models, the deformations would be smaller and another distribution with depth could be expected (decreasing with depth).

If looking closer at the input parameters for Creep-SCLAY1S, it can be seen that many of them are based on the critical state friction angle, ϕ'_{cv}, especially parameters describing initial stresses and anisotropy. Thus, it might be deceptive to just change some of the parameters based on ϕ'_{cv} when calibrating the Creep-SCLAY1S model. Although, this source of error is not considered to be that significant since the derivation of these parameters depends on other parameters than ϕ'_{cv} as well. As a consequence of the ϕ'_{cv}-dependency, the sensitivity analysis of K_0^{NC} and K_0 might be misleading since the "new" values are retrieved with formulations based on w_L instead of ϕ'_{cv}. Thus, other methods, than using ϕ'_{cv} for retrieving K_0^{NC} and K_0 might not be compatible with the other input parameters. However, the relationships based on w_L (from Larsson et al. (2007)), are based on empirical studies done on Scandinavian clays, which implies that these K_0^{NC} and K_0 values are more realistic than the ones obtained with Jaky's formula. Another thing adding to the uncertainty of the sensitivity analysis is that only one parameter is changed for each clay layer, which is not very realistic as all parameters for the clay cohere to some extent.

When looking at the real excavation process so far, it is not exactly executed like the one in the numerical model simulations, which partially could explain the observed difference between the measured values and the numerical predictions. For instance, heaps of soil were left while excavating for the second level waling beam (phase 8), which will counteract the bottom heave due to the additional soil weight. For clarification, the heaps of soil can be seen in Figure 6.2.

Figure 6.2: Heap of soil in the studied excavation.

Another aspect that is not considered in the numerical modelling is the installation effects. From Figure 5.22 in Section 5.6 (grey line) it is evident that the installation effects are prominent and could affect the predictions to a large extent. Also, to properly study the deformations after the finalized excavation it is necessary to consider activities such as casting of the concrete slab etc. Further, the piles within the excavation have not been modelled in a completely realistic way, which also adds to

the uncertainty of the prediction. In reality, auger drilling was used for the first 18 m below the excavation bottom, which would implicate a slight mass displacement when this part of the pile is installed. Further, the mass displacement from the piles below the pre-augering is not considered either (down to level -60 m).

During the excavation process it was noticed that the top layer of clay in the excavation was dry and that formation of cracks has occurred. In the numerical model simulation the excavation bottom is modelled as cohesive material, but considering the cracks, it is more suitable to model the top layer as a dry crust. The cracks result in an increased permeability and a lower strength of the top soil layer, which is not accounted for. These cracks could both affect the stability and the predicted heave profile. Since the clay shrinks, it would decrease the upwards moving displacements. Figure 6.3 shows the formation of cracks in the excavation bottom (phase 8).

Figure 6.3: Cracks on excavation bottom in studied excavation.

7

Conclusion & Recommendations

Numerical modelling is a very useful tool when modelling soil behaviour, but it should be used more as an indication on the expected behaviour than definite answers. Even though if measured values show compliance with numerical predictions, it could be for the wrong reason. For instance, larger displacements are predicted with the Creep-SCLAY1S model compared to the NGI-ADP model. However, the Creep-SCLAY1S model is considered to predict the development of deformations/stresses with time in a more realistic way. If the design complied more with reality, such as if piles would be incorporated in the design, there could be a risk of underestimating the deformations or forces/bending moments with the NGI-ADP model. Except suitable constitutive model and representative input values, it should be emphasized that the implementation of surrounding structures and stress history are of great importance when predicting the behaviour of clay.

To conclude, both studied numerical models have their advantages and drawbacks. The Creep-SCLAY1S model seemingly incorporates many aspects of Scandinavian clay behaviour that the NGI-ADP model does not. Perhaps most importantly, compared to the NGI-ADP model, it is an effective stress based model. Thus, allowing for consolidation analysis which could be crucial for design of excavations, as overall stability will decrease due to dissipation of negative excess pore pressures. As it incorporates rate-dependency, it can also account for if the field strain rate is lower than the laboratory test strain rate. However, the complexity of the Creep-SCLAY1S model is time consuming, both for laboratory testing, derivation of input parameters to the model and for the understanding of the user. Therefore, these factors are crucial to have in mind to be able to obtain reasonable predictions with the Creep-SCLAY1S model, as there are more input parameters that could lead to uncertainties. Another thing that is important to have in mind when using the different numerical models, is what purpose the study has. If longer time periods are studied, it is recommended to use rate-dependent models, like the Creep-SCLAY1S model. However, the complexity could be an issue if the user does not understand the model correctly. For shorter time spans or undrained response, models that are total stress based, like the NGI-ADP model are suitable as pore pressures will not have any notable effect. However, since deep and complex excavations may stay open during longer periods of time than previously, the modelling of time-dependent response of clay will be important since the stability of excavations becomes more critical with time. Thus, use of effective stress based models are strongly recommended.

7.1 Further Work

This thesis can be elaborated in many ways as mentioned in the discussion. There are some aspects that are both more interesting, and also the things that are considered to have the potential to give most improvement. These can be divided into different categories. The first is related to the in-situ and laboratory testing, as well as derivation of input parameters. Here, the input parameters could be altered to fit the time of actual input. In addition to this, further studies on the most sensitive parameters, k, κ^*, OCR, and K_0^{NC} and K_0 would be of interest.

The second category is related to the numerical modelling, where 3D modelling could be used instead of 2D plane strain, as the estimation with the 2:1 method showed that there is a notable difference. Here, the effect of small strain stiffness could be incorporated as well, since the influence area with depth evidently was unrealistically large in the models. Further and more extensive studies on uncertainties and sensitivity in the numerical models would also be of interest.

The last category includes the incorporation of real life construction techniques and effects of soil response. For instance, modelling the heap of soil on the excavation bottom, including the bottom plate, installation effects and modelling the top clay layer of the excavation bottom as dry clay. It would also be of interest to do more extensive comparison with measured values (Class C prediction), for instance for more phases and also for settlements, horizontal displacements, structural forces and bending moments.

References

Ahmad, N. (2017). *Nicoll highway collapse.* Retrieved 2019-02-09, from http://eresources.nlb.gov.sg/infopedia/articles/SIP_430_2004-12-17.html

Amavasai, A., Sivasithamparam, N., Dijkstra, J., & Karstunen, M. (2018, January). Consistent class a & c predictions of the ballina test embankment. *Computers and Geotechnics*, *93*, 75-86.

Andresen, A., & Kolstad, P. (1979). *The ngi 54-mm samplers for undisturbed sampling of clays and representative sampling of coarser materials* (Tech. Rep.). Oslo: Norges geotekniske institutt.

Billington, E. (1988). Generalized isotropic yield criterion for incompressible materials. *Acta mechanica*, *72*(1-2), 1–20.

Claesson, P. (2003). *Long term settlements of soft clays* (Ph.D. dissertation). Chalmers University of Technology.

Clayton, C. (2011). Stiffness at small strain: research and practice. *Géotechnique*, *61*(1), 5–37.

COI. (2005). *Report on the incident at the mrt circle line worksite that led to the collapse of the nicoll highway on 20 april 2004.* Ministry of Manpower, Singapore.

DeGroot, D. J., Poirier, S. E., & Landon, M. M. (2005). Sample disturbance – soft clays. *Studia Geotechnica et Mechanica*, *27*, 3–4.

Dijkstra, J., Karstunen, M., Gras, J.-P., & Karlsson, M. (2015). Creep and deformation characteristics in geomaterials.

Ekholm, K. (2017). *Hisingsbron: Från utredning till detaljprojektering.* Retrieved 2019-02-13, from https://docplayer.se/48513630-Hisingsbron-fran-utredning-till-detaljprojektering-kristoffer-ekholm-trafikkontoret.html (Trafikkontoret)

Ergun, M. U. (2008). Deep excavations. *EJGE*, *8*, 1-34.

Google Maps. (2019). *Google maps.* Retrieved 2019-02-13, from https://www.google.se/maps

Grimstad, G., Andresen, L., & Jostad, H. P. (2012). Ngi-adp: Anisotropic shear strength model for clay. *International journal for numerical and analytical methods in geomechanics*, *36*(4), 483–497.

Grimstad, G., Degago, S. A., Nordal, S., & Karstunen, M. (2010). Modelling creep and rate effects in structured anisotropic soft clays. *Acta Geotechnica*, *5*(1), 69-81.

Hansbo, S. (1960). Consolidation of clay, with special reference to influence of vertical sand drains. In *Swedish geotechnical institute proc.*

Jamal, H. (2017). *Total stress and effective stress analysis in soil.* Retrieved 2019-02-01, from `https://www.aboutcivil.org/soil-bearing-capacity-stress-analysis.html`

Janbu, N. (1969). The resistance concept applied to deformations of soils. In *Proceedings of the 7th international conference on soil mechanics and foundation engineering, mexico city* (Vol. 2529, p. 191-196).

Karlsrud, K. (2003). *Teknisk notat 2g-201-deformasjonsparametere for bruk i geotekniske beregninger.* Norges Geotekniske Institutt, Oslo, Norway.

Karlsrud, K., & Andresen, L. (2008). Design and performance of deep excavations in soft clays. In *International conference on case histories in geotechnical engineering* (p. 1-26). Arlington, USA.

Karlsson, M., Bergström, A., & Dijkstra, J. (2015). *Comparison of the performance of mini-block and piston sampling in high plasticity clay* (Tech. Rep.). Gothenburg: Chalmers University of Technology.

Karstunen, M., & Amavasai, A. (2017). *Best soil: Soft soil modelling and parameter determination* (Tech. Rep.). Göteborg: Chalmers University of Technology.

Karstunen, M., & Koskinen, M. (2008, August). Plastic anisotropy of soft reconstituted clays. *Canadian Geotechnical Journal*, *45*, 314-328.

Karstunen, M., Krenn, H., Wheeler, S. J., Koskinen, M., & Zentar, R. (2005, June). Effect of anisotropy and destructuration on the behavior of murro test embankment. *International Journal of Geomechanics*, *5*, 87-97.

Kempfert, H., & Gebreselassie, B. (2006). *Excavations and foundations in soft soils* (1st ed.). Berlin: Springer-Verlag.

Knappet, J. A., & Craig, R. F. (2012). *Craig's soil mechanics* (8th ed.). Abingdon: Spon Press.

Kullingsjö, A. (2007). *Effects of deep excavations in soft clay on the immediate surroundings - analysis of the possibility to predict deformations and reactions against the retaining system* (Unpublished doctoral dissertation). Chalmers University of Technology.

Ladd, C., & Foott, R. (1974). New design procedure for stability of soft clays. *Journal of Geotechnical and Geoenvironmental Engineering*, *100*, 763-786.

Lantmäteriet. (2019). *Historiska kartor.* Retrieved 2019-02-12, from `https://historiskakartor.lantmateriet.se`

Lanzky, R., & Palmquist, D. (2015). *Sample quality and disturbance in soft marine clay.* Chalmers University of Technology. Retrieved from `http://publications.lib.chalmers.se/records/fulltext/233364/233364.pdf`

Larsson, R. (1986). *Consolidation of soft soils* (Tech. Rep.). Linköping: SGI.

Larsson, R. (2008). *Jords egenskaper* (Tech. Rep.). Linköping: SGI.

Larsson, R., Sällfors, G., Bengtsson, P.-E., Alén, C., Bergdahl, U., & Eriksson, L. (2007). *Skjuvhållfasthet - utvärdering i kohesionsjord* (Tech. Rep.). Linköping: SGI.

Leoni, M., Karstunen, M., & Vermeer, P. A. (2008). Anisotropic creep model for soft soils. *Géotechnique*, *58*(3), 215–226.

Leroueil, S. (2006). The isotache approach—where are we 50 years after its development by professor šuklje? In *Proc., 13th danube-european conf. on geotechnical engineering* (pp. 55–88).

Lunne, T., Berre, T., & Strandvik, S. (1997). Sample disturbance effects in soft low plastic norwegian clay. In *Symposium on recent developments in soil and pavement mechanics* (p. 81-102). Rotterdam.

Meijer, K., & Åberg, A. (2007). *Krypsättningar i lera: en jämfölse mellan två beräkningsprogram.* Chalmers University of Technology.

Mises, R. v. (1913). Mechanik der festen körper im plastisch-deformablen zustand. *Nachrichten von der Gesellschaft der Wissenschaften zu Göttingen, Mathematisch-Physikalische Klasse*, *1913*, 582–592.

Olsson, M. (2010). Calculating long-term settlement in soft clays-with special focus on the gothenburg region.

Olsson, M. (2013). *On rate-dependency of gothenburg clay* (Ph.D. dissertation). Chalmers University of Technology.

Persson, J. (2004). The unloading modulus of soft soil: a field and laboratory study.

Petalas, A. (2018). *Numerical modelling.* Chalmers University of Technology. (Lecture in Infrastructural Geo-engineering)

Plaxis. (2018a). Plaxis 2d material models manual [Computer software manual].

Plaxis. (2018b). Plaxis 2d reference manual [Computer software manual].

Plaxis. (2018c). Plaxis scientific manual [Computer software manual].

Rankka, K. (2003). *Kvicklera - bildning och egenskaper* (Tech. Rep. No. 526). Linköping: SGI.

Rankka, K., Andersson-Sköld, Y., Hultén, C., Larsson, R., Leroux, V., & Dahlin, T. (2004). *Quick clay in sweden* (Tech. Rep. No. 65). Linköping: SGI.

SGU. (2019). *Sgus kartgenerator.* Retrieved 2019-02-14, from `http://apps.sgu.se/kartgenerator/maporder_en.html`

Sivasithamparam, N. (2012). *Modelling creep behaviour of soft soils* (Tech. Rep.). Glasgow: University of Strathclyde.

Sivasithamparam, N., Karstunen, M., & Bonnier, P. (2015, September). Modelling creep behaviour of anisotropic soft soils. *Computers and Geotechnics*, *69*, 46-57.

Skanska Teknik. (2018a). *Beräknings-pm - broramp ne* (Tech. Rep.). Göteborg: Skanska Teknik.

Skanska Teknik. (2018b). *Kompletternade markgeoteknisk undersökrningsrapport - broramp ne* (Tech. Rep.). Göteborg: Skanska Teknik.

Stadsbyggnadskontoret. (2019). *Historiska kartor.* Retrieved 2019-02-12, from `https://goteborg.se/wps/portal/start/byggande--lantmateri-och-planarbete/stadsbyggnadskontorets-kundservice/historiskt-material/kartor`

Stadsmuseet. (1999). Kulturhistoriskt värdefull bebyggelse i göteborg - ett program för bevarande. In G. Lönnroth (Ed.), (p. 22-55). Graphium Västra Aros, Västerås.

Svanø, C. S. . N. S., G. (1991). A soil model for consolidation and creep. In *Proceedings of the 10th ecsmfe, firenze* (p. 269-272).

Sällfors, G. (2013). *Geoteknik - jordmateriallära* (5th ed.). Göteborg: Cremona.

Taylor, D. W. (1942). *Research on consolidation of clays* (Vol. 82). Massachusetts Institute of Technology.

Terzaghi, K. (1923). Die berechnug der durchlassigkeit des tones aus dem verlauf

der hydromechanischen spannungserscheinungen. *Sitzungsber. Akad. Wiss. (Wien). Math.-Naturwiss. Kl., Abt. Iia*, *132*, 125-138.

Terzaghi, K., Peck, R. B., & Mesri, G. (1996). *Soil mechanics in engineering practice* (3rd ed.). New York: John Wiley & Sons, Inc.

Tornborg, J. (2017). *Svälltryck på grund av avlastning i lös lera* (Tech. Rep.). Tech. Rep.). Gothenburg: Svenska Byggbranschens Utvecklingsfond.

Tornborg, J. (2018, April).

Tornborg, J. (2019). *Tidsberoende effekter av schakt i lös lera.* Chalmers University of Technology.

Trafikverket. (2016a). *Ansökan om tillstånd enligt miljöbalken - västlänken och olskroken planskildhet* (Tech. Rep.). Gothenburg: Author.

Trafikverket. (2016b). *Mål och förväntade effekter för Västsvenska paketet.* Retrieved 2019-02-13, from `https://www.trafikverket.se/nara-dig/Vastra-gotaland/Vastsvenska-paketet/Mal-och-forvantade-effekter-for-paketet/`

Trafikverket. (2016c). *Pm inventering grundvattenberoende grundläggning* (Tech. Rep.). Gothenburg: Author.

Wang, R., Liu, G., & Liu, D. (2009). *Discussion on design method for retaining structures of metro station deep excavations in shanghai* (Tech. Rep.). Shanghai: Department of Geotechnical Engineering of Tongji University.

Wheeler, S. J., Näätänen, A., Karstunen, M., & Lojander, M. (2003). An anisotropic elastoplastic model for soft clays. *Canadian Geotechnical Journal*, *40*, 403-418.

Wood, D. M. (1990). *Soil behaviour and critical state soil mechanics* (1st ed.). Cambridge: Cambridge University Press.

Wood, T. (2015). Re-appraisal of the dilatometer for in-situ assessment of geotechnical properties of swedish glacio-marine clays. In *Dmt 2015 3rd international conference on the flat dilatometer, rome, italy, june.*

Wood, T. (2016). *On the small strain stiffness of some scandinavian soft clays and impact on deep excavations* (Unpublished doctoral dissertation). Chalmers University of Technology, Gothenburg.

Yang, X., Jia, Y., Liu, H., & Shan, H. (2009, September). Characteristics and causes of the preconsolidation stress of soils in the yellow river delta. *Journal of Ocean University of China*, *8*, 215-222.

Šuklje, L. (1957). The analysis of the consolidation process by the isotache method. In *Proceedings of the 4th international conference on soil mechanics and foundation engineering, london* (Vol. 1, p. 200-206).

A

Appendix: Foundation Type

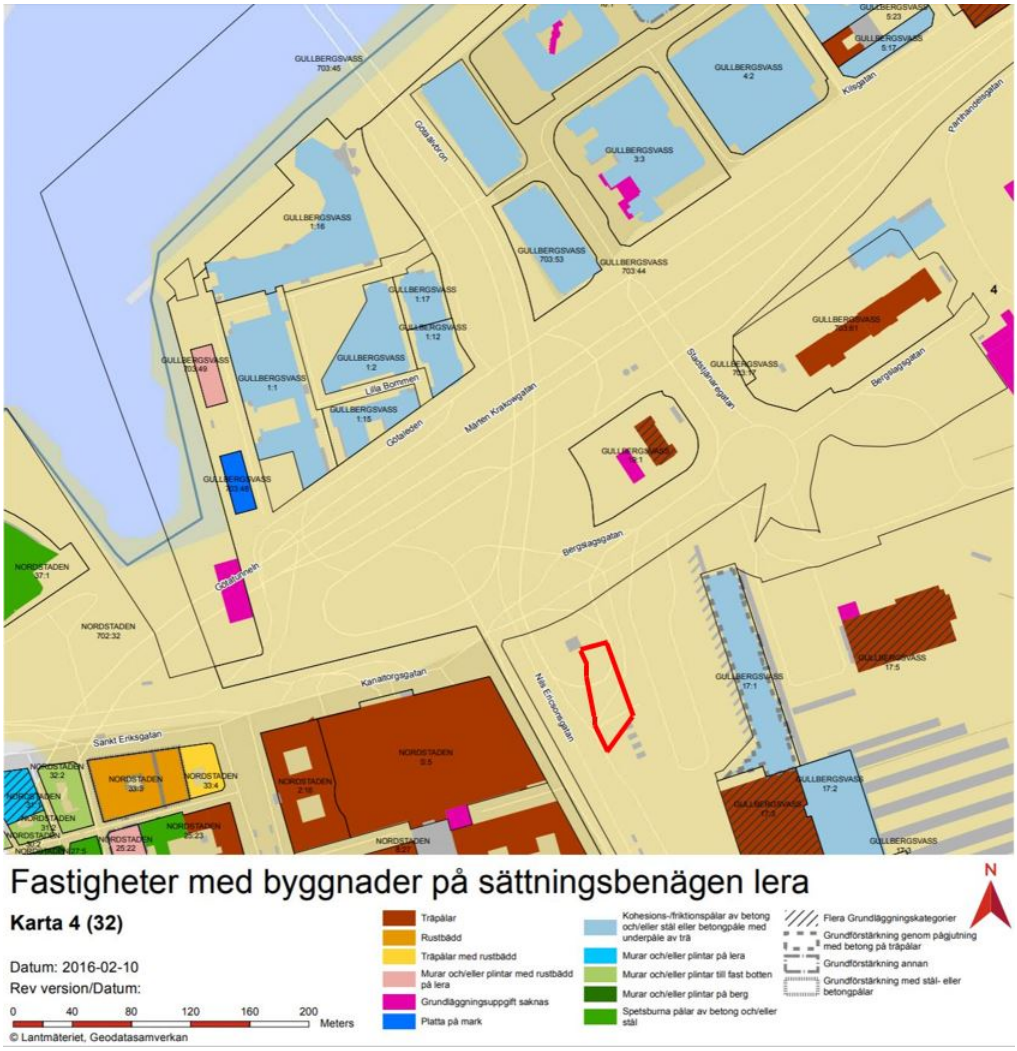

Figure A.1: Foundation types in the nearby area with excavation marked in red (Trafikverket, 2016c).

B

Appendix: Soil Properties

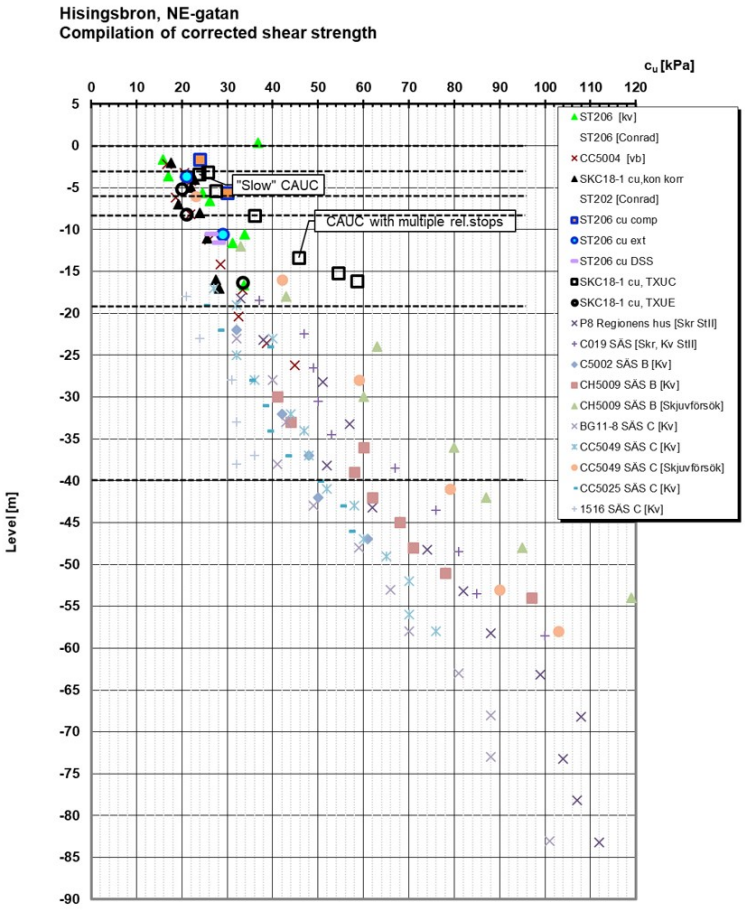

Figure B.1: Shear strength.

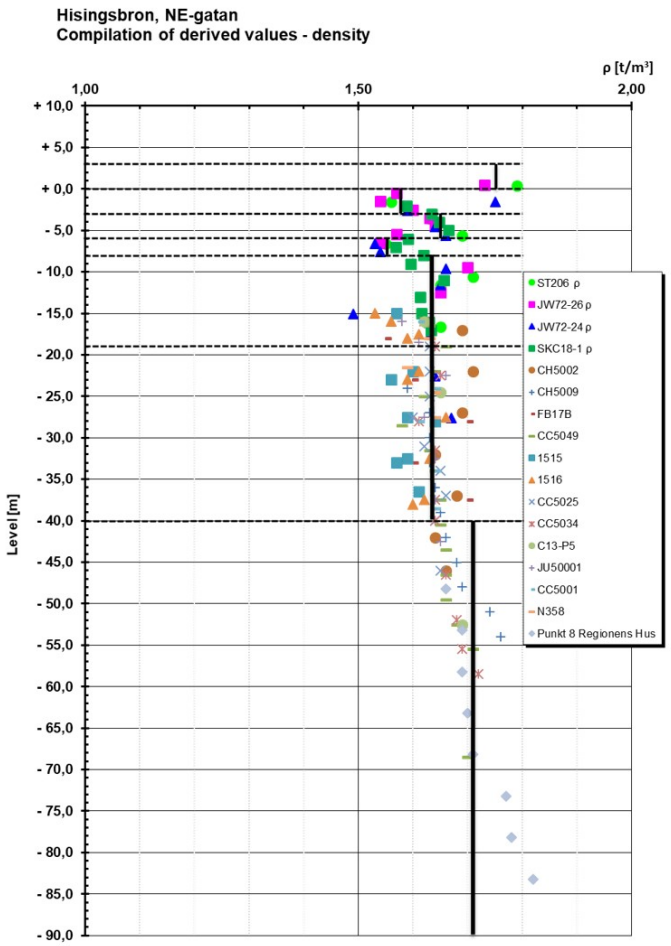

Figure B.2: Density.

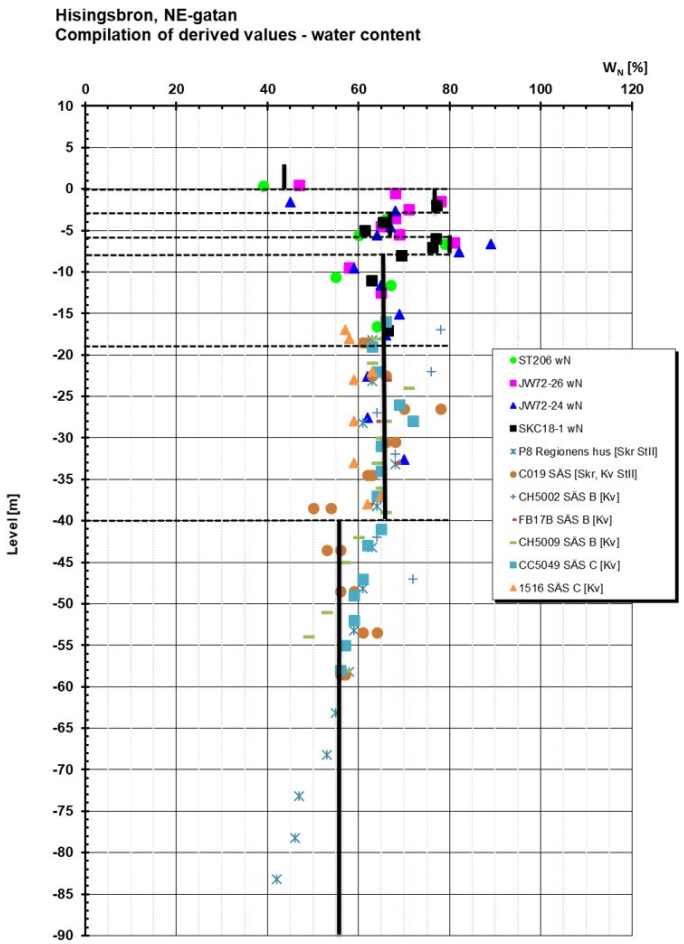

Figure B.3: Water content.

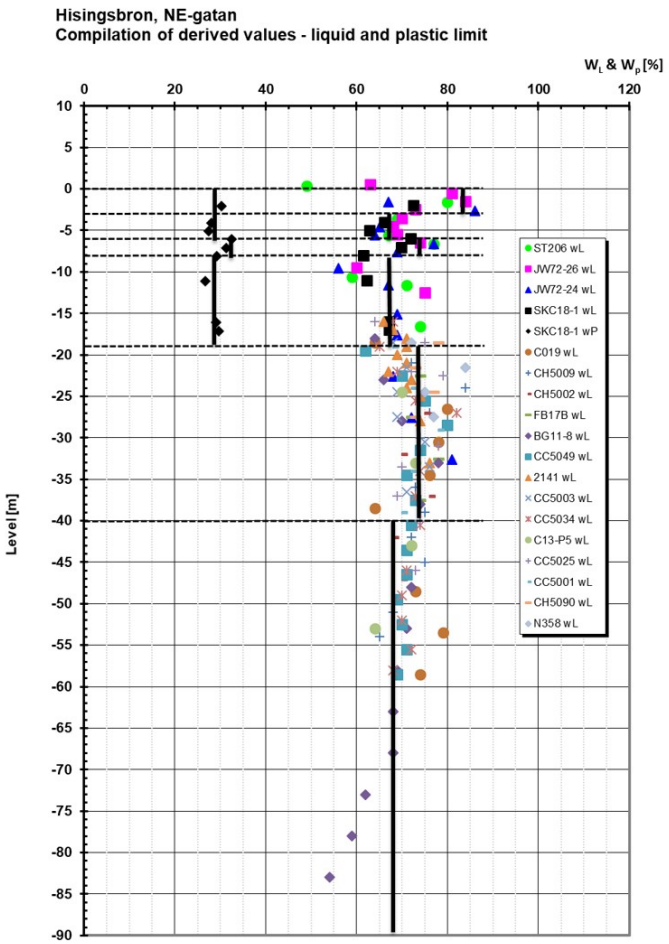

Figure B.4: Liquid and plastic limit.

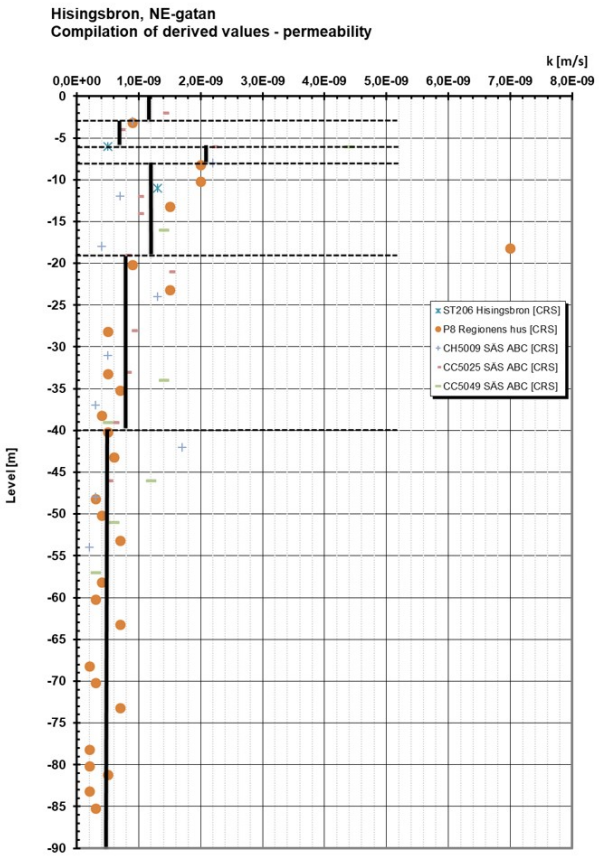

Figure B.5: Permeability.

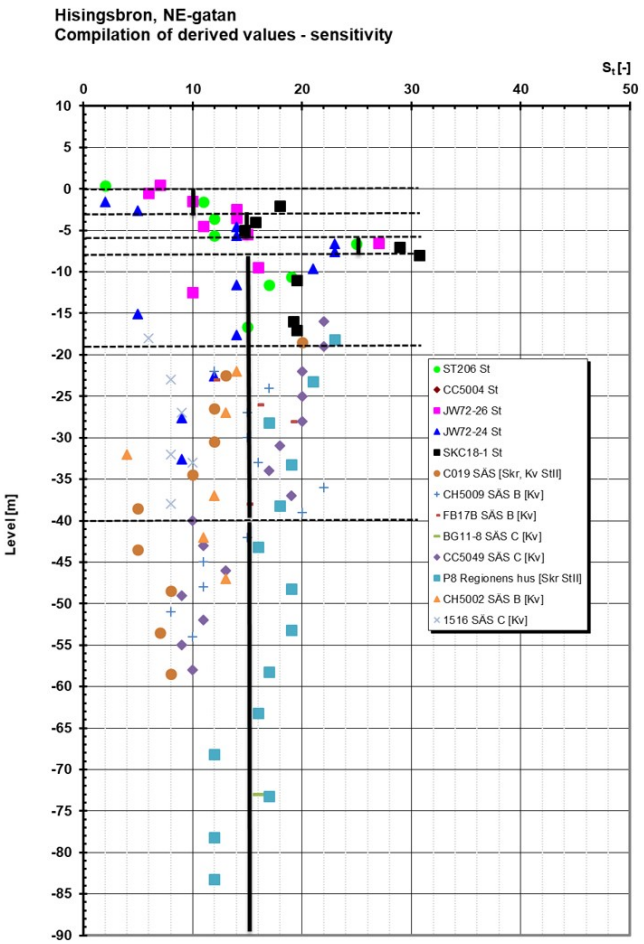

Figure B.6: Sensitivity.

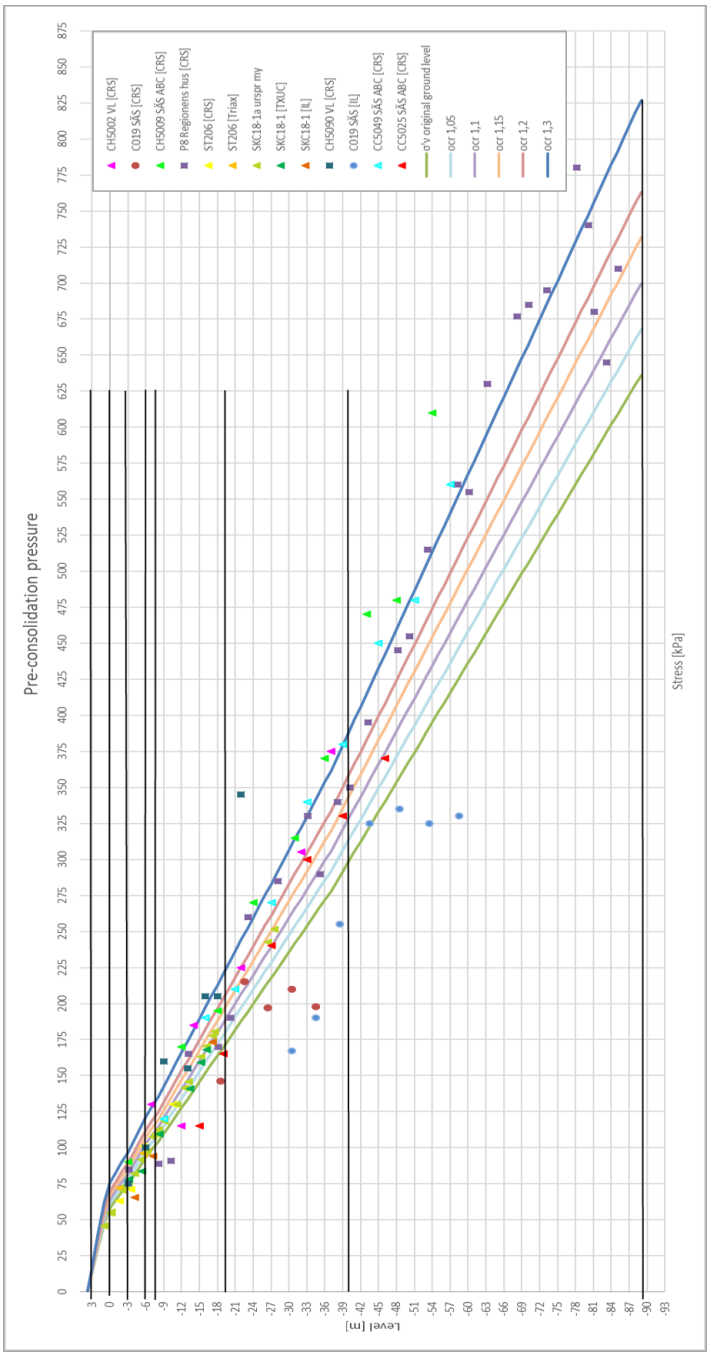

Figure B.7: Compilation of σ'_c with OCR trend-lines, chosen layers marked with black lines. The triangular markers are the values closest to the excavation, followed by the rectangular markers and then by the circular markers which are furthest away.

C

Appendix: Parameters for Numerical Model

Table C.1: Calculated parameters for Creep-SCLAY1S model.

Parameter	Clay 1	Clay 2	Clay 3	Clay 4	Clay 5	Clay 6
ϕ'_c	35	35	34.3	34	34	34
ϕ'_e	43	43	37	39.8	39.8	39.8
K_0	0.43	0.44	0.45	0.46	0.49	0.51
K_0^{NC}	0.43	0.43	0.44	0.44	0.44	0.44
OCR	1	1.05	1.1	1.15	1.2	1.3
ν'	0.15	0.15	0.15	0.15	0.15	0.15
$\kappa*$	0.011	0.011	0.017	0.005	0.005	0.005
λ_i*	0.057	0.057	0.046	0.062	0.062	0.062
M_c	1.42	1.42	1.39	1.37	1.37	1.37
M_e	1.1	1.1	1	1.06	1.06	1.06
α_0	0.55	0.55	0.53	0.53	0.53	0.53
ω	42	42	65	34	34	34
ω_d	0.96	0.96	0.94	0.93	0.93	0.93
χ_0	9	14	24	14	14	14
a	8	8	8	8	8	8
b	0.5	0.5	0.5	0.5	0.5	0.5
μ_i*	1.9E-3	1.9E-3	2E-3	1.5E-3	1.5E-3	1.5E-3
τ	1	1	1	1	1	1

Table C.2: Classification of sample quality for IL Oedometer tests.

Sample	$\mathbf{\Delta e/e_0}$	Rating
7m - Test 1	0.047	Good to fair
7m - Test 2	0.047	Good to fair
10m - Test 1	0.049	Good to fair
10m - Test 2	0.049	Good to fair
20m - Test 1	0.039	Very good to excellent
20m - Test 2	0.045	Good to fair

Table C.3: Classification of sample quality for CRS tests.

Sample	ε_p [%]	SQD	Rating
6m - Test 1	5.5	D	Poor
6m - Test 2	3	C	Fair
7m	3	C	Fair
8m	4	C	Fair
9m	2.8	C	Fair
10m	2.9	C	Fair
12m	5.5	D	Poor
14m - Test 1	3.5	C	Fair
14m - Test 2	2.7	C	Fair
14m - Test 3	3.8	C	Fair
16m	3.1	C	Fair
18m	2.7	C	Fair
19m	3.6	C	Fair
20m	-	-	-

Table C.4: Parameters for clay layers in NGI-ADP model.

Parameter	Unit	Clay 1	Clay 2	Clay 3
γ_{unsat}	kN/m^3	16	16	16.5
γ_{sat}	kN/m^3	16	16	16.5
G_{ur}/s_u^A	-	200	200	200
γ_f^C	%	1.5	1.5	1.5
γ_f^E	%	5	5	5
γ_f^{DSS}	%	3.163	3.163	3.163
$s_{u,ref}^A$	kN/m^2	23.56	23.56	64.48
y_{ref}	m	0	-3	-25
$s_{u,inc}^A$	kN/m^2/m	0	1.86	2.23
s_u^P/S_u^A	-	0.726	0.72	0.73
τ_0/s_u^A	-	0.27	0.5	0.52
s_u^{DSS}/s_u^A	-	0.806	0.81	0.81
ν'	-	0.2	0.2	0.2
k	m/s	1E-9	1E-9	1E-9
R_{inter}	-	0.5	0.5	0.5
K_0	-	0.75	0.65	0.65

Table C.5: Properties of filling material.

Parameter	Fill	Fill - embankment
γ_{unsat}	18	18
γ_{sat}	21	21
E'	10E3	40E3
E_{oed}	11.11E3	44.44E3
G	4167	16.67E3
ν'	0.2	0.2
ϕ'	35	42
c'_{ref}	0.1	0.1
V_s	47.65	95.31
V_p	77.82	155.6
k	0.0864	0.0864
R_{inter}	0.67	0.67

Table C.6: Properties of sheet pile walls.

Parameter	AU23 S355	PU12 S355
EA_1	3.641E6	2.94E6
EA_2	182.1E3	147E3
EI	68.1E3	29.03E3
w	1.363	1.1
M_p	644.7	413.8
$N_{p,1}$	7456	3360
$N_{p.2}$	372.8	168

Table C.7: Properties of struts.

Parameter	CHS406(10)	CHS558(12.5)
EA	1.29E6	2.89E6
$L_{spacing}$	6	6

Table C.8: Parameters for Soft Soil interfaces.

Parameter	Unit	Interface 1	Interface 2	Interface 3	Interface 4
γ_{unsat}	kN/m^3	15.4	16.2	15.2	16
γ_{sat}	kN/m^3	15.4	16.2	15.2	16
k	m/s	1.2E-9	0.7E-9	2.1E-9	1.2E-9
ϕ'_c	°	35	35	34.3	34.5
K_0^{NC}	-	0.43	0.43	0.44	0.44
OCR	-	1	1.05	1.1	1.15
ν'_{ur}	-	0.15	0.15	0.15	0.15
$\kappa*$	-	0.019	0.019	0.014	0.014
$\lambda*$	-	0.15	0.15	0.13	0.24
c'_{ref}	kN/m^2	1	1	1	1
R_{inter}	-	0.5	0.5	0.5	0.5

D

Appendix: Soil Test

D.1 Calibration of Tests at Depth 7-8 m

In Figure D.1, D.2 and D.3 the lab-test-results from 7-8 m depth is plotted against fitted curves from soil test in Plaxis. To calibrate the soil against the triaxial test results the triaxial soil test function in Plaxis was used. For the triaxial compression and extension a K_0 of 0.59 was used and a σ'_{v0} of 76.2 kPa was calculated from the assumed densities and water table presented in Figure 4.4. The samples used for triaxial compression and extension were retrieved from a depth of 8.26 m which corresponds to a level of -5.26 m. The σ'_c was estimated to be 81 kPa from the triaxial compression plot. The used OCR was 1.06.

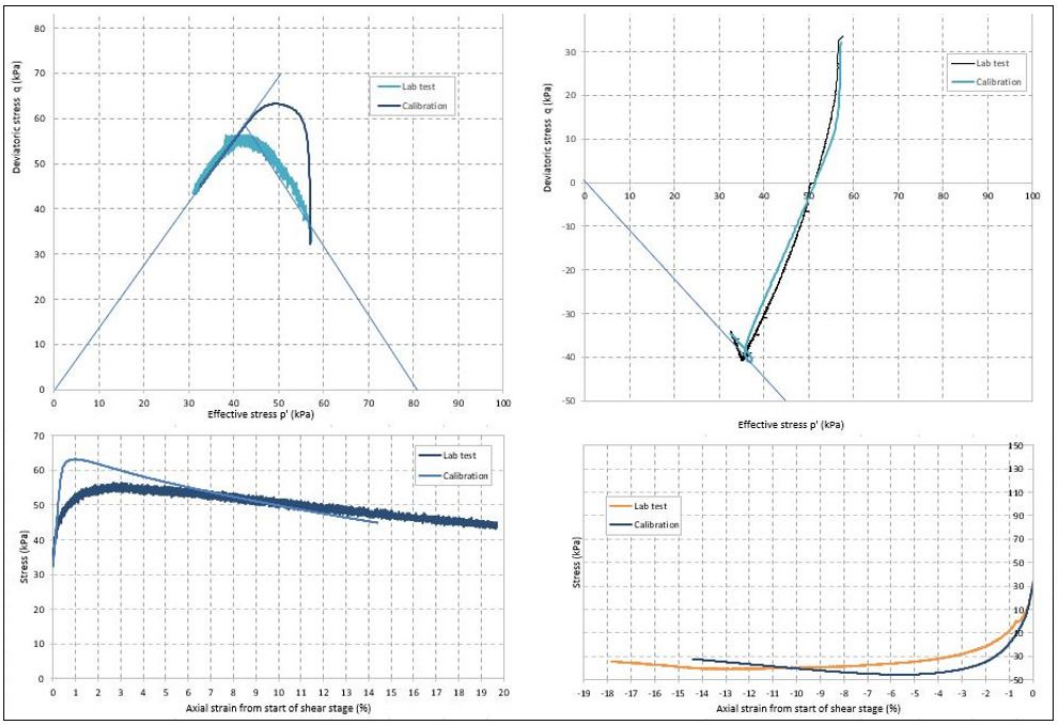

Figure D.1: Calibration against triaxial test, level -5.26 m.

When calibrating for the IL Oedometer test result, the general soil test function was used. The sample used in the IL Oedometer test was retrieved from a depth of 7.1 m which corresponds to a level of -4.1 m. The σ'_c was estimated to 73 kPa which was used as POP. The initial stresses was set to -5 kPa in all directions.

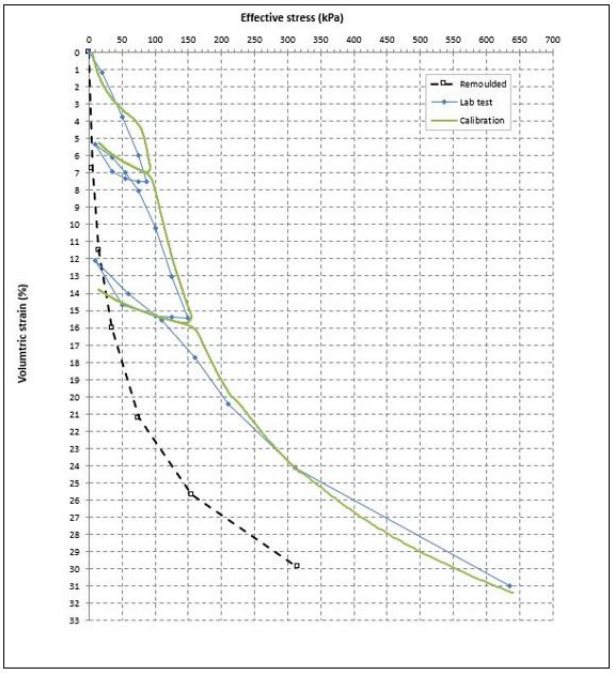

Figure D.2: Calibration against IL Oedometer test, level -4.1 m.

When calibrating for the CRS test result, the general soil test function in Plaxis was used. The sample used for the CRS test was retrieved at a depth of 7.1 m, which corresponds to a level of -4.1 m. The σ'_c was estimated to 58 kPa which was used as POP.

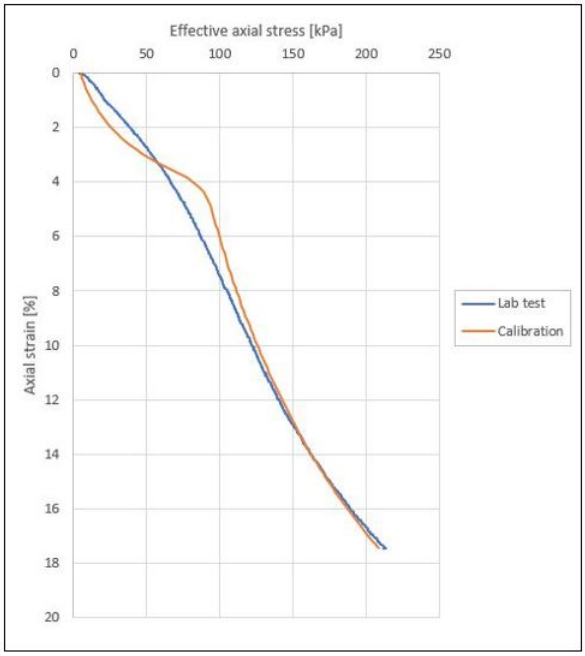

Figure D.3: Calibration against CRS test, level -4.1 m.

D.2 Calibration of Tests at Depth 10-11 m

In Figure D.4, D.5 and D.6 the lab-test-results from 10-11 m depth is plotted against fitted curves from soil test in Plaxis. To calibrate the soil against the triaxial test results the triaxial soil test function in Plaxis was used. For the triaxial compression and extension a K_0 of 0.593 and 0.597 was used respectivly and a σ'_{v0} of 92.7 kPa was calculated from the assumed densities and water table presented in Figure 4.4. The samples used for triaxial compression and extension was retrieved from a depth of 11.2 m and 11.1 m which corresponds to a level of -8.2 m and -8.1 m. The σ'_c was estimated to be 108 kPa from the triaxial compression plot. The used OCR was 1.16.

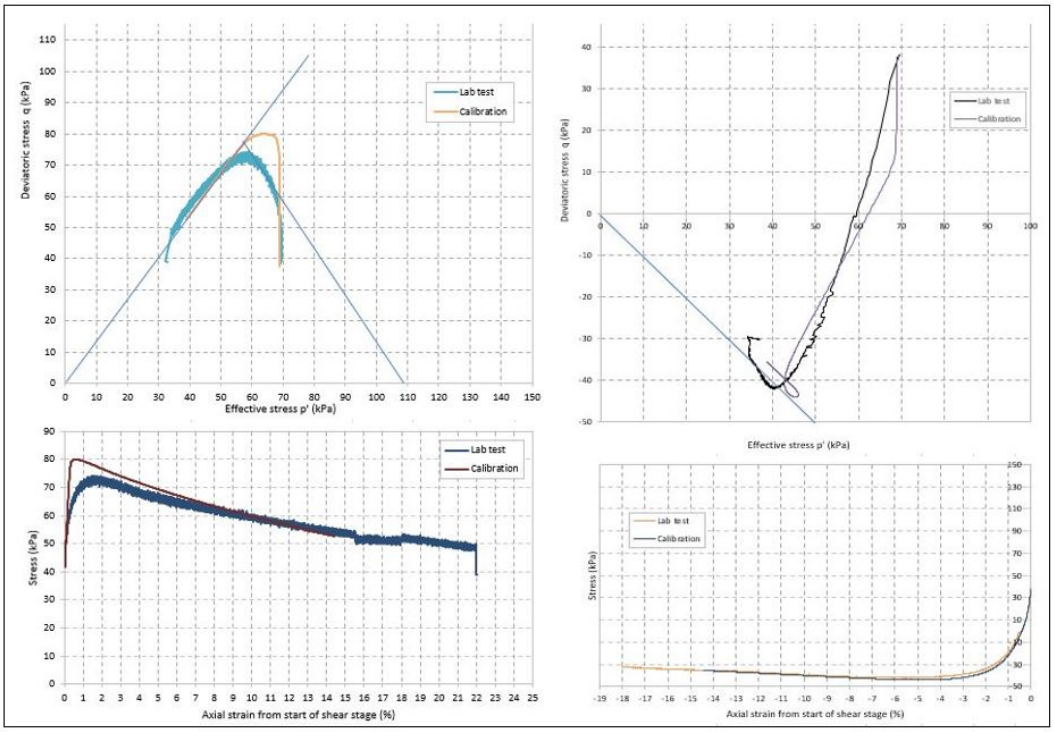

Figure D.4: Calibration against triaxial test, level -8.24 m.

When calibrating for the IL Oedometer test result, the general soil test function was used. The sample used in the IL Oedometer test was retrieved from a depth of 10.1 m which corresponds to a level of -7.1 m. The σ'_c was estimated to 93 kPa which was used as POP. The initial stresses was set to -5 kPa in all directions.

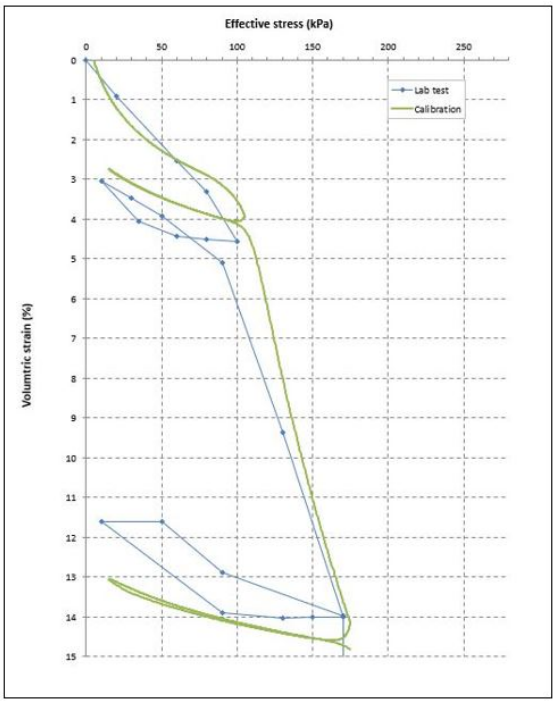

Figure D.5: Calibration against IL Oedometer test, level -7.1 m.

When calibrating for the CRS test result, the general soil test function in Plaxis was used. The sample used for the CRS test was retrieved at a depth of 10.1 m, which corresponds to a level of -7.1 m. The σ_c' was estimated to 101 kPa which was used as POP.

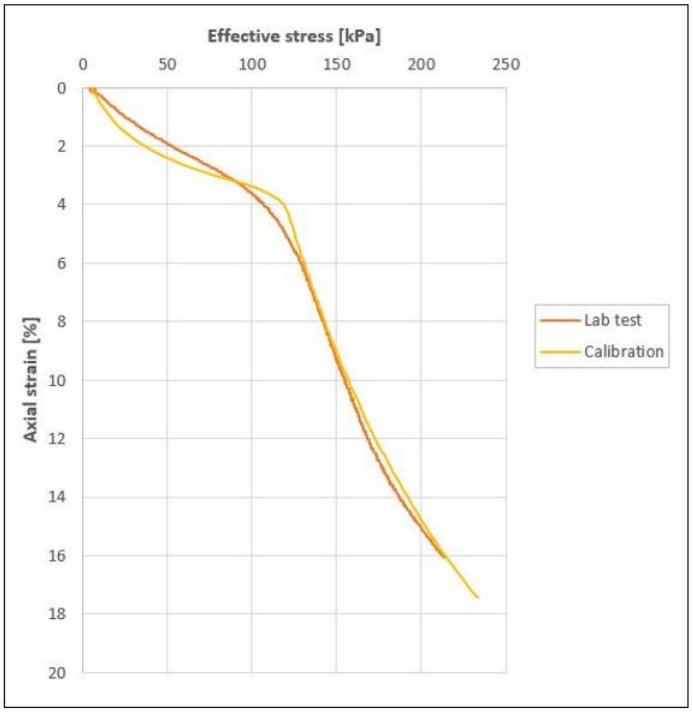

Figure D.6: Calibration against CRS test, level -7.1 m.

D.3 Calibration of Tests at Depth 19-20 m

In Figure D.7, D.8 and D.9 the lab-test-results from 19-20 m depth is plotted against fitted curves from soil test in Plaxis. To calibrate the soil against the triaxial test results the triaxial soil test function in Plaxis was used. For the triaxial compression and extension a K_0 of 0.59 was used and a σ'_{v0} of 139.9 kPa was calculated from the assumed densities and water table presented in Figure 4.4. The samples used for triaxial compression and extension was retrieved from a depth of 19.1 m which corresponds to a level of -16.1 m. The σ'_c was estimated to be 168 kPa from the triaxial compression plot. The used OCR was 1.2.

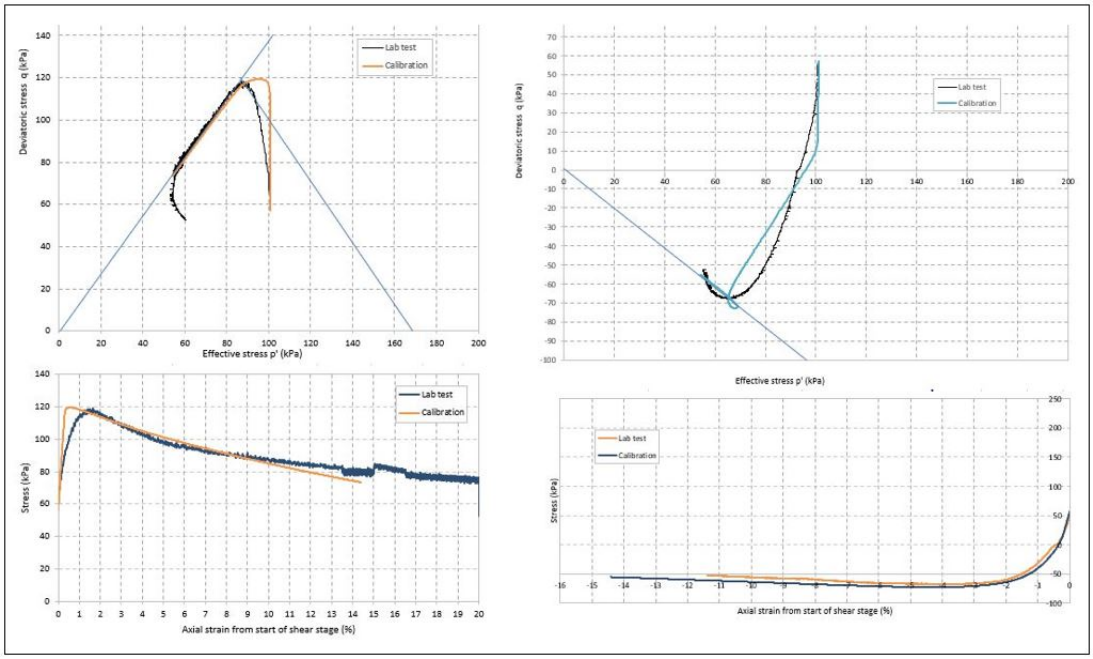

Figure D.7: Calibration against triaxial test, level -16.1 m.

When calibrating for the IL Oedometer test result, the general soil test function was used. The sample used in the IL Oedometer test was retrieved from a depth of 20 m which corresponds to a level of -17 m. The σ'_c was estimated to 165 kPa which was used as POP. The initial stresses was set to -7 kPa in all directions.

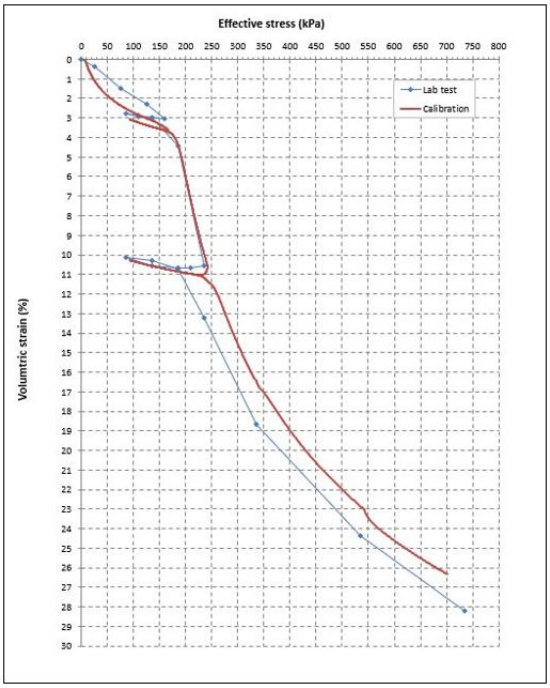

Figure D.8: Calibration against IL Oedometer test, level -17 m.

When calibrating for the CRS test result, the general soil test function in Plaxis was used. The sample used for the CRS test was retrieved at a depth of 19 m, which corresponds to a level of -16 m. The σ'_c was estimated to 183 kPa which was used as POP

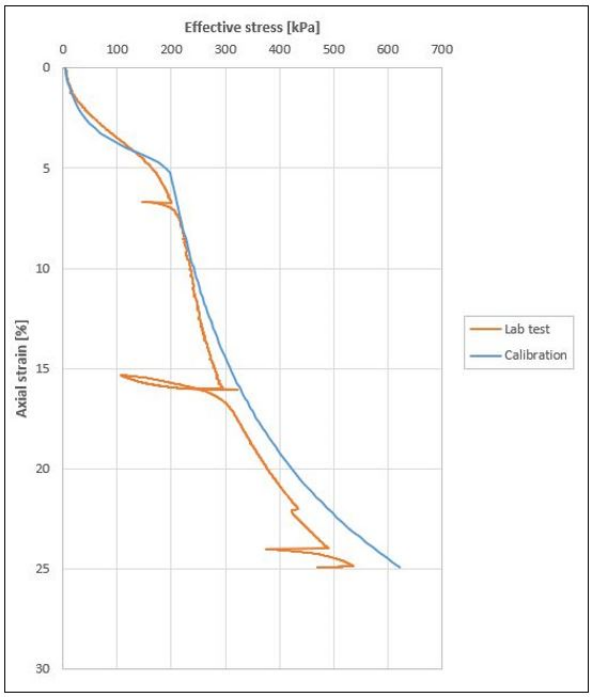

Figure D.9: Calibration against CRS test, level -16 m.

E

Appendix: Construction Sequence

Table E.1: Construction sequence with NGI-ADP in Plaxis.

Phase	Description	Type of procedure
Initial phase	Soil activation and calculation of initial stresses	K_0-procedure
Phase 1	Installation of existing wooden piles	Plastic
Phase 2	Construction of existing embankment	Plastic
Phase 3	Consolidation to current conditions	Not included
Phase 4	Excavation for unloading down to +2.8m	Plastic
Phase 5	Installation of sheet pile wall	Plastic
Phase 6	Excavation for first level waling beam down to +1m	Plastic
Phase 7	Installation of first strut level	Plastic
Phase 8	Excavation for second level waling beam down to -1m	Plastic
Phase 9	Installation of second strut level	Plastic
Phase 10	Final excavation down to -2.55m	Plastic

F

Appendix: Result

F.1 Displacements in Soil

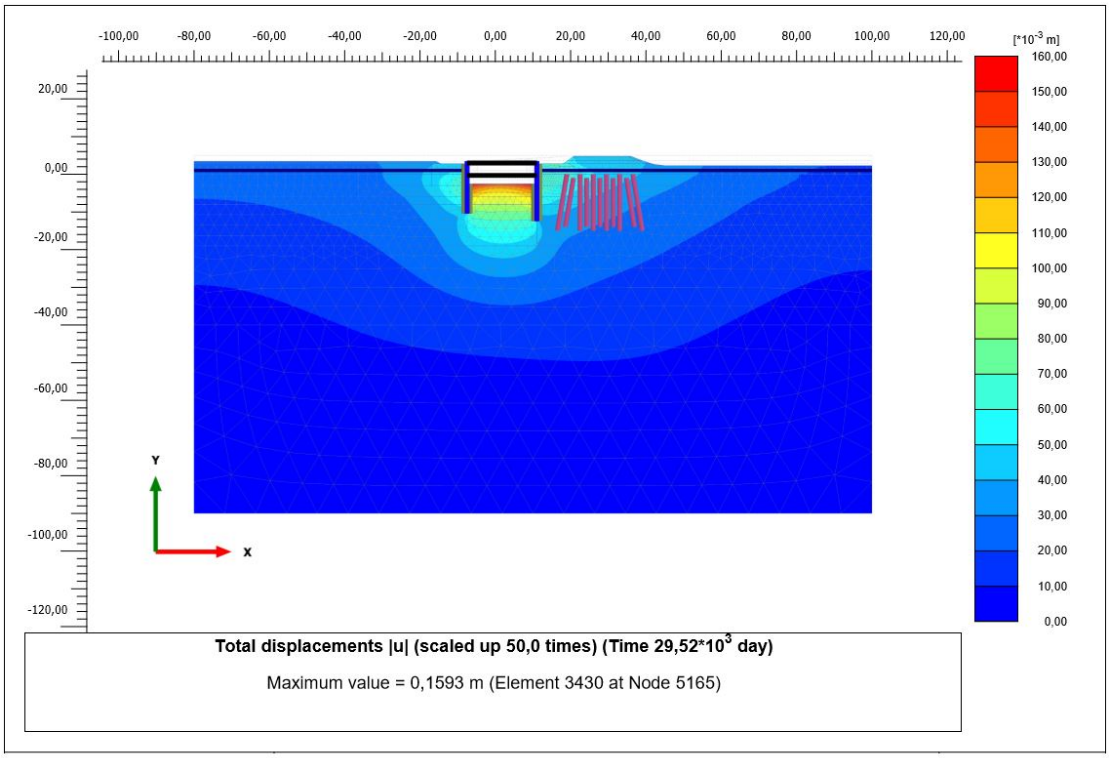

Figure F.1: Total displacements for last excavation stage using Creep-SCLAY1S model.

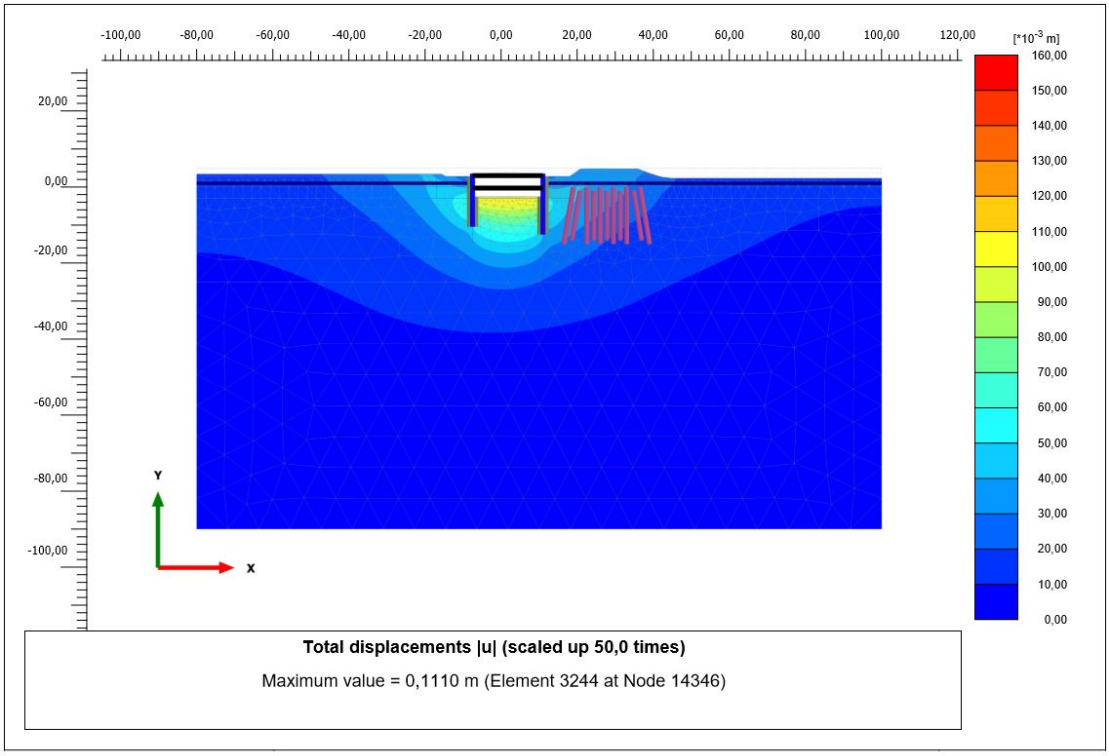

Figure F.2: Total displacements for last excavation stage using NGI-ADP model.

Table F.1: Bottom heave in point A (center of excavation bottom) with Creep-SCLAY1S and NGI-ADP. Displacements are reset to 0 after Phase 3.

Phase	u_y [m] Creep-SCLAY1S	u_y [m] NGI-ADP
Phase 1 - Installation of existing wooden piles	-0.001	0
Phase 2 - Construction of existing embankment	-0.019	-0.045
Phase 3 - Consolidation to current conditions	-0.903	-
Phase 4 - Excavation for unloading down to +2.8m	0.022	0.012
Phase 5 - Installation of sheet pile wall	0.021	0.011
Phase 6 - Excavation for first level waling beam down to +1m	0.055	0.031
Phase 7 - Installation of first strut level	0.057	0.031
Phase 8 - Excavation for second level waling beam down to -1m	0.098	0.073
Phase 9 - Installation of second strut level	0.104	0.073
Phase 10 - Final excavation down to -2.55m	0.141	0.111
Phase 11 - Consolidation for 1 month	0.150	-
Phase 12 - Consolidation for 3 months	0.166	-
Phase 13 - Consolidation for 1 year	0.200	-

Analytical 2:1 method for 2D plane strain, where $\Delta\sigma_y$ is the change in stress at a depth y.

$$\Delta\sigma_y = \frac{b \cdot q}{(b + y)} \tag{F.1}$$

where
b = width [m]
q = applied/removed load at ground surface (negative for unloading) [kPa/m]
y = depth [m]

Vertical displacements at depth y.

$$u_y = \sum h \frac{\Delta\sigma_y}{M_{ul}} \tag{F.2}$$

where
$\Delta\sigma_y$ = stress change at depth y [kPa]
M_{ul} = unloading modulus [kPa]
h = thickness of clay [m]

Table F.2: Horizontal displacement in point B (location of inclinometer) with Creep-SCLAY1S and NGI-ADP. Displacements are reset to 0 after Phase 3.

Phase	u_x [m] Creep-SCLAY1S	u_x [m] NGI-ADP
Phase 1 - Installation of existing wooden piles	0	0
Phase 2 - Construction of existing embankment	0.010	-0.001
Phase 3 - Consolidation to current conditions	-0.057	-
Phase 4 - Excavation for unloading down to +2.8m	-0.004	-0.001
Phase 5 - Installation of sheet pile wall	-0.004	-0.001
Phase 6 - Excavation for first level waling beam down to +1m	-0.039	-0.009
Phase 7 - Installation of first strut level	-0.038	-0.009
Phase 8 - Excavation for second level waling beam down to -1m	-0.055	-0.022
Phase 9 - Installation of second strut level	-0.055	-0.022
Phase 10 - Final excavation down to -2.55m	-0.057	-0.022
Phase 11 - Consolidation for 1 month	-0.056	-
Phase 12 - Consolidation for 3 months	-0.056	-
Phase 13 - Consolidation for 1 year	-0.056	-

Table F.3: Settlement in point C (tram track closest to excavation) with Creep-SCLAY1S and NGI-ADP. Displacements are reset to 0 after Phase 3.

Phase	u_y [m] Creep-SCLAY1S	u_y [m] NGI-ADP
Phase 2 - Construction of existing embankment	-0.061	-0.061
Phase 3 - Consolidation to current conditions	-0.819	-
Phase 4 - Excavation for unloading down to +2.8m	-0.001	0
Phase 5 - Installation of sheet pile wall	-0.002	0
Phase 6 - Excavation for first level waling beam down to +1m	-0.006	-0.002
Phase 7 - Installation of first strut level	-0.006	-0.002
Phase 8 - Excavation for second level waling beam down to -1m	-0.010	-0.010
Phase 9 - Installation of second strut level	-0.011	-0.010
Phase 10 - Final excavation down to -2.55m	-0.014	-0.018
Phase 11 - Consolidation for 1 month	-0.015	-
Phase 12 - Consolidation for 3 months	-0.016	-
Phase 13 - Consolidation for 1 year	-0.022	-

F.2 Bending Moments

Table F.4: Horizontal displacement in right-hand sheet pile wall with Creep-SCLAY1S and NGI-ADP.

Phase	u_x^{min}/u_x^{max} [m] Creep-SCLAY1S	u_x^{min}/u_x^{max} [m] NGI-ADP
Phase 5 - Installation of sheet pile wall	-0.004/0.002	-0.002/0
Phase 6 - Excavation for first level waling beam down to +1m	-0.045/-0.013	-0.011/-0.006
Phase 7 - Installation of first strut level	-0.044/-0.012	-0.011/-0.006
Phase 8 - Excavation for second level waling beam down to -1m	-0.061/-0.023	-0.039/-0.010
Phase 9 - Installation of second strut level	-0.061/-0.022	-0.039/-0.010
Phase 10 - Final excavation down to -2.55m	-0.068/-0.030	-0.054/-0.010
Phase 11 - Consolidation for 1 month	-0.070/-0.029	-
Phase 12 - Consolidation for 3 months	-0.071/-0.027	-
Phase 13 - Consolidation for 1 year	-0.072/-0.020	-

Table F.5: Bending moment in right-hand sheet pile wall with Creep-SCLAY1S and NGI-ADP.

Phase	M_{min}/M_{max} [kNm/m] Creep-SCLAY1S	M_{min}/M_{max} [kNm/m] NGI-ADP
Phase 5 - Installation of sheet pile wall	-0.3/0	0/0
Phase 6 - Excavation for first level waling beam down to +1m	-5.6/22	-1.1/8.1
Phase 7 - Installation of first strut level	-6.6/22.9	-1.1/8.0
Phase 8 - Excavation for second level waling beam down to -1m	-67.0/10.1	-64.4/5.0
Phase 9 - Installation of second strut level	-61.8/6.7	-64.4/5.0
Phase 10 - Final excavation down to -2.55m	-53.3/10.9	-66.6/15.8
Phase 11 - Consolidation for 1 month	-54.3/21.7	-
Phase 12 - Consolidation for 3 months	-58.8/30.9	-
Phase 13 - Consolidation for 1 year	-66.9/34.1	-

F.3 Sensitivity Analysis

Table F.6: Increased values for K_0^{NC} and K_0.

Parameter	Clay 1	Clay 2	Clay 3	Clay 4	Clay 5	Clay 6
K_0^{NC}	0.76	0.64	0.69	0.64	0.69	0.65
K_0	0.76	0.66	0.73	0.70	0.77	0.75

F.4 Effect of Piles

Table F.7: Parameters for steel and concrete piles.

Parameter	Unit	Outer steel pile	Inner steel pile	Outer concrete pile	Inner concrete pile
E	kN/m^2	210E6	210E6	13E6	13E6
γ	kN/m^3	32	32	25	25
Diameter	m	0.3239	0.3239	-	-
Width	m	-	-	0.270	0.270
$L_{spacing}$	m	3.6	4.9	3.6	4.9
Axial skin resistance	-	Multi-linear	Multi-linear	Multi-linear	Multi-linear
Lateral skin resistance	-	Linear	Linear	Linear	Linear
$T_{lat,start,max}$	kN/m	0.5	0.5	0.5	0.5
$T_{lat,end,max}$	kN/m	1	1	1	1
F_{max}	kN/m	1	1	1	1

Table F.8: Parameters for axial skin resistance.
Steel piles: 0.5·c_{uk}
Concrete piles: 0.7·c_{uk}

Distance [m]	Axial skin resistance - Steel pile	Axial skin resistance - Concrete pile
2.35	9.5	13.3
6	11.5	16.1
8	11	15.4
19	18	25.2
40	34	47.6
59.35	49	68.6

Table F.9: Bottom heave in point A (center of excavation bottom) with Creep-SCLAY1S and Modified Creep-SCLAY1S. Displacements are reset to 0 after Phase 3.

Phase	u_y [m] Creep-SCLAY1S	u_y [m] Modified Creep-SCLAY1S
Phase 1 - Installation of existing wooden piles	-0.001	-0.001
Phase 2 - Construction of existing embankment	-0.019	-0.019
Phase 3 - Consolidation to current conditions	-0.903	-0.904
Phase 4 - Excavation for unloading down to +2.8m	0.022	0.022
Phase 4.5 - Installation of steel & concrete piles	-	0.020
Phase 5 - Installation of sheet pile wall	0.021	0.020
Phase 6 - Excavation for first level waling beam down to +1m	0.055	0.044
Phase 7 - Installation of first strut level	0.057	0.045
Phase 8 - Excavation for second level waling beam down to -1m	0.098	0.076
Phase 9 - Installation of second strut level	0.104	0.080
Phase 10 - Final excavation down to -2.55m	0.141	0.127
Phase 11 - Consolidation for 1 month	0.150	0.136
Phase 12 - Consolidation for 3 months	0.166	0.151
Phase 13 - Consolidation for 1 year	0.200	0.184